

University of Ninevah
College of Electronic Engineering



**Simulation and Implementation of Wireless Power
Transfer System**

Zakarya Ammar Al-Atraqchi

**M.Sc. Thesis in
Electronic Engineering**

**Supervised by
Dr. Ahmad Thanoon Younis
Dr. Yasir M.Y. Ameen**

2020 A.C.

1442 A.H.

University of Ninevah
College of Electronic Engineering



Simulation and Implementation of Wireless Power Transfer System

A Dissertation Submitted by
Zakarya Ammar Al-Atraqchi

To
The Council of College of Electronic Engineering
University of Ninevah
In Partial Fulfillment of the Requirements
For the Degree of Master of Sciences
In
Electronic Engineering

Supervised by
Dr. Ahmad Thanoon Younis
Dr. Yasir M.Y. Ameen

2020 A.C.

1442 A.H.



Abstract

Wireless power transfer (WPT) is a technique introduced to transfer power in a wireless fashion. Inductive coupling WPT systems have been dominant for use in wireless chargers due to their flexibility and particular use compared to conventional cable charging systems. The efficiency of the WPT depends on many factors, this may include the coupling between the transmitter and receiver coils, inverter losses, and rectifier losses.

In this thesis, a resonant inductive wireless system has been designed for a power range up to 250W considering issues such as the effect of the resonant frequency, the efficiency of the system, inductive coils coupling factor, and system losses. The developed WPT system has been simulated using MATLAB and ANSYS MAXWELL and many investigations have been accomplished on the coils and the circuit of the system. These may include the effect of changing coil parameters on the coupling factor and how to improve it and also studies several factors that have been affected on the WPT system circuit. Finally, a prototype has been developed in the laboratory to implement and realize the designed WPT system and to show how the system efficiency can be improved practically. Also, a new method to calculate the compensations element was presented, simulation and realization are applied which is based on the leakage-inductance instead of self-inductance.

TABLE OF CONTENTS

| Subject | | Page |
|--|--|-------------|
| Abstract | | I |
| Table of contents | | II |
| List of figures | | VI |
| List of tables | | II |
| List of abbreviations | | XIII |
| List of symbols | | IIV |
| CHAPTER ONE | | |
| INTRODUCTION | | |
| 1.1 | Preface | 1 |
| 1.2 | Literature review | 2 |
| 1.3 | Aims of the dissertation | 5 |
| 1.4 | layout of the dissertation | 6 |
| CHAPTER TWO | | |
| BASICS THEORIES OF WPT SYSTEMS AND THEIR APPLICATIONS | | |
| 2.1 | Introduction | 7 |
| 2.2 | Wireless power transmission technologies | 7 |
| 2.3 | The basic concept of the resonant inductive coupling WPT system. | 9 |
| 2.3.1 | Maxwell's equations | 9 |
| 2.3.2 | The resistance and the skin depth | 10 |
| 2.3.3 | Resonance | 11 |
| 2.3.4 | Quality factor (Q) | 14 |
| 2.3.5 | Coupled resonators | 15 |

| Subject | | Page |
|---|--|------|
| 2.3.6 | Self-inductance | 16 |
| 2.3.7 | Coupling factor (k) | 16 |
| 2.4 | Basic realization of the resonant inductive WPT system | 17 |
| 2.4.1 | Inverter | 18 |
| 2.4.1.1 | Inverter topologies | 18 |
| 2.2.1.2 | Inverter switching device | 22 |
| 2.4.2 | Rectifier | 22 |
| 2.4.3 | Compensation elements | 23 |
| 2.5 | Calculation of electrical parameters for the WPT system | 24 |
| 2.6 | Main point that must be observed in WPT systems | 27 |
| 2.6.1 | The efficiency of the transfer power. | 27 |
| 2.6.2 | Transmission power | 27 |
| 2.6.3 | Transmission distance | 27 |
| 2.6.4 | Displacement flexibility | 28 |
| 2.7 | WPT system benefits and applications | 28 |
| CHAPTER THREE | | |
| DESIGN AND SIMULATION OF RESONANT WPT SYSTEM | | |
| 3.1 | Introduction | 29 |
| 3.2 | Coils design | 29 |
| 3.2.1 | Simulation of an inductive coil. | 29 |
| 3.2.2 | Design and simulation of a specific coil for the WPT system | 31 |
| 3.2.2.1 | Calculation of the skin effect and R_{ac} | 34 |
| 3.3 | The design considerations of the induction coils for the WPT system | 35 |
| 3.3.1 | The effect of changing the diameter of the wire on the coil parameters | 35 |

| Subject | | Page |
|--|---|-------------|
| 3.3.2 | The effect of changing the coil's inner radius on its parameters | 36 |
| 3.3.3 | The effect of changing the gap between the turns on the coil's parameters | 37 |
| 3.3.4 | The effect of changing coil's shape and alignment coupling factor | 38 |
| 3.3.5 | Efficiency investigation of the WPT system coils with two types of cross-sections | 39 |
| 3.3.5.1 | Design and simulation of symmetrical and asymmetrical coils | 39 |
| 3.3.5.2 | Inductive coupling WPT realization | 41 |
| 3.4 | WPT system circuit design and simulation | 43 |
| 3.5 | System efficiency measurement simulation at the different applied voltage | 46 |
| 3.6 | Performance study of the entire WPT system. | 47 |
| 3.6.1 | Find the appropriate load resistance for the WPT system | 47 |
| 3.6.2 | The effect of changing the load resistance on the WPT system | 49 |
| 3.6.3 | Effect of changing resonant frequency (f_r) on the WPT system | 52 |
| 3.6.4 | Comparative study of resonant frequency calculation | 55 |
| 3.6.5 | Simulation of a 250-watt WPT with a various air gap | 61 |
| CHAPTER FOUR | | |
| IMPLEMENTATION OF RESONANT WPT SYSTEM | | |
| 4.1 | Introduction | 64 |
| 4.2 | WPT system design | 64 |
| 4.2.1 | Inverter design | 65 |
| 4.2.1.1 | Input DC supply voltage | 66 |
| 4.2.1.2 | Trigger circuit | 67 |
| 4.2.1.3 | Optocoupler | 67 |

| Subject | | Page |
|------------------------------------|---|-------------|
| 4.2.1.4 | Switching device | 67 |
| 4.2.2 | Coil implementation | 68 |
| 4.2.2.1 | Inductive coil | 68 |
| 4.2.2.2 | Specific coil for the WPT system | 70 |
| 4.2.3 | Compensation capacitors | 70 |
| 4.2.4 | Rectifier circuit | 70 |
| 4.2.4.1 | Diode bridge | 71 |
| 4.2.4.2 | Output capacitor | 71 |
| 4.2.5 | Output load | 71 |
| 4.3 | Implementation of the WPT system with a Silicon inverter | 71 |
| 4.4 | Comparison between WPT System using Silicon and Silicon Carbide inverter | 75 |
| 4.5 | Implementation of the WPT system with leakage-inductance and self-inductance-based resonant frequency calculation | 77 |
| CHAPTER FIVE | | |
| CONCLUSIONS AND FUTURE WORK | | |
| 5.1 | Conclusions | 80 |
| 5.2 | Future work | 82 |
| REFERENCES | | |
| References | | 83 |

LIST OF FIGURES

| Figure | Title | Page |
|----------------------|---|-----------|
| CHAPTER TWO | | |
| 2.1 | Classification of wireless power transfer technologies. | 8 |
| 2.2 | Skin effect for the copper wire. | 11 |
| 2.3 | An LCR series circuit. | 12 |
| 2.4 | An equivalent circuit of the coupled two-resonator system. | 15 |
| 2.5 | Two types of coupled circuits mode | 17 |
| 2.6 | General diagram of RIPT system. | 18 |
| 2.7 | DC to AC half-bridge inverter circuit. | 19 |
| 2.8 | Current direction flow in half-bridge inverter (a) for time period ($0 < t < T_1$) (b) for time period ($T_1 < t < T_2$). | 19 |
| 2.9 | Load voltage and switches current in the half-bridge inverter. | 20 |
| 2.10 | Circuit diagram of the full-bridge inverter. | 20 |
| 2.11 | Current flow for the period a. ($0 < t < T_1$). b. ($T_1 < t < T_2$). | 21 |
| 2.12 | Load voltage and current in the Full-bridge inverter. | 21 |
| 2.13 | Rectifier circuit with resistive load and capacitive output filter. | 23 |
| 2.14 | The basic topologies: (a) SS, (b) SP, (c) PS, (d) PP. | 24 |
| 2.15 | WPT system with SS compensation elements. | 24 |
| 2.16 | IPT systems architecture. | 27 |
| 2.17 | Misalignment of WPT systems. | 28 |
| CHAPTER THREE | | |
| 3.1 | The geometry of the two coils Tx and Rx. | 30 |
| 3.2 | Transmitter and receiver coils filed distribution. | 31 |

| Figure | Title | Page |
|--------|---|------|
| 3.3 | Circular Litz wire coils simulation. | 32 |
| 3.4 | Variation of the coupling factor and mutual factor with various air-gap between Rx and Tx. | 33 |
| 3.5 | The circular Litz wire Tx and Rx coils filed distribution | 33 |
| 3.6 | Circular coils geometry. | 35 |
| 3.7 | The effect of changing the diameter of the wire on the coils turns number, wire length l , volume, and weight while keeping the same k between the coils. | 36 |
| 3.8 | The effect of changing r_{in} on the coupling factor, outer radius, number of turns, and coils self-inductance. | 37 |
| 3.9 | The effect of changing the gap between the turns on the coupling factors between the transmitter and receiver circular coils, self-inductance, and the coils turns number. | 38 |
| 3.10 | Effect of changing the coil's shape on the coupling factor. | 39 |
| 3.11 | Wire cross-section | 40 |
| 3.12 | (a) Symmetric coils with circular cross-section wire, (b) Symmetric coils with rectangular cross-section-wire, (c) Asymmetric coils with circular cross-section-wire, (d) Asymmetric coils with rectangular cross-section-wire. | 40 |
| 3.13 | Simulation circuit of (a) SS topology (b) SP topology | 42 |
| 3.14 | The efficiency of the circular coils with various topologies and distances (a) Rectangular cross-section (b) Circular cross-section | 43 |
| 3.15 | The WPT system circuit. | 44 |
| 3.16 | The whole MATLAB WPT circuit with the measurement devices. | 45 |
| 3.17 | The WPT system stages efficiency of the WPT system. | 46 |
| 3.18 | The inverter losses of the WPT system at different V_{in} | 47 |
| 3.19 | Efficiency carve with various R_L at $V_{in} = 150$ V and $f_r = 40$ kHz | 49 |
| 3.20 | Variation of V_{in} and V_{out} with R_L at 250 W out power. | 50 |

| Figure | Title | Page |
|---------------------|--|------|
| 3.21 | Variation of the input power with changing R_L | 50 |
| 3.22 | System efficiency with changing R_L | 51 |
| 3.23 | MOSFET voltage and current waveforms. | 51 |
| 3.24 | Tx coil voltage and current. | 52 |
| 3.25 | Input and voltage with changing f_r and 250-watt output power. | 54 |
| 3.26 | Input current value with changing f_r to get the 250-watt output power. | 45 |
| 3.27 | The power efficiency of the WPT system with changing f_r and 250-watt output power. | 55 |
| 3.28 | Switching voltage and current at $V_{in}=60V$ for Leakage-inductance-based calculation. | 57 |
| 3.29 | Switching voltage and current at $V_{in}=60V$ for L_{Self} -based inductance calculation. | 57 |
| 3.30 | The input voltage and current before the Tx coil at $V_{in}=60V$ (a) L_{leak} -based calculation (b) L_{Self} -based calculation | 58 |
| 3.31 | The input voltage and current for the rectifier circuit at $V_{in}=60V$ (a) L_{leak} -based calculation(b) L_{Self} -based calculation | 59 |
| 3.32 | Tx and Rx coils voltage L_{leak} -based calculation at $V_{in} = 60$ V | 60 |
| 3.33 | Tx and Rx coils voltage L_{Self} -based calculation at $V_{in} 60$ V. | 60 |
| 3.34 | Input applied voltage with changing air-gap and 250-watt output power. | 62 |
| 3.35 | Input current with changing air-gap and 250-watt output power. | 62 |
| 3.36 | The power efficiency of the WPT system with changing air-gap and 250-watt output power. | 63 |
| Chapter Four | | |
| 4.1 | Wireless power transfer system general configuration. | 64 |
| 4.2 | Inverter circuit using Silicon MOSFET. | 65 |
| 4.3 | Inverter circuit using Silicon Carbide MOSFET. | 66 |

| Figure | Title | Page |
|---------------|--|-------------|
| 4.4 | Inductive coils. | 68 |
| 4.5 | Induction Tx and Rx coils. | 69 |
| 4.6 | Laboratory measurement L for Cooker coils. | 69 |
| 4.7 | Circular Litz Wire Coils. | 70 |
| 4.8 | Rectifier circuit. | 71 |
| 4.9 | Silicon-inverter WPT system experiment. | 72 |
| 4.10 | Experimental results verification with simulation for input and output power. | 73 |
| 4.11 | Experimental results verification with simulation for efficiency. | 73 |
| 4.12 | Voltage and current across Tx coil at $V_{in} = 50V$. | 74 |
| 4.13 | Voltage and current across Rx coil at $V_{in} = 50V$. | 74 |
| 4.14 | Input and output power comparison between Silicon and Silicon Carbide inverter in the WPT system. | 75 |
| 4.15 | Input current comparison between Silicon and Silicon Carbide inverter in the WPT system. | 76 |
| 4.16 | Efficiency comparison between Silicon and Silicon Carbide inverter in the WPT system. | 76 |
| 4.17 | Practical experiment setup of the leakage and self-inductance-based calculation in the WPT system. | 77 |
| 4.18 | Experimental transmitter stage resonant voltage and current waveform at $V_{in} = 60V$ leakage-inductance-based. | 78 |
| 4.19 | Experimental receiver stage resonant voltage and current waveform at $V_{in} = 60V$ leakage-inductance-based. | 79 |
| 4.20 | Experimental results verification with simulation for input and output power based on self-inductance calculation. | 79 |

LIST OF TABLES

| Table | Title | Page |
|----------------------|--|-----------|
| CHAPTER THREE | | |
| 3.1 | Tx and Rx coils parameter | 30 |
| 3.2 | Simulation results of Tx and Rx. | 30 |
| 3.3 | Assumed value for WPT system | 31 |
| 3.4 | Circular Litz wire coils parameters. | 32 |
| 3.5 | The circular Litz wire coils simulation results. | 32 |
| 3.6 | The calculation of R_{ac} . | 34 |
| 3.7 | The geometry for the designed coils. | 41 |
| 3.8 | Coils simulation result parameter for a circular cross-section. | 41 |
| 3.9 | Coils simulation result parameter for a rectangular cross-section. | 41 |
| 3.10 | DC and AC Resistances. | 42 |
| 3.11 | WPT circuit elements. | 46 |
| 3.12 | The simulation results for the efficiency calculations for the different voltages applied. | 46 |
| 3.13 | Simulation result to find RL_A at $V_{in} = 150 \text{ V}$. | 48 |
| 3.14 | f_{SW} value for each R_L with 250 W output power | 52 |
| 3.15 | The circuit's parameter value to study the resonant frequency effect. | 53 |

| | | |
|---------------------|---|-----------|
| 3.16 | f_r and f_{sw} and compensation capacitor value. | 53 |
| 3.17 | Results based on leakage-inductance calculations. | 56 |
| 3.18 | Results on self-inductance calculations. | 56 |
| 3.19 | Simulation of a 250-watt WPT with various air gap circuit elements. | 61 |
| CHAPTER FOUR | | |
| 4.1 | Experimental result for WPT system with silicon inverter. | 72 |
| 4.2 | Experimental Results of WPT using Silicon Carbide inverter. | 75 |
| 4.3 | Experimental results based on leakage-inductance calculations | 77 |
| 4.4 | Experimental results based on self inductance calculations. | 78 |

LIST OF ABBREVIATIONS

| Abbreviation | Name |
|--|---|
| WPT | Wireless Power Transfer |
| RICPT | Resonance Inductive Coupling Power Transmission |
| CCPT | Capacitance Coupling Power Transmission |
| EM | Electromagnetic |
| MIT | Massachusetts Institute of Technology |
| T_x | Transmitter |
| R_x | Receiver |
| SS | Series - Series |
| PS | Parallel - Series |
| PP | Parallel - Parallel |
| SP | Series-Parallel |
| IPT | Induction Power Transfer |
| MOSFET | Metal Oxide Semiconductor Field Effect Transistor |
| IGBT | Insulated Gate Bipolar Transistor |
| AC | Alternating Current |
| DC | Direct Current |
| BW | bandwidth |
| XL | Inductive reactance |
| XC | capacitive reactance |
| S | Switch |
| <i>D₁, D₂, D₃, D₄</i> | Diode |

LIST OF SYMBOLS

| Symbol | Name |
|-----------------------|--------------------------------|
| E | Electric field |
| B | Magnetic flux density |
| t | Time |
| J | Current Density |
| H | Magnetic field |
| D_e | Electric flux density |
| ρ₀ | Charge density |
| μ | Magnetic permeability |
| R_{dc} | Dc resistance |
| l | Length |
| A | Cross-section region |
| ρ | Resistivity |
| δ | Skin effect |
| f | Frequency |
| μ₀ | Absolute magnetic permeability |
| f_r | Resonant frequency |
| R | Resistor |
| Z | Impedance |
| ω₀ | Angular resonant frequency |
| ω | Frequency |
| L | Inductance |
| C | Capacitor |
| Q | Quality factor |
| κ | Coupling factor |
| V_g | Voltage source with amplitude |
| R_g | Generator resistance |
| M | Mutual inductance |

| | |
|------------|--|
| Φ | Flux |
| ϵ | Magnetic flux |
| V_{dc} | Input DC voltage |
| T | The time during this period |
| V_{in} | Supply voltage |
| R_{LB} | Battery resistance |
| r | Wire radius |
| r_{in} | Coil's inner radius |
| d | The gap between turns |
| N | Number of turns |
| D | Air-gap |
| V_{out} | Output voltage |
| A_n | Actual area |
| A_f | The inner area of the wire that no current passes from it |
| r_f | The radius of the inner cross-section of the wire that no current passes |
| R_{on} | MOSFET on resistance |
| R_{LA} | Appropriate load resistance |
| R_L | Load resistance |

CHAPTER ONE

INTRODUCTION

CHAPTER ONE

INTRODUCTION

1.1 Preface

Wireless power transfer (WPT) is a concept of transferring energy between two circuits without any cables connecting between them. In the last years, the resonant inductive coupling of the WPT has become one of the most demanded technologies. WPT can be extremely useful for charging technologies and power transfer to the medical device [1][2].

There are three basic methodologies for the wireless transmission of energy. These include longitudinal acoustic compression wave, resonance inductive coupling power transmission (RICPT), and electromagnetic propagation coupling capacitance coupling power transmission (CCPT), the WPT system has been discontinued by longitudinal acoustic compression waves [3].

However, because of technical limitations, the concept was not developed and commercialized widely. Later on, in 2007, researchers at the Massachusetts Institute of Technology (MIT) have successfully shown the ability to transfer wireless power[4]. Since then the technology of wireless power transfer used as a solution to terminate hazards charges and the disadvantage related to cables and to provide the power required by on-demand charging devices, making them more flexible and energy-efficient also it provides better durability for the product (such as dustproof and waterproof) for contact-free devices[5]. In last years, WPT systems were the favorite for charging technology which provides different power levels such as electric vehicles, mobile applications, laptop computers, tablets, and biomedical devices [6].

However, depending on different factors, WPT systems can be divided into different types, depending on the distance from the radiant source, the characteristics of the Electromagnetic (EM) fields change and the methods of wireless transmission. They can be classified to [7][8][9]:

1. Near-field
2. Far-field

This study focuses on near-field technology only, and far-field technology is beyond the scope of this research. The design of a near-field medium power WPT system is accomplished in this dissertation and several studies are performed on the coils and the circuit of the WPT system.

1.2 Literature review

The literature review on WPT system technology will include a conceptual context and a device description.

Nikola Tesla first presented the idea of WPT in the late 19th century. He managed to power 200 lamp bulbs from a distance of 40km, by constructing the Warden-Clyffe Tower that used to transfer electrical energy globally without using wire via the ionosphere [10].

In 1996 Zierhofer et al. presented their work illustrated that the system geometry is affected by the amount of coupling between two coupled coils, also the work showed how the distribution of the coil winding along their radii (planar or spiral coil) increases the coupling factor compared to the concentration of the coil on the outside of the coil [11].

In 2007, Prof. Soljagic with the research team at MTI presented a wireless power supply for a 60 W bulb using two coils with an air gap of 2-meter separate between the transmitter (Tx) and receiver (Rx) coils at rough efficiency 45% [12].

In 2011, Ram Rakhyani, et al. presented the Development and optimization of four-coil based on resonance systems and achieved performance that twice much as conventional two-coil WPT system. With coil diameters 64 mm for high-quality and 22 mm for low-quality coils, and an air gap distance of 20 mm, that achieved 82% power transfer efficiency with resonant frequency 700 kHz. using four-coil with high-quality-factor This research succeeds in decoupling the source and load resistance effects of Tx and Rx coils resulting in a significant efficiency enhancement [13].

In 2013, relay resonators used to increase the air gap between the transmitter and receiver for the WPT systems was investigated by W. Zhong,[14].

In the same year, M. V. Reddy has presented the concept of the WPT system, efficiency, and transmission and distribution losses. It has also been discussed the WPT technological development [15].

In 2016 Tommaso Campi presented a different type of compensation topologies SS (series-series) and LCC compensations which were examined and compared in terms of system efficiency, the system operating at the resonant frequency $f_r = 85 \text{ kHz}$ and transferring power of 1 kW, which has been investigated adopting two different compensation topologies: SS and LCC (inductance capacitor) compensations. The power efficiency is 95% for SS and 93% for LCC with a 20 cm air gap between Tx and Rx coils [16].

In 2017, Fuxin Liu¹ presented a double-frequency MCR (magnetic coupling resonant) wireless power transfer system which has two loads is comprehensively studied as a representative model. The proposed methodology was verified experimentally using two prototypes of the circuit configurations [17].

In 2018 Vincenzo Cirimele presented the analysis of the effects of the variation in Tx and Rx coils compared to the basic construction, in which the Tx and Rx coils have the same diameter. Three cases are considered using accurate electromagnetic modeling to examine the properties of the transmission and the induced losses in the body of the vehicle, with a gap between Tx and Rx coils of 200 mm, the power efficiency of 97.6% is achieved [18].

In the same year, Suhad H. Jasim presented four basic topologies for comparative analysis of wireless power transmission with inductive connection, allowing designers to select the most acceptable topology for the application requirements. The efficiency of the four topologies for power transmission series - series (SS), parallel - series (PS), parallel - parallel (PP), series-parallel (SP)) was derived. It has been concluded that SS is best suited for biomedical devices.[19].

In 2019, Masood Rehman presented the investigation of two basic topologies, i.e. SS and SP for symmetrical and asymmetrical coils. Both compensation topologies were theoretically analyzed and the topologies then modeled using two different combinations of circular coils. In the first case, two symmetrical coils were designed, in which the Tx and Rx coils had the same diameter, while in the second case the Tx coil was constructed with larger dimensions than the Rx coil. The overall result showed that the SP topology offers better efficiency if Tx is greater than Rx than the SS equivalent, while SS offers high efficiency if the Tx and Rx coils are symmetrical [20].

Also, in this year, M Fareq offered to study for manufacture WPT system using inductive coupling and provided information about the power efficiency of the system which was not influenced by the things that put between the Tx and Rx coils such as hands, books, and plastics types[21].

In 2020, Lihao Wu presented a WPT system. It has been built and tested a 1 kW prototype. The results of this experiment appeared that the power transfer was stable which achieved a constant transfer efficiency (96.1%) within a range of (100-200) mm air gap. The same transfer efficiency was obtained within the horizontal tolerance of 240mm at a 100 mm air gap, while at a 200 mm air gap within a horizontal tolerance of 100 mm [22].

In the same year, Seyit Ahmet Sis presented a WPT system efficiency analysis by introducing the harmonics of the voltage waveform of a typical inverter circuit into an analytical model of the WPT system for the first time. The simulation results showed that the total harmonic distortion (THD) of the source voltage waveform can be minimized by using a duty cycle of 75%. [23].

1.3 Aims of the study

Previously, there were many challenges faced by those who worked on the WPT system. Although these challenges remain, the constraints and problems are minimized every day due to ongoing research on the WPT system. This study aims at minimizing the limitations of the transmission of power wirelessly by contributing to various techniques which include the following:

1. Designing a WPT system using induction power transfer (IPT) topology that transfers about (100-250) Watt. The design procedures are based on the following:
 - Choosing the suitable transmitter circuit and analyzing it.
 - Choosing the suitable receiver circuit and analyzing it.
 - Designing the coupling coil.
 - Choosing suitable compensation elements.

2. Simulation of the designed WPT system using a computer program (MATLAB, ANSYS MAXWELL)
3. Validation of the simulation results by implementing the designed WPT system in the laboratory.

1.4 Layout of the dissertation

This study consists of five chapters:

- Chapter one presents an introduction and literature review.
- Chapter two explores the background and basic theories of the WPT system and its applications.
- Chapter three introduces the design details of a WPT system and coils design. The experimental results are also introduced in this chapter.
- Chapter four explores the implementation of the WPT system and coils.
- Chapter five gives the conclusions and some suggestions for future work.

CHAPTER TWO

BASICS THEORIES OF WPT SYSTEMS AND THEIR APPLICATIONS

CHAPTER TWO

BASICS THEORIES of WPT SYSTEM AND THEIR APPLICATIONS

2.1 Introduction:

In the inductive WPT system, the power is inductively transferred from the Tx to the Rx coil, as a result of mutual coupling between them. It is the same as the definition of a transformer. The main difference is that the coupling between the Tx and Rx coils is strong in a transformer, while the coupling is weak in a WPT system because of the large air gap or magnetic material between the Tx and Rx coils. Most WPT systems do not use ferrite or other magnetic materials, so the flux flows through the air. Such systems have reduced coupling, but on the other hand, they have no core losses. The large leakage of inductance on both coils transmitter (Tx) and receiver (Rx) is resulting due to the low coupling between them, and this also causes reducing the flux of magnetization. Thus, a greater current of magnetization is needed to increase the flux [24].

This chapter presents the basic theories of the WPT system the inductive coupling between the coils and the WPT system application.

2.2 Wireless power transmission technologies

Wireless power transmission WPT is a general term that describes the different technologies for power transmission using electromagnetic fields EM. These technologies vary in the range that can transfer power over, but all of them using time-varying electric fields. Fig.2.1 shows the classification of wireless Power Transmission technologies according to the distance of the power transmission [25].

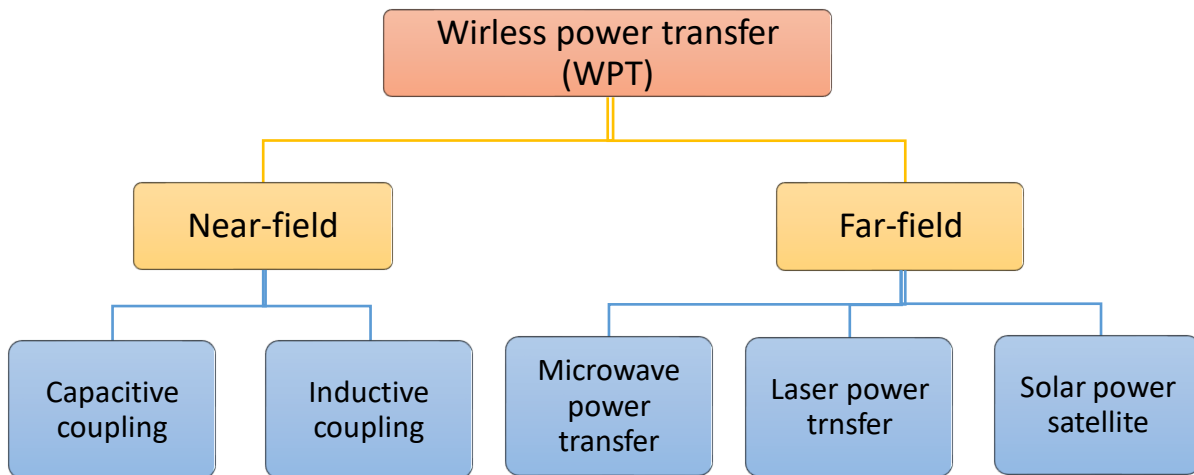


Fig. 2.1 Classification of wireless power transfer technologies.

The major difference between the near field and far field transmission is the transmission distance and the range of the frequency. When the electromagnetic field is resonant at a lower frequency from (20 kHz to 12.5 MHz) and the transmission distance is a few centimeters, in this case, the WPT system is part of the near-field power transfer. On the other hand, when the range of resonant frequency is in the (Gigahertz) and the transmission distance is longer, in this case, the WPT system falls in the far-field transfers, such as the transmission using the microwave[26][27]. In the far-field power transmission, the power decreases depending on the square of the distance between Tx and Rx, also The Rx antenna is not affected by the transmitted power unless it is coupled with the Tx antenna by the far-field technique [27][28]. The far-field power transmission is outside the scope of this research.

The efficiency of the power transfer in the near field technologies is mostly higher than the far-field technologies. The capacitive coupling depends in general on the available area of the device because of the plate's area of capacitance, as well as frequency, increases which increases the amount of the power transfer. Nevertheless, it is difficult to obtain sufficient power to charge a handheld mobile

electronic device[27]. However, the inductive coupling method is appropriate for short as well as mid-range distances which depend on the size and shape of the coils or antennas for transmitter Tx and receiver Rx and the resonant frequency[29].

2.3 The basic concept of the resonant inductive coupling WPT system

The theory of inductive coupling stems from the following concepts:

2.3.1 Maxwell's equations

Maxwell's equations refer that electromagnetic waves EM are propagated in a field depend on the relationships between the magnetic field, the electric field, space, and time. An antenna is used to transmit and receive radio waves. Theoretically, all electromagnetic waves can be used for WPT. The efficiency of WPT relies on the coupling coefficient, which also relies on the gap distance between the Tx and Rx coils. The Tx and Rx coils or resonators are electromagnetically mutual coupled for inductive coupling wireless power transfer and resonant coupling wireless power transfer systems. The electromagnetic phenomena can be describe using the following four of Maxwell's equations:

$$\nabla \times \mathbf{E} = -\frac{\partial \mathbf{B}}{\partial t} \quad (2-1)$$

Eq. (2-1) represents Faraday's induction law which is described by "the instantaneous electromotive force (emf) or voltage induced in a circuit due to changing magnetic field is directly proportional to the change of that magnetic field"[30].

$$\nabla \times \mathbf{H} = \mathbf{J} + \frac{\partial \mathbf{D}_e}{\partial t} \quad (2-2)$$

Eq. (2-2) represents Ampère's circuital law which is described by "a magnetic field is formed around a closed loop of a conductor or coil. when the current passes through it, the magnetic field produced by the current is proportional to the size of

that conductor or coil with a proportionality constant equivalent to the free space permeability" [30] [24].

$$\nabla \cdot \mathbf{D}_e = \rho_0 \quad (2-3)$$

Eq. (2-3) represents the Gauss' law Which is described by "the electric flux through any closed surface is proportional to the total electric charge enclosed by this surface" [24].

$$\nabla \cdot \mathbf{B} = 0 \quad (2-4)$$

Eq. (2-4) represents the Non-entity of Magnetic Charge [31]. Where E: the electric field (V/m), \mathbf{D}_e : the electric flux density (C/m²), \mathbf{H} : the magnetic field (A/m), $\mathbf{B} = \mu\mathbf{H}$: the magnetic flux density (T), J: the current density (A/m²), ρ_0 : charge density (C/m³), and μ : the magnetic permeability (H/m).

2.3.2 The resistance and the skin depth

The dc resistance (R_{dc}) is the wire resistance when the applied voltage is DC or low-frequency AC, it can be written as a relationship between the resistivity (ρ) of the wire length (l), and cross-section region (A) as given in Eq. (2-5).

$$R_{dc} = \frac{\rho l}{A} \quad (2-5)$$

As the frequency rises, the current which charges distribution in the conductor will change from a consistent spread throughout the whole conductor volume to a surface distribution only, this phenomenon is called the skin effect. Skin effect (depth) δ is the calculation of how the current distribution varies with frequency shifts [32].

Also, the skin depth is defined as "the depth from the conductor's outer surface to a point where the current density is reduced 1/e (i.e. about 37 %) of its value at the surface". Which can be calculated mathematically using Eq. (2-6)[33]:

$$\delta = \frac{1}{\sqrt{\pi f \mu_0}} \quad (2-6)$$

Where: μ_0 is the conductor's absolute magnetic permeability, f is the frequency of the current. The skin effect for the copper wire is shown in Fig.2.2 [33]. By using δ to find the actual conductor area value which the current passes through it, then substituting it in Eq. (2-5) to find R_{ac} .

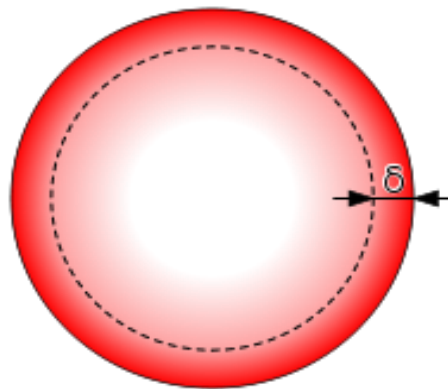


Fig. 2.2 Skin effect for the copper wire[33].

Skin depth δ is the length scale for the penetration currents and the fields inside the conductor [32].

2.3.3 Resonance

The electrical resonance happens in the electrical circuit at a certain frequency called resonant frequency (f_r). At that frequency, an imaginary part of the impedances and the admittances of the circuit are equal so they cancel each other. The resonance of a circuit containing capacitors and inductors happens because the inductor's contracting magnetic field produces an electrical current in its windings which charges the capacitor and when it discharging it creates an electrical current that builds the inductor's magnetic field. This process is continuously repeated, creating a resonant frequency [34]. The magnitude of the transfer function when the output is taken over the LCR series resistor R shown in Fig. 2.3 can be written by Eq. (2-7)

$$|H(\omega)| = \left| \frac{V_o(\omega)}{V_i(\omega)} \right| = \frac{R}{Z} = \frac{R}{\sqrt{R^2 + \left(\omega L - \frac{1}{\omega C}\right)^2}} = \frac{\omega CR}{\sqrt{\omega^2 C^2 R^2 + (\omega^2 LC - 1)^2}} \quad (2-7)$$

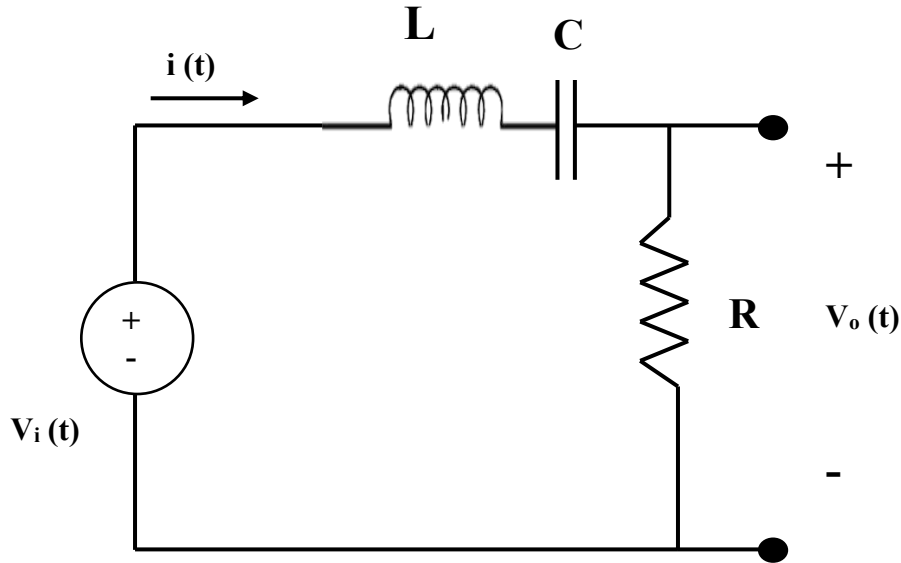


Fig. 2.3 An LCR series circuit

$$|H(\omega)| = 1 \text{ corresponds to } \omega^2 LC - 1 = 0 \text{ or equivalently to } \omega = \omega_0 = \frac{1}{\sqrt{LC}}.$$

The maximum output value of the transmission function or in other words the maximum output for voltage occurs when the circuit at the resonance frequency. The impedance Z of the LCR series circuit is shown in Eq. (2-8) [35]:

$$|Z| = \sqrt{R^2 + \left(\omega L - \frac{1}{\omega C}\right)^2} \quad (2-8)$$

The resonance peak of the two points at both sides is called half-power points, depending on that power drops to the (one half) of the resonance peak. The voltage drops through the resistor at these points is $\left(\frac{1}{\sqrt{2}}\right)$ times of the voltage drops through it at resonance peak. The bandwidth (BW) is the frequency separation between these two points.

$$\frac{1}{\sqrt{2}} = \frac{R}{\sqrt{R^2 + \left(\omega L - \frac{1}{\omega C}\right)^2}} \quad (2-9)$$

By Squaring both sides, to outcome Eq. (2-10).

$$\frac{1}{2} = \frac{R^2}{R^2 + (\omega L - \frac{1}{\omega C})^2} \quad (2-10)$$

By solving Eq. (2-10), the roots can be given in Eq. (2-11) & Eq. (2-12):

$$\omega_1 = -\frac{R}{2L} + \sqrt{\left(\frac{R}{2L}\right)^2 + \frac{1}{\omega_0^2}} \quad (2-11)$$

$$\omega_2 = \frac{R}{2L} + \sqrt{\left(\frac{R}{2L}\right)^2 + \frac{1}{\omega_0^2}} \quad (2-12)$$

Therefore, the bandwidth is given in Eq. (2-13):

$$B = \omega_2 - \omega_1 = \frac{R}{L} \quad (2-13)$$

As given in Eq. (2-13) the bandwidth B is in proportion to the resistance R of the circuit. Thus, the small values of R will be sharp at the resonance frequency.

By multiply two expressions ω_1 and ω_2 from above, it can be obtained:

$$\omega_0 = \sqrt{\omega_1 \omega_2} \quad (2-14)$$

That means for the LCR series circuit the resonance frequency is the geometric mean of a half-power frequencies. The most important characteristics of the series RLC circuit at resonant can be summarized by [34]:

- The capacitive reactance X_C and the inductive reactance X_L are equal.
- The total value of the impedance Z in the circuit will be minimum which is equal to resistance R.
- The current of the circuit will be the maximum value when the impedance is reduced.
- The voltage across the resistor equal to the supply voltage.

- The phase of the voltage and the current are the same making zero phase angle between them because the entire circuit is purely resistive and therefore the resultant reactance is zero.
- The power factor will be unity.
- The resonance frequency of the RLC series circuit is calculated by:

$$f_r = \frac{1}{2\pi\sqrt{LC}} \quad [\text{Hz}] \quad (2-15)$$

2.3.4 Quality factor (Q)

A coil's Q-factor is a measure of the inductor's energy-saving capability, it is an important parameter. In addition to its inductance, each coil has a small resistance. The lower the resistance R level, the higher the coil's efficiency or Q factor. This is mainly because a lower value of resistance R is lower power consumption and draws a very small current line. So, the obtained quality factor of the coil is a ration of the energy stored in the circuit proportional to the energy dissipated in the circuit as shown in Eq.(2-16) [27]:

$$Q = \frac{\text{Energy stored in the circuit}}{\text{Energy dissipated in the circuit}} \quad (2-16)$$

Therefore, at operating frequency (ω), the quality factor of a coil is described by the ratio between the reactance X_L and the resistance R of the coil as shown in Eq. (2-17) & Eq. (2-18):

$$Q = \frac{X_L}{R} \quad (2-17)$$

Then

$$Q = \frac{2\pi f_r L}{R} \quad (2-18)$$

The quality factor (Q) value can be from zero to infinity, with predicted values varying generally from 10 to 100. The quality factor (Q) relies primarily on the materials used as well as the size and shape of a coil[27][36].

2.3.5 Coupled resonators

If the two resonators were put close to each other having a mutual coupling between each other, that will increase the possibility of the resonator to transfer energy. This transferred energy has an efficiency that relies on the energy-coupling rate κ between the resonators as well as the characteristic parameters for each of them. Therefore, a couple can be used to describe the dynamics of these resonators system [37].

Fig.2.4 illustrates an equivalent circuit system of the coupled two-resonator which has a series resonant circuit.

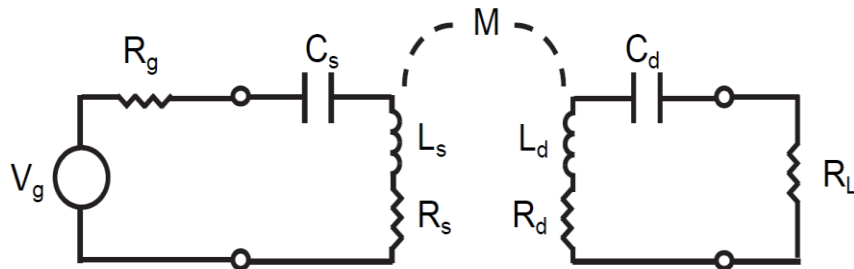


Fig. 2.4 An equivalent circuit of the coupled two-resonator system.

The above circuit has a generator that provides a sinusoidal voltage to the system with amplitude (V_g), frequency (ω) and has a resistance (R_g). While L_s is a source coil inductor and L_d is device coil inductor, and M is the mutual inductance coupling between these resonators, where:

$$M = k\sqrt{L_s L_d} \quad (2-19)$$

Each coil for the source and device has a capacitor in series to create a resonator, while the R_s and R_d represent the parasitic resistances (each has a

radiative loss and ohmic loss) of the coil and resonant capacitor for the respective resonators. The R_L represents the load resistance which equivalent to AC resistance [37].

2.3.6 Self-inductance

The isolated circuit was used to connect magnetic flux because the variation in current inside the circuit relies on the circuit's geometry. The current transition causes changes in the Flux Φ of a static stationary circuit [35].

$$\frac{d\Phi}{dt} = \frac{d\Phi}{dI} \frac{dI}{dt} \quad (2-20)$$

The ratio of Φ Flux change to a fixed stationary circuit is due to the current flux transfer to the current change called circuit self-inductance (L). Using induction faraday law for the Electromagnetic field, the fluctuation in current across the circuit (thus magnetic flux) will produce the voltage (emf) through it as follows:

$$\mathcal{E} = -\frac{d\Phi}{dt} = \frac{d\Phi}{dI} \frac{dI}{dt} = -L \frac{dI}{dt} \quad (2-21)$$

2.3.7 Coupling-factor (k)

The coupling factor (k) is a unitless value that determines a connection of any WPT system between the primary and secondary coils. The better power transfer efficiency is achieved when the coupling factor is higher by decrease the loss of the magnetic flux as well as lower the heating. Fig.2.5 shows two types of coupled circuits mode, the first one is tightly-coupled and the second one is loosely-coupled.

At the tightly-coupled circuit, the (Tx) coil and (Rx) coil are aligned to have the same diameter size, and the air gap between the two coils is less value than the diameter of the coils. This setup means that the receiver coil captures most of the magnetic flux to convert it into an electrical current.

While, in loosely coupled systems the distance between, the transmitter (Tx) and receiver (Rx) coils are more than coil diameter so that the magnetic flux will not be completely transmitted because the air gap between the transmitter coil (Tx) and receiver coil (Rx) is big or because the diameters of the coils do not match when the transmitter (Tx) coil is bigger than the receiver coil (Rx) [12].

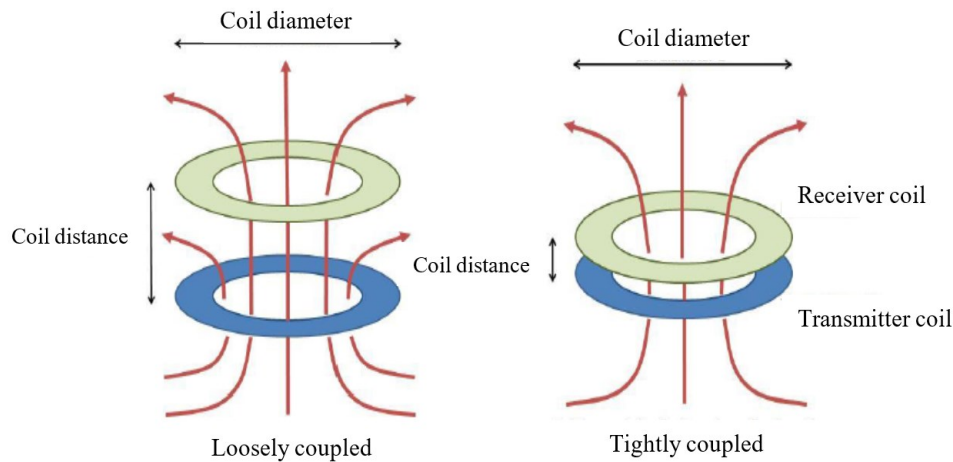


Fig. 2.5 Two types of coupled circuits mode [12].

Relying on the air gap between the transmitter (Tx) and receiver (Rx) coils, the magnetic flux produced at the Tx coil will not reach the Rx coil to contribute to the power transmission. The better mutual coupling means more flux received by the Rx coil [12].

2.4 Basic realization of resonant inductive WPT system:

Inductive power transfer includes the energy at the primary Tx coil generating a change in the magnetic field through the energy of the secondary Rx coil within the field. A circuit is designed with a small value of quality factor which is less than 10 due to the energy transmitted which diminishes very fast when chose a high value of the quality factor. the inductive charging is more usable and common for the low power portable devices because of the implementation facility, convenient operation, high efficiency in the small air gap, and guaranteed safety. Fig. 2.6 shows the general diagram for the IPT system [38][39].

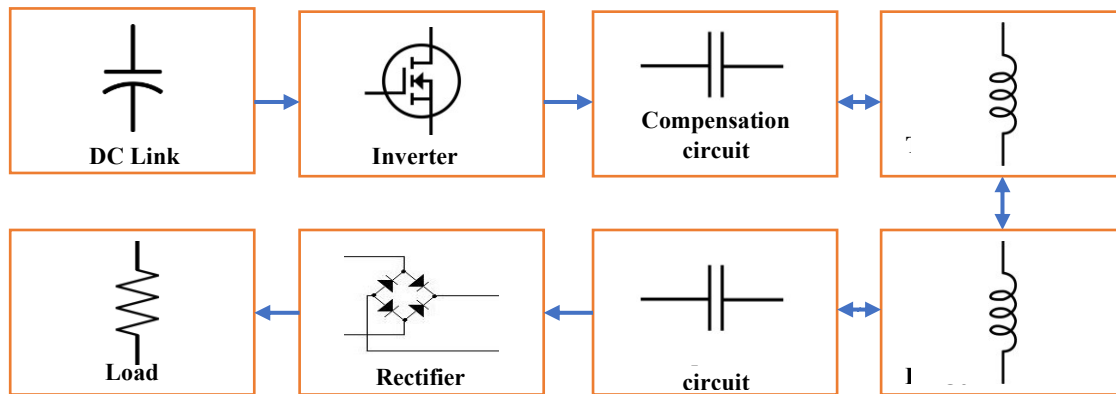


Fig. 2.6 General diagram of RIPT system.

The major components for the above IPT systems are explained as follows:

2.4.1 Inverter

The inverter (DC-AC) is the first stage located on the primary side of the WPT system and it is supplied by the DC voltage to generate the AC voltage whose frequency depends on the pulses that are applied on the gate of the CMOS. The alternating current generated in the output of the inverter flows into the primary Tx coil to cause a current to flow inside the secondary Rx coil [40].

2.4.1.1 Inverter topologies

To perform a DC to AC inverter stage, two different topologies are available: the first one can use a half-bridge inverter and the second one is a full-bridge inverter [41].

1. Half-bridge inverter

This kind of DC-AC inverter needs to use two types of electronic switches. It is often used for these purposes by the IGBT or MOSFET as a switch. Fig. 2.7 shows a half-bridge inverter circuit diagram. The DC source is equally split into two parts. Depending on the frequency of the gate pulses, the switch-on and switch-off times are determined and the output voltage is generated.

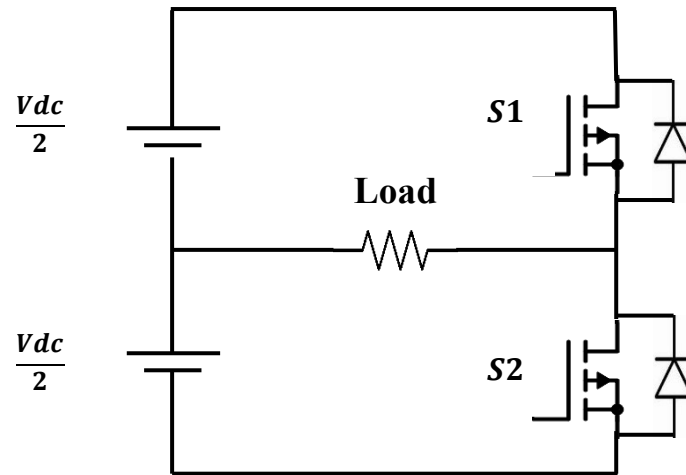


Fig. 2.7 DC to AC half-bridge inverter circuit.

In the first half cycle ($0 < t < T_1$) and during this period switch (S_1) is triggered (ON) and switch (S_2) is not triggered (OFF). In this period, the current will flow in the direction of the arrow as illustrated in Fig.2.8 (a) and the half-cycle of AC output is completed. The current flow from the load is right to left and the load voltage is equal to $(+V_{dc}/2)$. In the second half cycle ($T_1 < t < T_2$), and during this period the S_1 is not triggered (OFF), S_2 is triggered (ON) and the lower voltage source is connected with the load. The current flow from the load in the left to the right direction and load voltage is equal to $(-V_{dc}/2)$. In this period, the current will flow as illustrated in Fig.2.8 (b) and the other half cycle of AC output is completed.

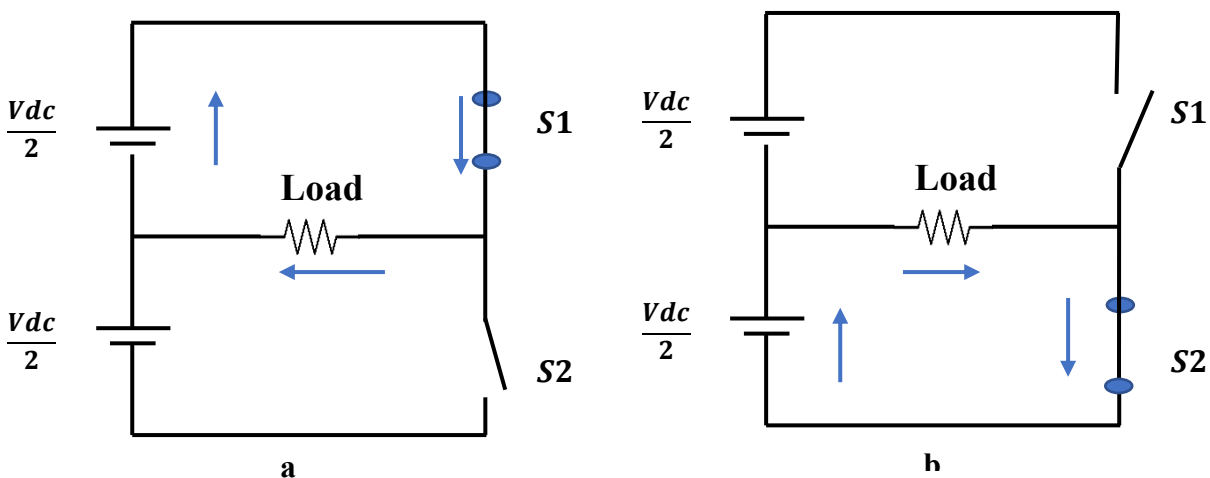


Fig. 2.8 Current direction flow in half-bridge inverter (a) for time period ($0 < t < T_1$) (b) for time period ($T_1 < t < T_2$).

The load voltage and switches current in the half-bridge inverter for the first and second periods are shown in Fig.2.9 [42][43][44].

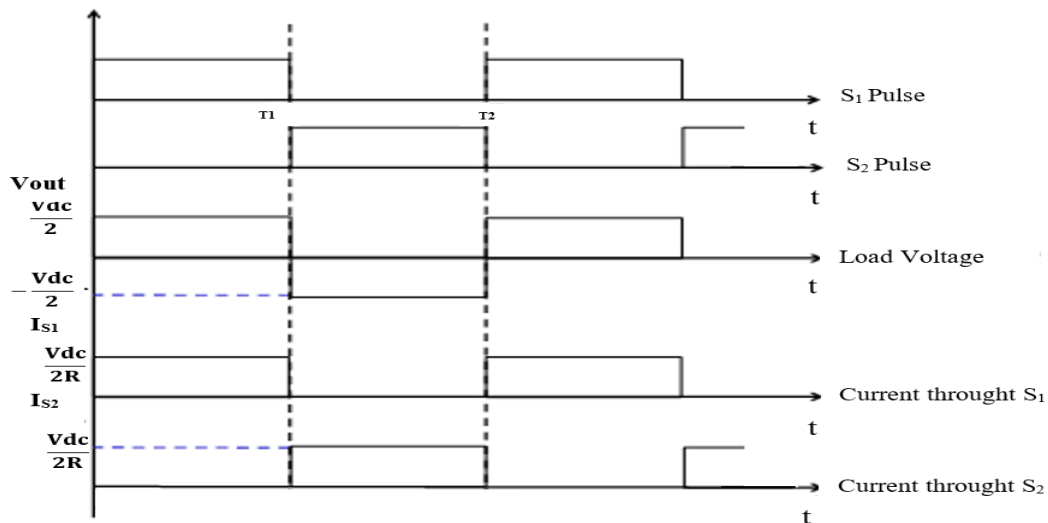


Fig. 2.9 Load voltage and switches current in the half-bridge inverter.

2. Full bridge inverter

Four switches are used in this type of inverter. The main difference between HB (half-bridge) and FB (full-bridge) inverter is the max. value of output voltage. In an HB inverter, the peak voltage is half of the DC input supply voltage, while in a FB inverter, the peak voltage is equal to the DC input supply voltage. Fig.2.10 illustrates the circuit diagram of a FB inverter. Both switches S_1 & S_2 operating at the same time and the gate pulse are the same, while both S_3 & S_4 switches are operating at the same time and they have the same gate pulses.

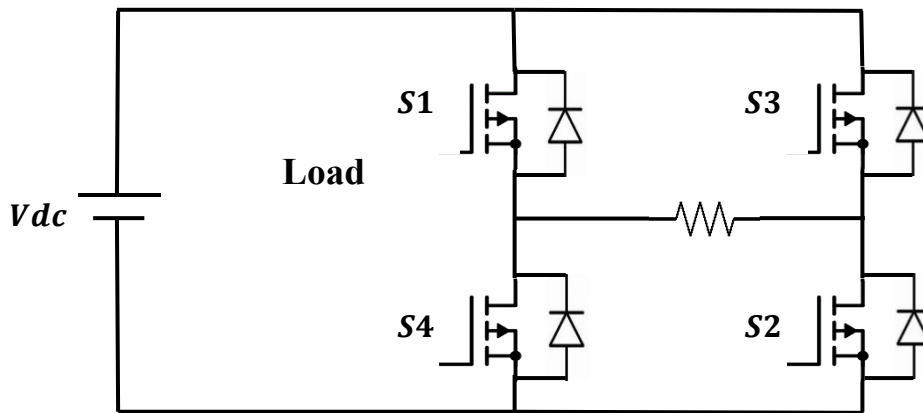


Fig. 2.10 Circuit diagram of the full-bridge inverter.

For the upper half cycle ($0 < t < T_1$), S_1 and S_2 get pulsed and the current will flow as illustrated in Fig. 2.11(a) below, in this period, the current flow from left to the right direction.

For the lower half cycle ($T_1 < t < T_2$), S_3 and S_4 get pulsed and the current will flow as illustrated in Fig. 2.11 (b). In this period, the current flow from right to left direction.

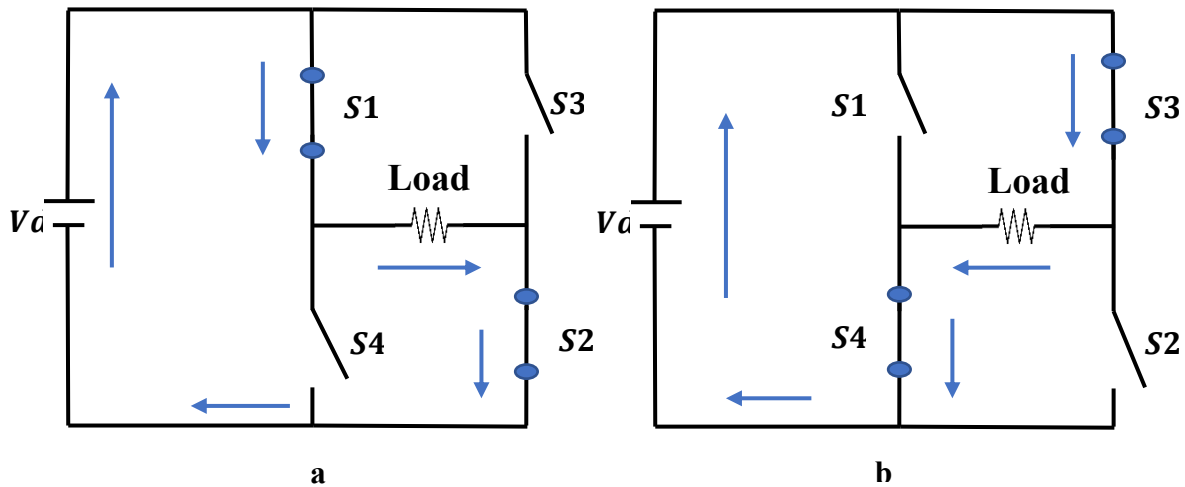


Fig. 2.11 Current flow for the period a. ($0 < t < T_1$). b. ($T_1 < t < T_2$).

The load voltage and current in the Full-bridge inverter for the first and second periods are shown in Fig.2.12 [42][43][44].

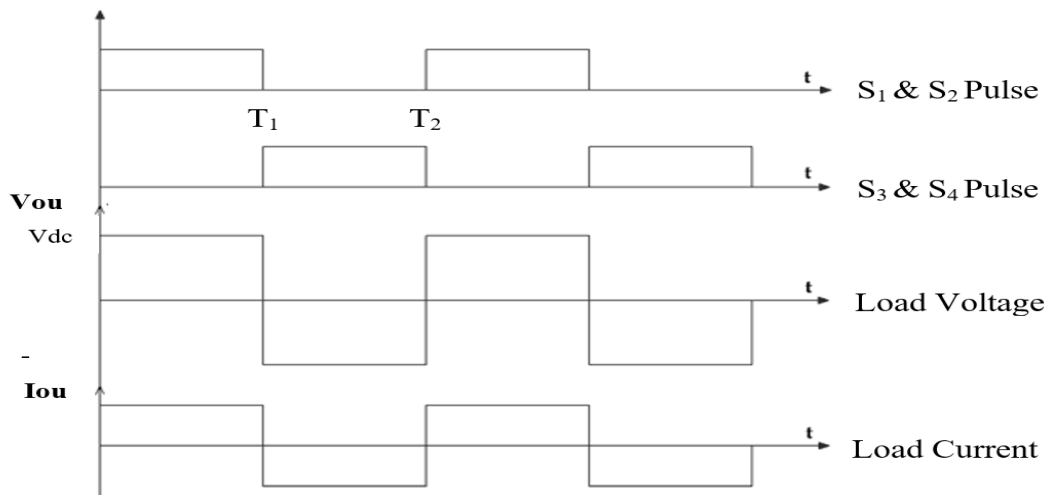


Fig. 2.12 Load voltage and current in the Full-bridge inverter.

2.4.1.2 Inverter switching device

In order to alternate the current direction and produce alternative power (AC) the switching device in inverters is needed, such as transistors and thyristors are used to perform switching.

Thyristors are work the same as mechanical switches (ON) & (OFF) mode which only has two modes to operate with it. It is used in basic models of inverters.

Transistors similar in switching capability to thyristors, but they instead respond to the voltage applied rather than current that has allowed to smoothly vary the transistor's internal resistance. So, in addition to ON and OFF functions.

There are two main types of transistors which is used in inverters:

- MOSFET: (Metal Oxide Semiconductor Field Effect Transistor).
- IGBT: (Insulated Gate Bipolar Transistor).

The MOSFET switching device type is suitable for operating at relatively low voltage, but the IGBT type withstands higher voltage and current. In this study, it has been used and compared between two types of MOSFET as a switching device:

- a. Silicon MOSFET
- b. Silicon Carbide MOSFET.

Silicon Carbide power devices have many important features over traditional Silicon devices [45]:

- Ultra-fast switching speeds.
- Lower switching losses.
- High-temperature operation.
- Low specific on-resistance.

2.4.2 Rectifier

A rectifier (AC-DC) stage that is located on the receiver side which required to convert voltage from high-frequency AC that comes from the inductive coils into DC voltage to supply the load.

Two types of AC-DC stage can be used in the WPT system depending on efficiency and controllability issues, passive and active rectifier. The passive-rectifier typically consists of a bridge of four conventional diodes, and this type of rectifier is used in this study[40][41]. The passive rectifier is illustrated in Fig.2.13 [46][47].

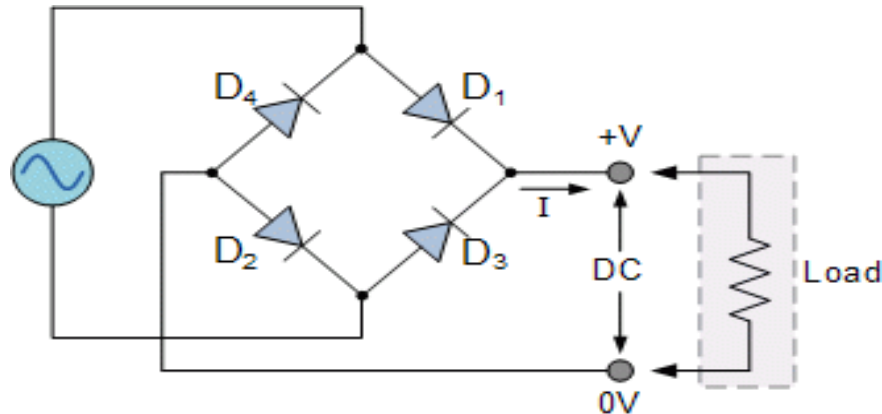


Fig. 2.13 Rectifier circuit with resistive load and capacitive output filter.

2.4.3 Compensation elements

A compensation circuit is required in order to maximize the efficiency of the power transfer from the source to the load. Since the coils are used as an inductive element to coupling the transmitter stage with the receiver stage, then the compensation elements which should be used are capacitors [48][49].

The compensation elements are connected in the transmitter stage (C1) and also in the receiver stage (C2). There are four types of compensation topologies according to the connection type between the coils and the compensation element, series-series (SS), series-parallel (SP), parallel-series (PS), and parallel-parallel (PP) as shown in Fig.2.14. The first word (letter) refers to the transmitter stage, while the second word refers to the receiver stage. The choosing of a certain topology rather than another depends on the particular application [50][51][52].

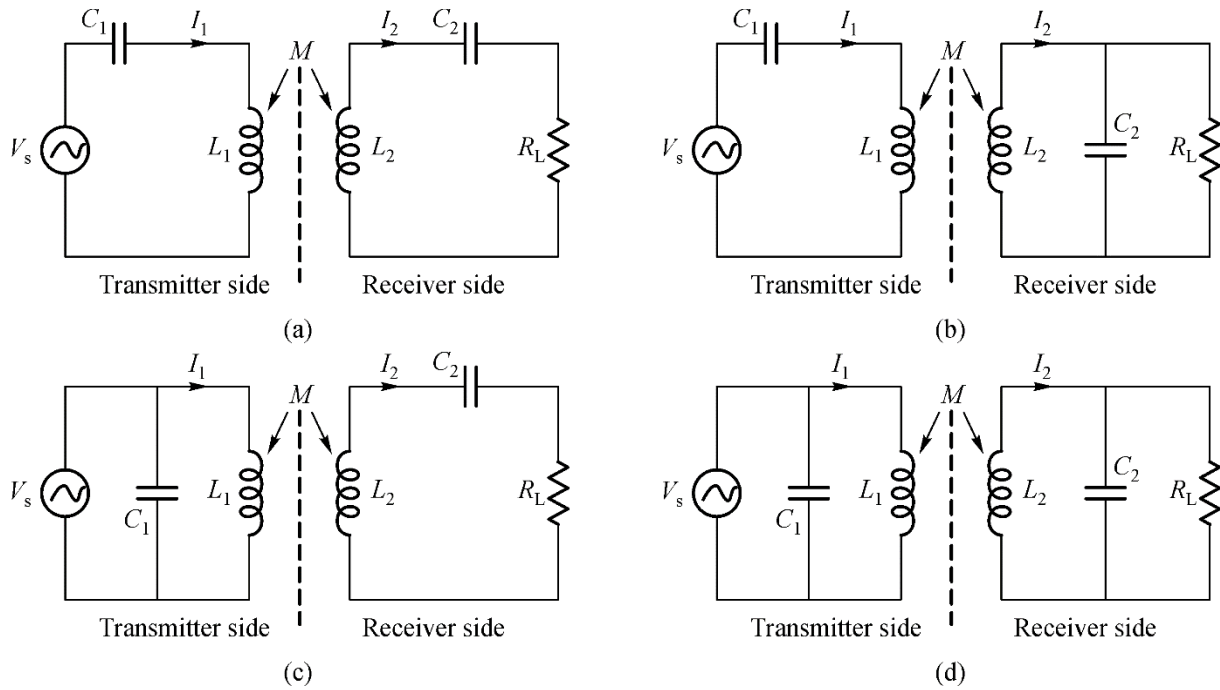


Fig. 2.14 The basic topologies: (a) SS, (b) SP, (c) PS, (d) PP.

The SS compensation topologies are depending only on the coil's self-inductance, regardless of what the load and the magnetically coupled link are. Therefore, the system is continuously operating in the resonant state in the case of misalignments between the transmitter and receiver coils [41].

2.5 Calculation of electrical parameters for the WPT system

The block diagram and components of the WPT system with the SS compensation element are illustrated in Fig. 2.15[33].

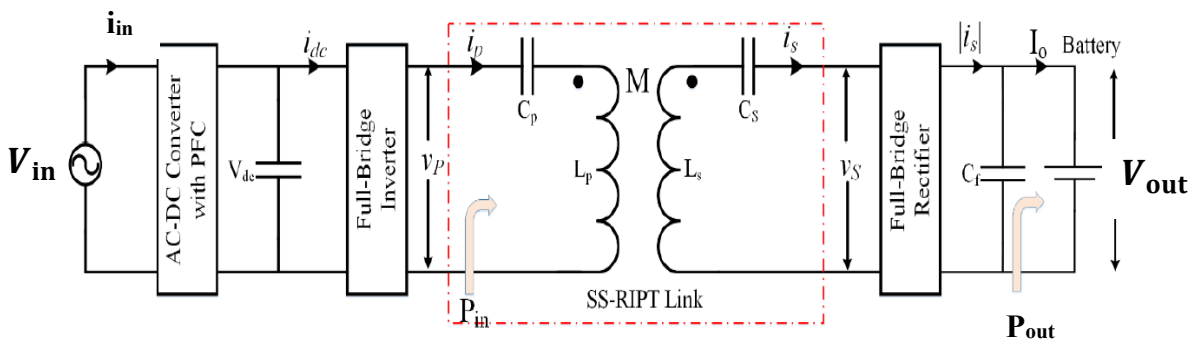


Fig. 2.15 WPT system with SS compensation elements[33].

The following presumptions are made to simplify the estimation of the WPT system parameters [33]:

- a) The WPT system efficiency is assumed to be 100% since the resistance value of the coil is unknown before making the link between the transmitter and receiver coils.
- b) The quality factor Q of the transmitter coils and the receiver coils are considered in order to receive primary and secondary currents that differ sinusoidally therefore only the first harmonic component (fundamental) of the voltage of the input V_p and output V_s of the WPT system is considered.
- c) All converter devices are assumed to be 100% efficient.
- d) The resonance in the transmitter and receiver stage is assumed to be ideal.

Let the needed power in the output be (P_o). Since the load side is a battery, then the defined by the manufacturer of the battery pack is the charging voltage. Then it can be represented the battery by a (DC) resistance R_{LB} as:

$$R_{LB} = \frac{V_{out}^2}{P_{out}} \quad (2-22)$$

According to [53] and [54], the equivalent resistance of a load, diode rectifier, and output filter capacitive can be given by Eq. (2-23). This resistance is seen on the receiver side of the WPT system.

$$R_L = \frac{8V_{out}^2}{\pi^2 P_{out}} \quad (2-23)$$

The v_s (secondary voltage) is a square wave because of the output capacitive filter. The value of the fundamental component of v_s (RMS) can be given by Eq. (2-24). And the I_S RMS (secondary current) value can be given by Eq. (2-25):

$$V_{Srms} = 2\sqrt{2} \frac{V_{out}}{\pi} \quad (2-24)$$

$$I_{Srms} = \frac{V_{Srms}}{R_L} \quad (2-25)$$

By using the above assumption (1), $P_{out} = P_{in}$ and since it has been assumed that $V_p = V_{in}$ (input applied voltage), then the value of the current in the primary side (RMS) can be given by Eq. (2-26) for a full-bridge inverter:

$$I_{Prms} = \frac{P_{in}}{V_{Prms}} \quad (2-26)$$

The mutual inductance (M) between the transmitter and receiver coils and the amount of power output from the system can be derived using (KVL) equation on the receiver side of the WPT system.

Eq. (2-11) is used to calculate the resonant frequency value of the system, and using the receiver coil inductance for calculation of the quality factor of the receiver coils Q_s . The value of Q_s should be selected between (2-10) as a higher value for lower harmonics in the waveform of the current and voltage. The value of the receiver coil can be given by Eq. (2-27) [33]:

$$L_{Rx} = \frac{Q_{Rx} * R_L}{\omega_r} \quad (2-27)$$

The coupling factor (k) can be obtained using Eq. (2-28):

$$k < \frac{1}{Q_s} \sqrt{1 - \frac{1}{4Q_s^2}} \quad (2-28)$$

Using Eq. (2-28) it can be decided the min. air-gap between the transmitter and the receiver coils, and also the max. value of k (coupling factor) coefficient. Once the value of the coupling factor is found, the transmitter coil inductance can be calculated using Eq. (2-29) and Eq. (2-30) [33]:

$$M = \frac{I_{Srms} * R_L}{I_{Prms} * \omega_r} \quad (2-29)$$

$$L_{Tx} = \frac{M^2}{L_{Tx} k^2} \quad (2-30)$$

Then after the above calculation of the parameters of the WPT system, the physical building of the coils will be started[33].

2.6 The main point that must be observed in WPT systems

The main point that must be observed in the WPT systems:

2.6.1 The efficiency of the transfer power

The most important technological issue for WPT systems is maximum power transfer efficiency. Fig.2.16 illustrates various system power efficiency along the transmission path. In previous studies, several works have been reported to improve the system efficiency, such as coils design and compensation circuit topologies, and the power control [55].

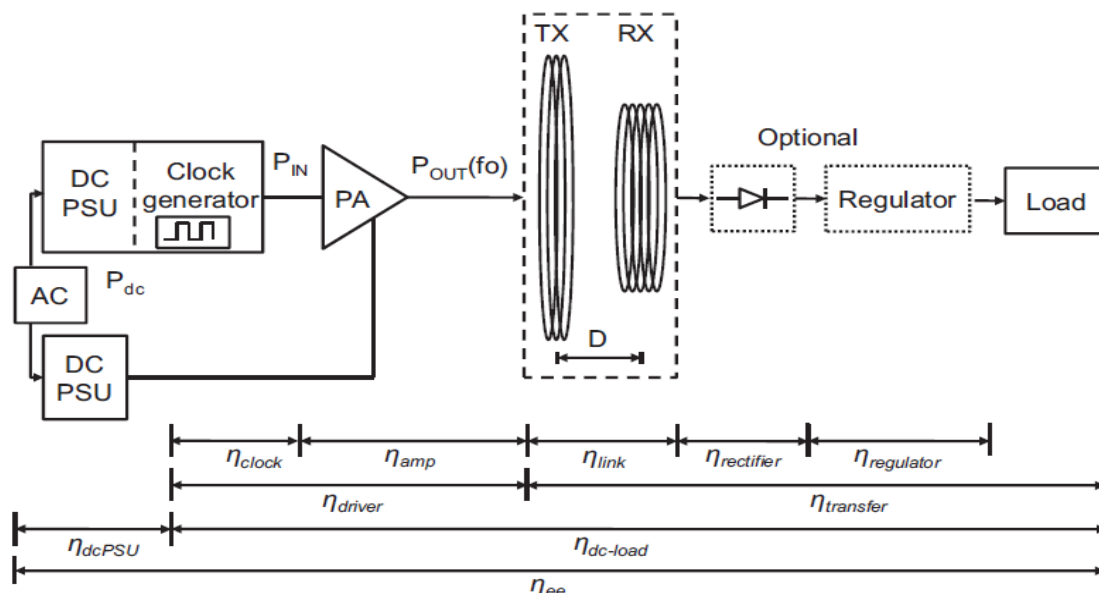


Fig. 2.16 IPT systems architecture [55].

2.6.2 Transmission power

One of the most important performance indexes for power WPT systems is the transmitted power capability. The power level is limited by the switching device because the WPT system is working at a relatively high-frequency[3].

2.6.3 Transmission distance

Is the air gap (distance) between the transmitter (Tx) and receiver (Rx) coils [56].

2.6.4 Displacement flexibility

The WPT system is very sensitive to alignments and the relative location between the coils of the transmitting (Tx) and receiving (Rx), In other words, the system efficiency deteriorates concerning a lateral or angular misalignment as illustrated in Fig.2.17 [57].

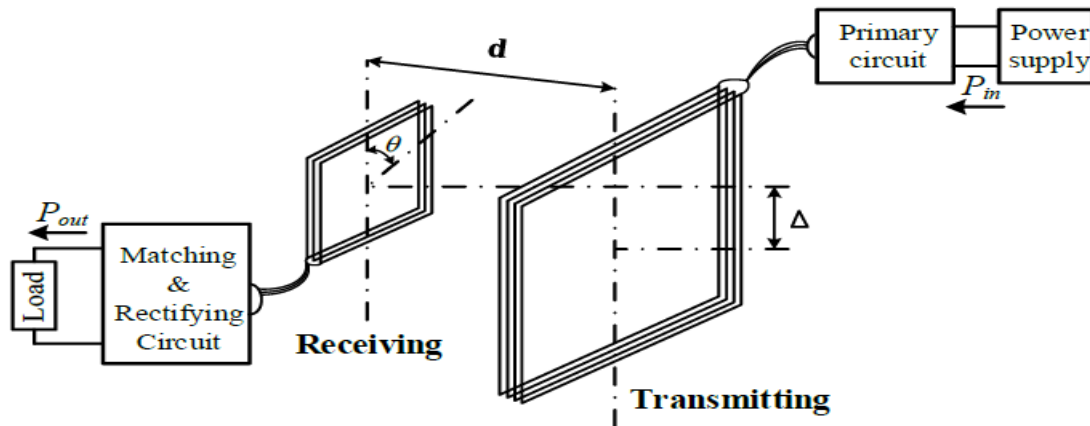


Fig. 2.17 Misalignment of WPT systems [57].

2.7 WPT system benefits and applications

There are many reasons for using resonant WPT system technology in many of the power transmission and charging devices, which mostly fall into one or more of the categories below[58]:

1. Removing the need for a power cable or battery replacement, so it makes the devices more compact and thus more suitable for consumers.
2. More safety for the power transfer devices to work in wet places.
3. Spatial freedom between the power source and the device.
4. Allows for the charging of multiple devices in order to reduce system costs.
5. High charging speeds.
6. It is possible to use it to charge vehicles and robots during their movement, which provides an increase in working time and service.

CHAPTER THREE

DESIGN AND SIMULATION OF RESONANT WPT SYSTEM

CHAPTER THREE

DESIGN AND SIMULATION OF RESONANT WPT SYSTEM

3.1 Introduction

In this chapter the ANSYS MAXWELL software is used to design the coils and evaluate the coils parameter such as inductance (L), DC resistance, mutual between two coils, magnetic flux, etc., and also ANSYS Simpler software can be used to evaluate the power transfer efficiency between two coils. The whole resonant IPT system has been designed and simulated using MATLAB software to study the performance of the designed system. WPT system with 250-watt power transfer is proposed in this chapter

3.2 Coils design

The spiral coil is a very common structure in the wireless transmission system because of its compact dimensions and very limited electromagnetic field characteristics. In this section, spiral coils are designed, simulated and some of their properties are studied.

3.2.1 Simulation of an inductive coil

Initially, a premade coil for cooking applications is adapted to the implementation of the WPT system, since the Litz wire used in the implementation of the WPT system coils was not available in the local markets. The simulation tool of the “ANSYS MAXWELL” software is used in order to determine the self-inductance for the Tx coil (L_{Tx}) and Rx coil (L_{Rx}), mutual (M) between two similar coils, and the coupling factor (k). The parameters of design are listed in Table 3.1. The geometry of the transmitter (Tx) and receiver (Rx) coils are illustrated in Fig.3.1.

The two coils are excited with a current value equal to (1A) to obtain the self-inductance (L) and the mutuality between the transmitter and receiver coils (M).

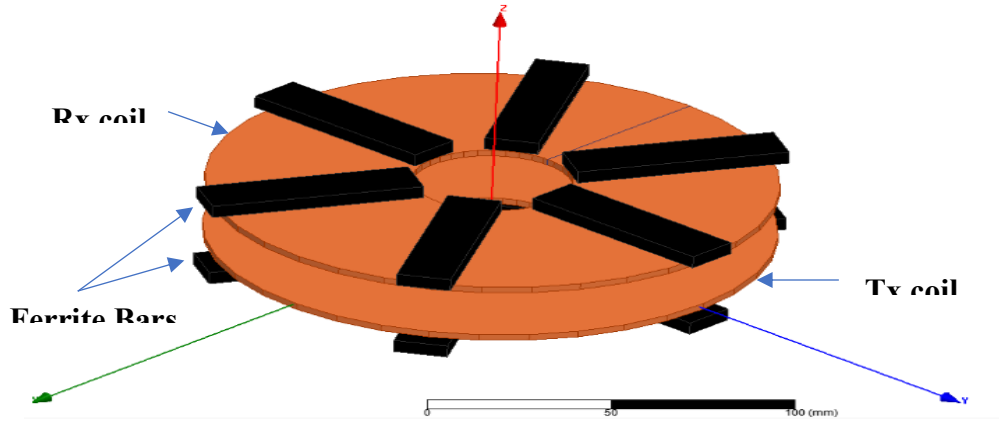


Fig. 3.1 The geometry of the two coils Tx and Rx.

Table 3.1 Tx and Rx coils parameter.

| Parameter | Value |
|----------------------------------|--------------------|
| Wire radius (r) | 0.8625 mm |
| Coil's inner radius (r_{in}) | 37.2 mm |
| The gap between turns (d) | 1 mm |
| Number of turns (N) | 28 |
| Ferrite Bar | 8 Bar (60*15*5) mm |

The simulation results of the two coils with different air-gap (D) are listed in Table 3.2, which is created using a magnetic solver in MAXWELL software.

Table 3.2 Simulation results of Tx and Rx.

| D [mm] | L_{Tx} [μ H] | L_{Rx} [μ H] | k | M [μ H] |
|----------|---------------------|---------------------|-------|----------------|
| 30 | 104.1 | 106.8 | 0.449 | 47.42 |
| 40 | 100.7 | 103.6 | 0.324 | 33.15 |
| 50 | 99.2 | 102 | 0.233 | 23.46 |
| 60 | 98.4 | 101.3 | 0.167 | 16.75 |
| 70 | 98.1 | 100.9 | 0.12 | 12 |

The field distribution of the Tx and Rx coils shown in Fig.3.2, that the field concentration in the central axis between the two coils is a result of the presence of the ferrites bar in transmitter and receiver coils.

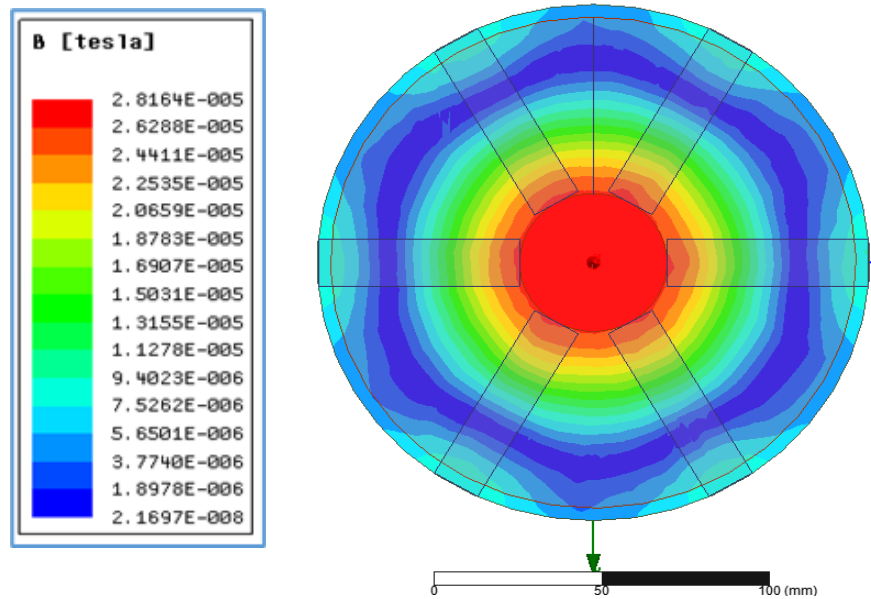


Fig. 3.2 Transmitter and receiver coils filed distribution.

3.2.2 Design and simulation of a specific coil for the WPT system

The first step in building a WPT system is to design and select the appropriate transmitter and receiver coils to deliver the required power as well as determine the distance required to transmit this power. Table 3.3 summarizes the assumed values as are necessary for some of the variables used to design the coils. It is worth mentioning that a Litz wire of 5x5x42/38DN is used to construct these coils.

Table 3.3 Assumed value for WPT system

| Power | V_{in} | V_{out} | R_L |
|-------|----------|-----------|------------|
| 250 W | 42 V | 114 V | 7 Ω |

Where V_{in} is the WPT system input voltage with the half-bridge inverter, V_{out} is the output voltage of the system, and R_L is the load value. Under these conditions, the values of L_{Rx} , L_{Tx} and M is calculated as mention in chapter two Eq (2-23) - (2-30).

Then the value of L_{Rx} and $L_{Tx} = 67.4 \mu\text{H}$. Then these values have been designed in MAXWELL using the same previous procedure. The coils parameters are shown in Table 3.4

Table 3.4 Circular Litz wire coils parameters.

| Parameter | Value |
|--------------------------------|----------|
| Wire radius (r) | 1.715 mm |
| Coil inner radius (r_{in}) | 37.5 mm |
| The gap between turns (d) | 1 mm |
| Number of turns (N) | 21 |

The geometry of the transmitter and receiver coils are illustrated in Fig. 3.3

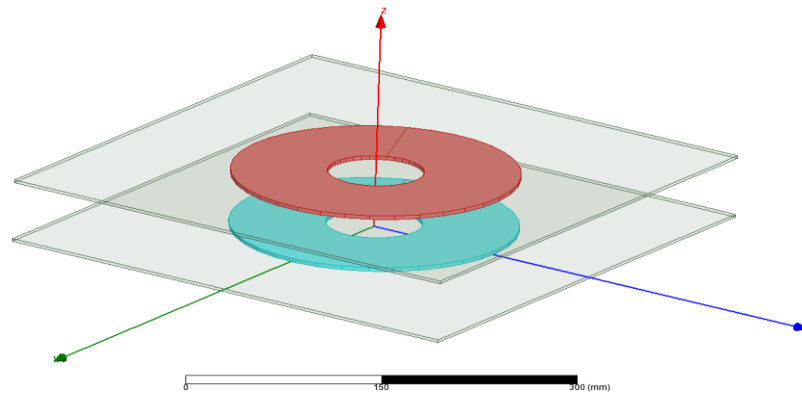


Fig. 3.3 Circular Litz wire coils simulation.

The simulation results of different air-gap and using the magnetic solver in MAXWELL software are shown in Table 3.5. These results involve the self-inductance of the transmitter and receiver coils, coupling factor, and the mutual (M) inductance.

Table 3.5 The circular Litz wire coils simulation results.

| D [mm] | L_{Tx} [μH] | L_{Rx} [μH] | k | M [μH] |
|--------|----------------------------|----------------------------|-------|---------------------|
| 30 | 67.4 | 67.5 | 0.524 | 35.37 |
| 40 | 67.5 | 67.6 | 0.427 | 28.89 |
| 50 | 67.4 | 67.6 | 0.352 | 23.82 |
| 60 | 67.4 | 67.6 | 0.292 | 19.76 |
| 70 | 67.5 | 67.5 | 0.244 | 16.5 |
| 80 | 67.5 | 67.7 | 0.205 | 13.89 |
| 90 | 67.3 | 67.4 | 0.173 | 11.72 |

Fig. 3.4 shows the relationship between the coupling factor, the mutual, and the air gap distances between Rx and Tx.

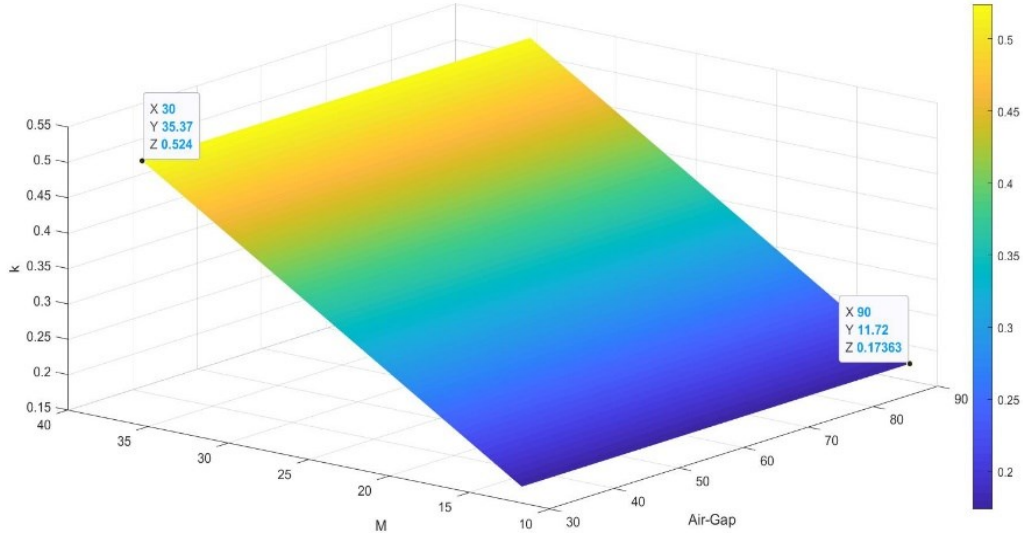


Fig. 3.4 Variation of the coupling factor and mutual factor with various air-gap between Rx and Tx.

The filed distribution of the designed Tx and Rx coils are shown in Fig.3.5.

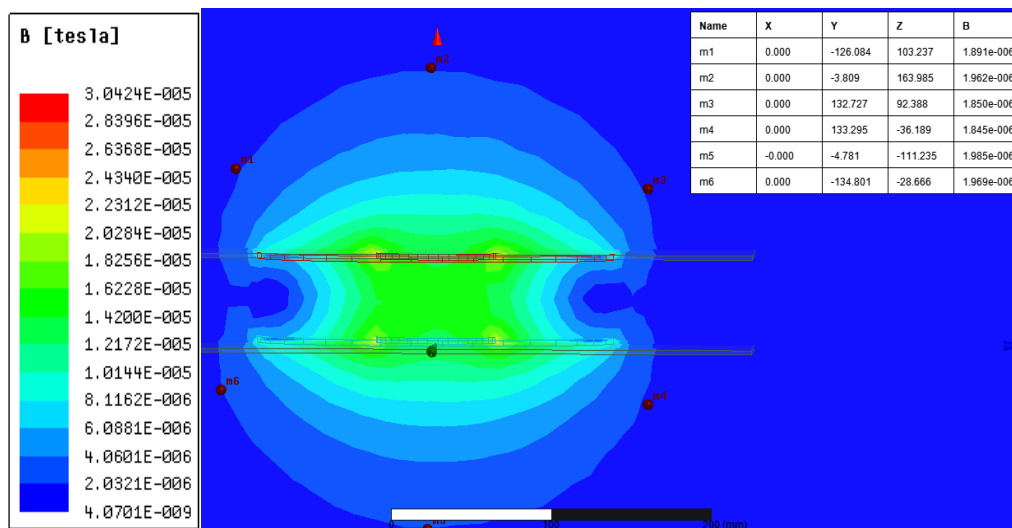


Fig. 3.5 The circular Litz wire Tx and Rx coils filed distribution.

3.2.2.1 Calculation of the skin effect and R_{ac}

The round conductor skin depth is given by Eq(2-2), the value of resonant frequency is chosen ($f_r = 40000$ Hz) and the mobility of the copper ($\mu = 4\pi \times 10^{-8}$ $\Omega\text{-m}$) also the resistivity is ($\rho = 1.72 \times 10^{-7}$ $\Omega\text{-m}$) at 20°C and ($\rho = 2.3 \times 10^{-7}$ $\Omega\text{-m}$) at 100°C . by substituting all these values in the above Eq. the value of the skin depth is (0.33 mm). Then calculating the AC resistance (R_{ac}) of the coil using Eq. (2-5) where $l = 10\text{m}$, A is the cross-section area of the wire that can be calculated by Eq. (3-1):

$$A = \pi * r^2 \quad (3-1)$$

Where r is the wire radius of the coil $r = 1.715$ mm.

To calculate the R_{ac} the actual area A_n , where the current passes as a result of skin effect can be found by Eq. (3-2):

$$A_n = A - A_f \quad (3-2)$$

Where A_f is the inner area of the wire that no current passes through it, and it is calculated using Eq. (3-3).

$$A_f = \pi * r_f^2 \quad (3-3)$$

Where r_f is the radius of the inner cross-section of the wire that no current passes is calculated by Eq.3.4:

$$r_f = r - \delta \quad (3-4)$$

By applied the above equations to find the R_{ac} as shown in Table 3.6.

Table 3.6 The calculation of R_{ac} .

| r_f [mm] | A_f [mm^2] | A [mm^2] | A_n [mm^2] | R_{ac} [$\text{m}\Omega$] |
|------------|-------------------------|-----------------------|-------------------------|-------------------------------|
| 1.385 | 6.02 | 9.24 | 3.22 | 64 |

3.3 The design considerations of the induction coils for the WPT system

In this section, some studies are investigated that related to the coil's design parameter such as the coupling factor between two coils, self-inductance (L) of each transmitter and receiver coils, and the geometry of the coil such as the gap between coils turns, wire diameter ...etc. as shown in Fig.3.6.

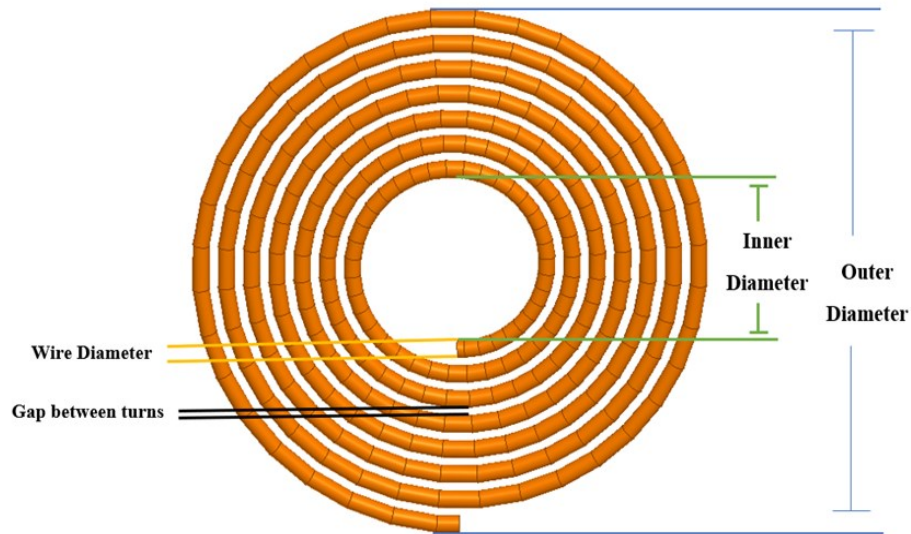


Fig. 3.6 Circular coils geometry.

3.3.1 The effect of changing the diameter of the wire on the coil parameters

A simulation process is applied to clarify the effect of changing the diameter of the wire (d) on the coil parameters.

The simulation process is completed for coils with an inner radius $r_{in} = 40\text{mm}$ to get the same coupling factor $k = 0.526$ at air-gap $D = 30\text{mm}$ between the transmitter (Tx) and receiver (Rx) coils and then changing the coil wire diameter for each coil every time to get the same coupling factor.

As the simulation results are shown in Fig 3.7, that when the wire diameter of the circular coils is increased while keeping the same coupling factor between the transmitter (Tx) and the receiver (Rx) coils, the turns number, wire length (l), and self-inductance (L) of the coils are decreased, but the volume and the weight of the coils are increased.

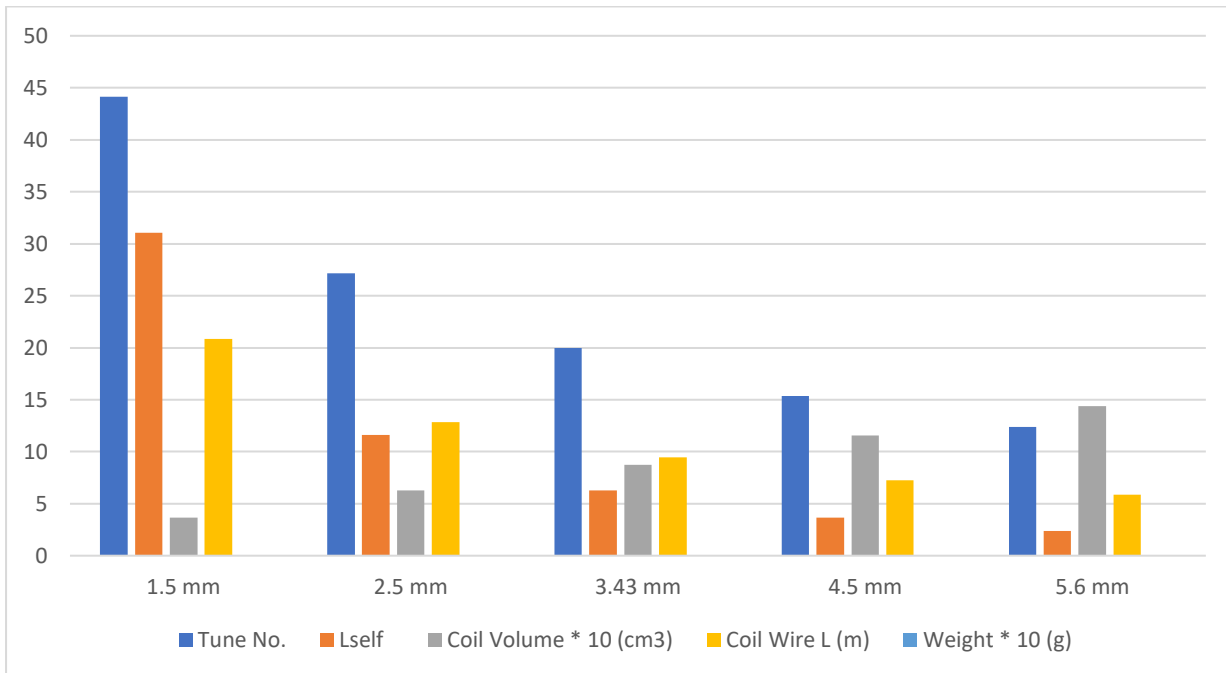


Fig. 3.7 The effect of changing the diameter of the wire on the coils turns number, wire length l , volume, and weight while keeping the same k between the coils.

3.3.2 The effect of changing the coil's inner radius on its parameters

A simulation process is applied to clarify the effect of changing the coil's inner radius r_{in} on the coupling factor between two symmetrical circular coils and the number of turns, using a fixed coil's wire length $l = 7.81m$, and $d = 3.43mm$.

The simulation results show in Fig 3.8 that when the coil's inner diameter of the transmitter (Tx) and receiver (Rx) coils is increased, the coupling factor (k) and the r_{out} are also increasing. But the number of turns is decreasing, and also the self-inductance (L) of the transmitter (Tx) and receiver (Rx) are slightly less. For example when the r_{in} increases by 100 percent the coupling factor increased by 1 percent and the number of turns decreased by 39 percent.

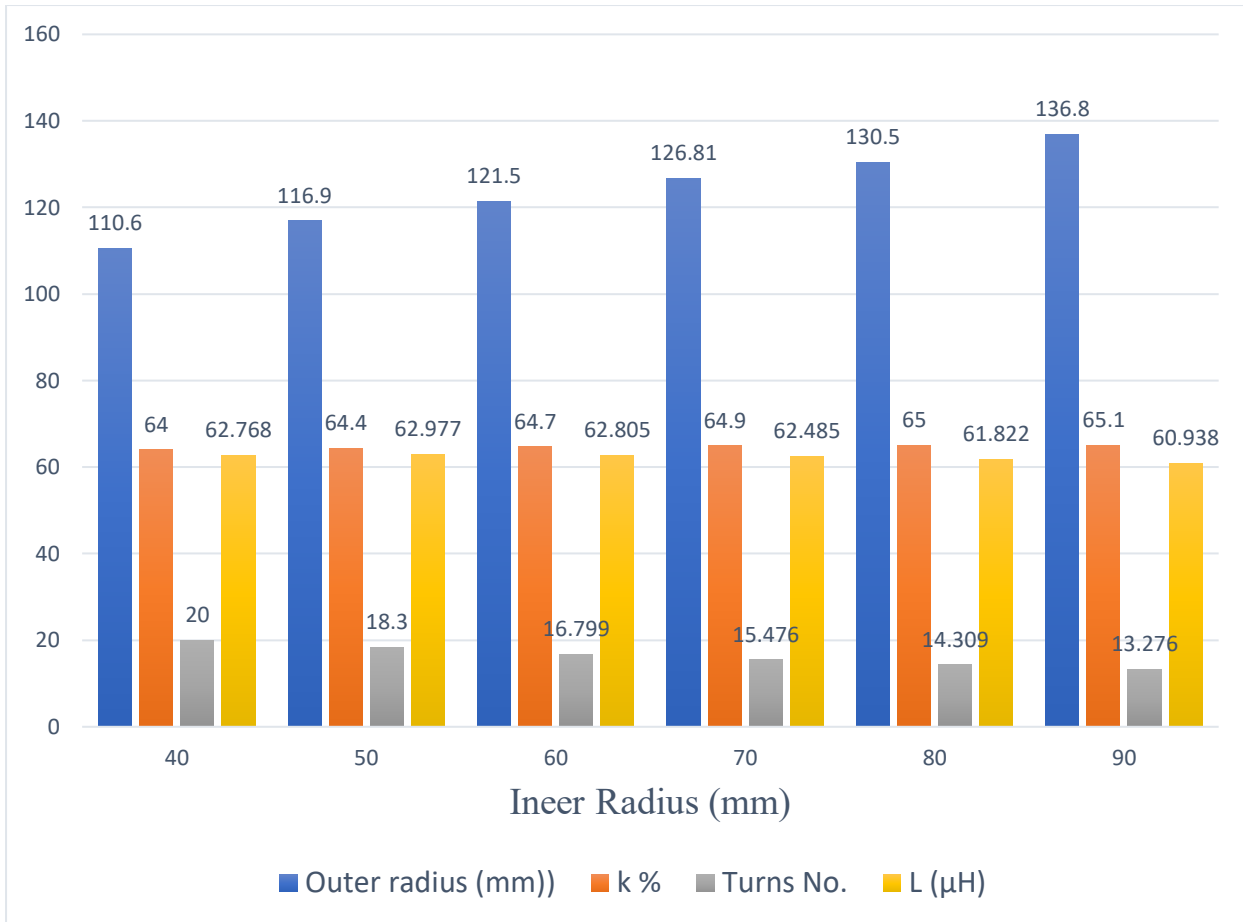


Fig. 3.8 The effect of changing r_{in} on the coupling factor, outer radius, number of turns, and coils self-inductance.

3.3.3 The effect of changing the gap between the turns on the coil's parameters

A simulation process is applied to illustrate the effect of changing the gap between the turns on the coupling factor between two circular symmetrical coils and the number of turns with a fixed wire length of the coils $l = 7.81m$ and $r = 3.43mm$. The experiment is done for coils with an inner radius $r_{in} = 40mm$, $d = 3.43 mm$, and $D = 40mm$ between the transmitter (Tx) and receiver (Rx) coils.

The simulation results show in Fig 3.9 that when the gap between turns of each Tx and Rx coils increased, the coupling factor is also increased, but the self-inductance and the coil's turns number are decreased.

For example, when the gap between the turn increase to 2.4 mm increases the coupling factor increased by 6.4 percent and the number of turns decreased by 27 percent.

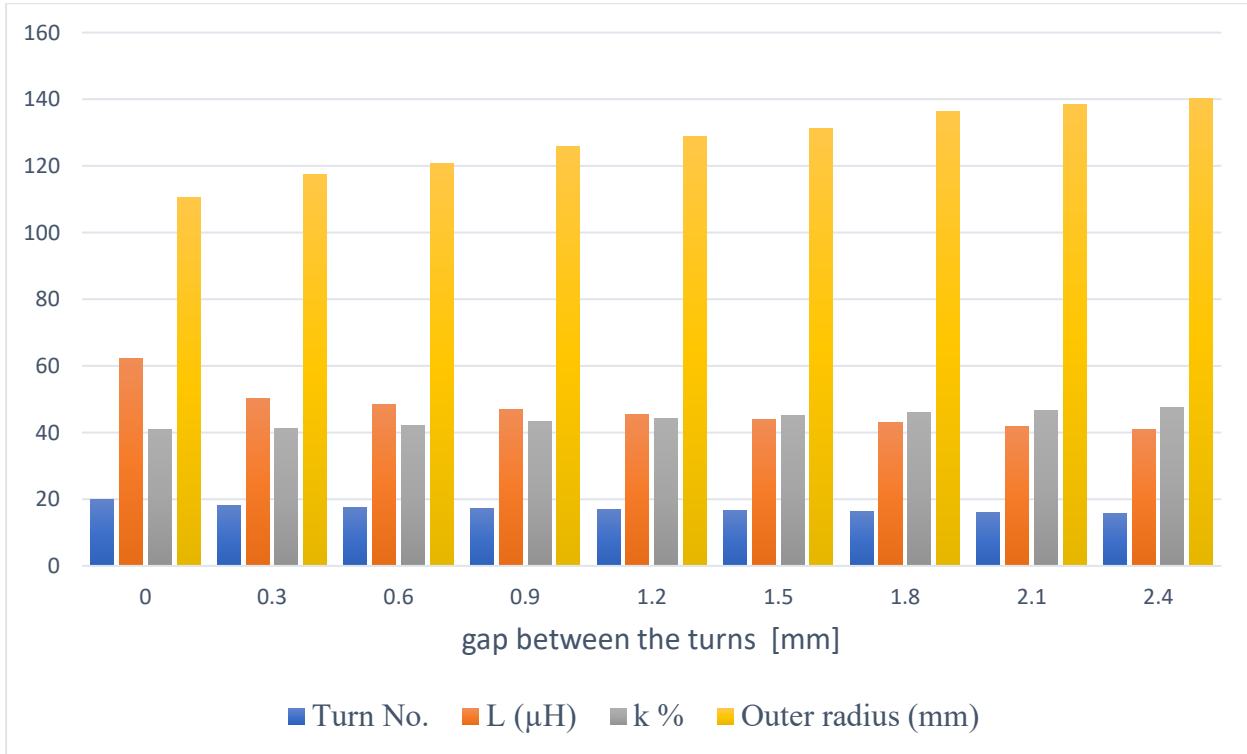


Fig. 3.9 The effect of changing the gap between the turns on the coupling factors between the transmitter and receiver circular coils, self-inductance, and the coils turns number.

3.3.4 The effect of changing the coil's shape and alignment coupling factor

A simulation process is applied to explain the effect of changing the coil's shape and alignment on the coupling factor between two symmetrical coils with a fixed coil wire length $l = 7.81 m$, and $d = 3.43mm$. The experiment is done for coils with an inner radius $r_{in} = 40mm$ and $D = 40mm$ between the transmitter (Tx) and receiver (Rx) coils.

The simulation results are illustrated in Fig 3.10 that the coils circular shape gives the best k than the other shape in all alignment percentage.

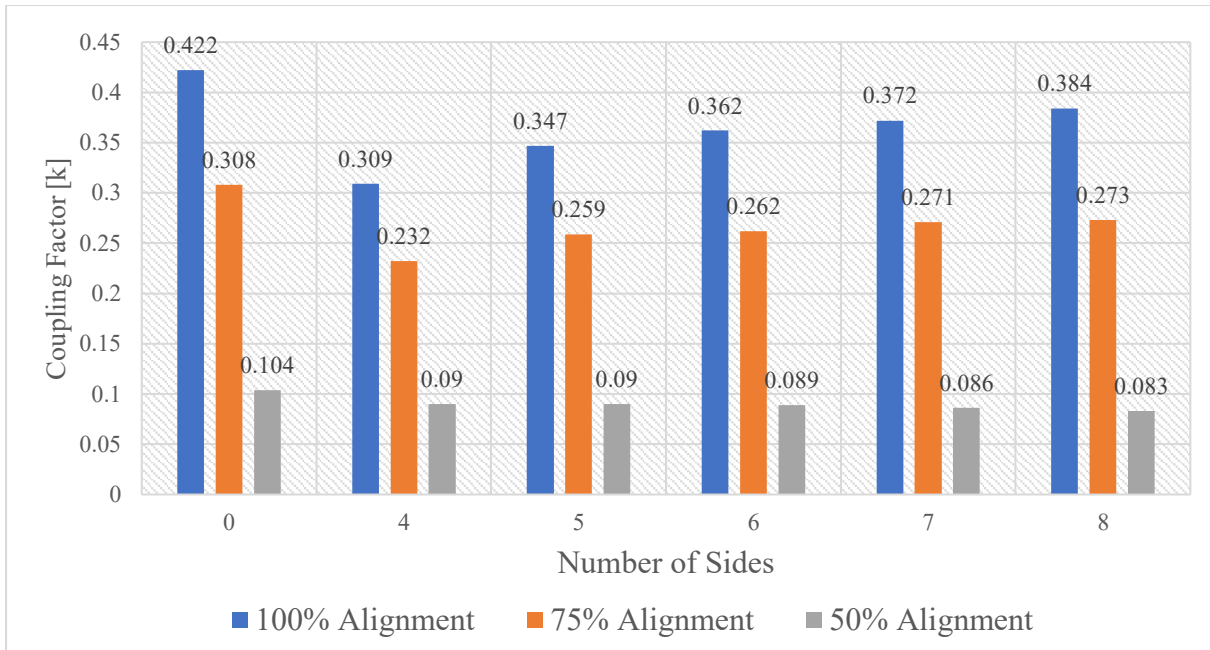


Fig. 3.10 Effect of changing the coil's shape on the coupling factor.

3.3.5 Efficiency investigation of the WPT system coils with two types of cross-sections wire

This work presents a simulation study of the influence of the changing the coils copper wire cross-section from circular to rectangular on the coil's parameters, also the effect of compensation circuits topologies types series-series (SS) and series-parallel (SP) on each type of the above coils by using symmetrical and asymmetrical coils.

3.3.5.1 Design and simulation of symmetrical and asymmetrical coils

The most common coil structure in the WPT system is spiral design because of its compact size and the electromagnetic field characteristics are very limited. The circular coils structure is chosen for this study and by using the MAXWELL software four different coils are designed by using two types of wire cross-sections as shown in Fig.3.11.

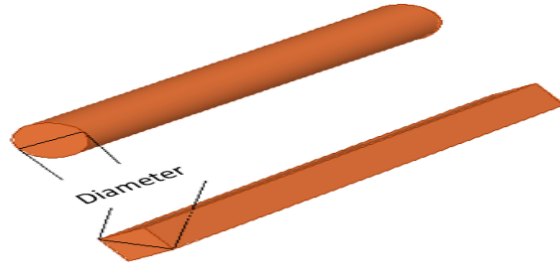


Fig. 3.11 Wire cross-section

In the first and the second cases, similar size coils are designed, one by using circular wire cross-section and the other case using rectangular wire cross-section as shown in Fig.3.12 (a)&(b). While in the (c) and (d) cases, the Tx coil is kept in the same size while the receiver coil is minimized, also by using circular and rectangular cross-section wire as illustrated in Fig.3.12 (c) & (d).

The asymmetric coils designed can be suitable for use in biomedical devices [20].

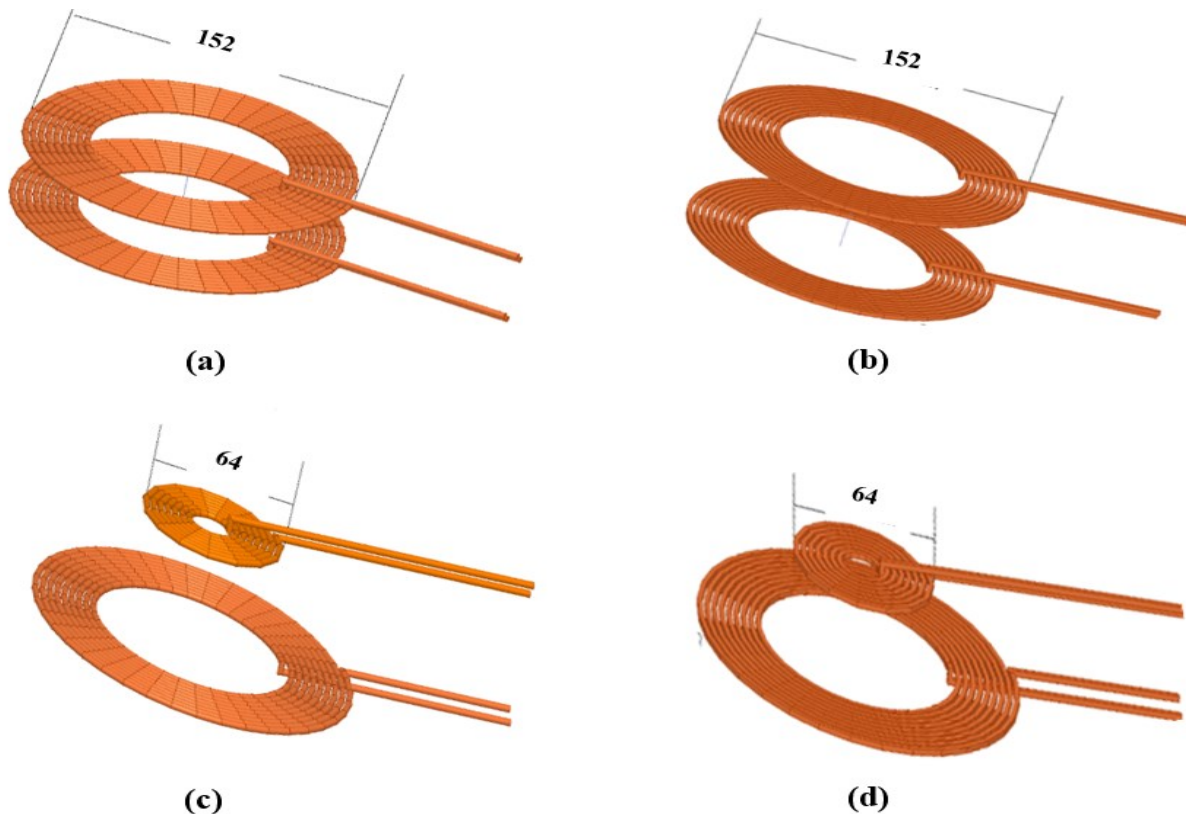


Fig. 3.12 (a) Symmetrical coils with circular cross-section wire, (b) Symmetrical coils with rectangular cross-section-wire, (c) Asymmetrical coils with circular cross-section-wire, (d) Asymmetrical coils with rectangular cross-section-wire.

The geometry for the designed coils is given in Table 3.7.

Table 3.7 The geometry for the designed coils.

| | Symmetric | | Asymmetric | |
|------------------------|-----------|---------|------------|---------|
| | Tx Coil | Rx Coil | Tx Coil | Rx Coil |
| Polygon Radius(mm) | 1.5 | 1.5 | 1.5 | 1.5 |
| Start Helix Radius(mm) | 45.5 | 45.5 | 45.5 | 9.1 |
| Radius Change (mm) | 3.5 | 3.5 | 3.5 | 3.2 |
| No. of Turns | 9 | 9 | 9 | 7 |

The MAXWELL software is used to analyze and simulate the above-designed coils by using the magnetic solver with an excitation current of (1 A). For transmitter and receiver coils, the value of the inductance and the coupling coefficients between them are obtained for four different air gaps as given in Table 3.8 and Table 3.9

Table 3.8 Coils simulation result parameter for a circular cross-section.

| Distance (mm) | Symmetrical | | | | Asymmetrical | | | |
|---------------|---------------------|---------------------|--------------|-------|---------------------|---------------------|--------|-------|
| | L_{Tx} (μ H) | L_{Rx} (μ H) | M (μ H) | K | L_{Tx} (μ H) | L_{Rx} (μ H) | M (nH) | k |
| 30 | 12.9 | 12.9 | 4.1 | 0.32 | 12.9 | 1.9 | 633.4 | 0.126 |
| 50 | 12.7 | 12.9 | 2.2 | 0.17 | 12.9 | 1.9 | 360.2 | 0.072 |
| 60 | 12.5 | 12.9 | 1.61 | 0.126 | 12.9 | 1.9 | 264.8 | 0.035 |
| 90 | 10.3 | 12.9 | 0.53 | 0.05 | 12.9 | 1.8 | 88.2 | 0.018 |

Where: (L_{Tx}) is the transmitter (Tx) coil self-inductance, (L_{Rx}) is the receiver (Rx) coil self-inductance.

Table 3.9 Coils simulation result parameter for a rectangular cross-section.

| Distance (mm) | Symmetrical | | | | Asymmetrical | | | |
|---------------|---------------------|---------------------|--------------|-------|---------------------|---------------------|--------|-------|
| | L_{Tx} (μ H) | L_{Rx} (μ H) | M (μ H) | K | L_{Tx} (μ H) | L_{Rx} (μ H) | M (nH) | k |
| 30 | 13 | 13 | 4.01 | 0.31 | 12.9 | 1.98 | 527 | 0.12 |
| 50 | 12.8 | 13 | 2.2 | 0.16 | 12 | 1.98 | 293 | 0.06 |
| 60 | 12.6 | 13 | 1.611 | 0.125 | 11.4 | 1.98 | 175 | 0.04 |
| 90 | 10.4 | 13 | 0.53 | 0.05 | 11.4 | 1.98 | 84 | 0.017 |

3.3.5.2 Inductive coupling WPT realization

As shown in Fig.3.13, the simulation software ANSYS Simplorer is used to simulate the designed coils with the SS and SP topology. The designed coils are imported from Maxwell software and putting it in the circuit, the software automatically takes the coils parameter to the circuit.

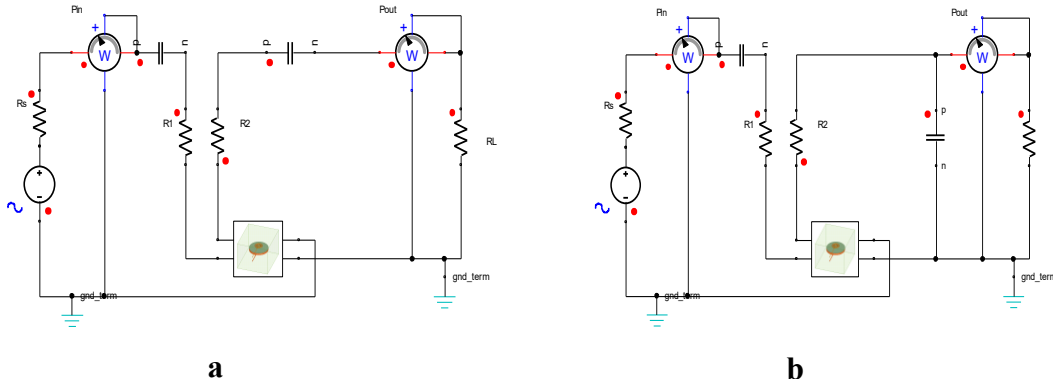


Fig. 3.13 Simulation circuit of (a) SS topology (b) SP topology

The efficiency is calculated at the resonance frequency $f_r = 100$ KHz. The results of Tables 3.8 and Tables 3.9 with an air gap distance of 30 mm are used to calculate the capacitance values. In the case of symmetrical structure, the calculated capacitance values for the transmitter side and the receiver side were $C = 0.194 \mu\text{F}$. Whereas, $C = 1.333 \mu\text{F}$ for the small coil on the receiver side and $C = 0.194 \mu\text{F}$ for the large coil side in an asymmetrical design. It is worth noting that the circuit is supplied with $V_s = 12$ V and loaded with $R_L = 10\Omega$. The values of R_{dc} and R_{ac} can be calculated and the result given in Table 3.10 takes into account the skin effect on the Litz wire at $f = 100$ kHz.

Table 3.10 DC and AC Resistances.

| Wire cross-section | Symmetric (m Ω) | | Asymmetric (m Ω) | | | |
|--------------------|-------------------------|------------------|--------------------------|-------------|-------------|-------------|
| | R_{dc} (Tx=Rx) | R_{ac} (Tx=Rx) | R_{dc} Tx | R_{ac} Tx | R_{dc} Rx | R_{ac} Rx |
| Circular | 8.47 | 32.1 | 8.47 | 32.1 | 2.726 | 10.4 |
| Rectangular | 13.34 | 37 | 13.34 | 37 | 4.212 | 11.8 |

The simulation is performed for the designed coils using two types of compensation circuits, i.e. SS and SP topologies for four different air gap distances. The efficiency is calculated from the reading of the wattmeter, which measures the input and output power. Fig.3.14 shows the calculated efficiency for the coils with both circular and rectangular cross-sections for air gap distances of 30 mm, 50 mm, 60 mm, and 90 mm.

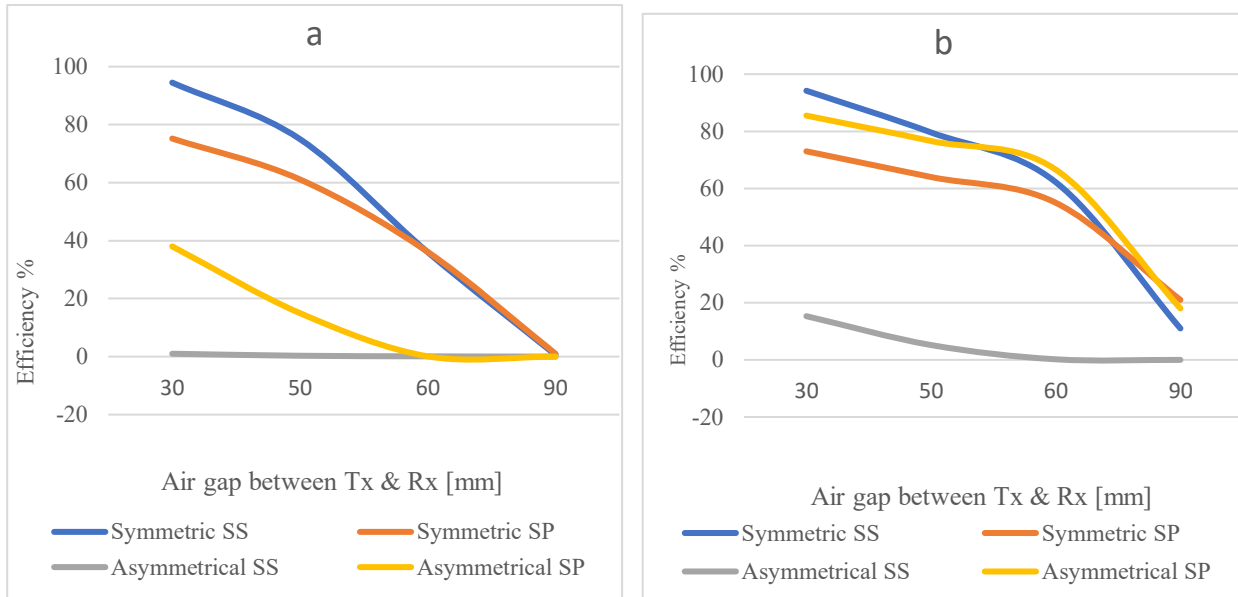


Fig. 3.14 The efficiency of the circular coils with various topologies and distances (a) Rectangular cross-section (b) Circular cross-section

The overall results show that the symmetrical coils in, which the transmitter (Tx) and receiver (Rx) coils have the same sizes, give higher energy transfer efficiency when an SS compensation circuit is used. While the asymmetrical coils, in which the Tx coil is larger than the Rx coil, a higher energy transfer efficiency is achieved using SP compensation topologies. It was also found from the results that the symmetrical coils with rectangular cross-section wire are more efficient in transmitting the power over the near distances (30mm) than the circular cross-section wire, while the circular cross-section wire is the better in the other distances. In the latter case, the asymmetric coils with a circular cross-section wire gave better efficiency for power transmission over all distances than the rectangular cross-section wire.

3.4 WPT system circuit design and simulation

This section describes the simulation process of the entire WPT system stages inverter, rectifier, and load by using MATLAB-Simulink software. The designed WPT system is selected to be able to transfer power to about 250 Watt. WPT system

consists of three-stage as shown in Fig.3.15. The first stage is the half-bridge inverter, which consists of dc voltage source connected in series with two series-connected capacitors to work as a two-voltage source. The inverter switches are semiconductor devices of the power MOSFET type with $R_{on} = 280 \text{ m}\Omega$. The gate of the MOSFET was triggered with the pulse with a frequency approximately equal to resonant frequency to generate a square wave with the same frequency as the applied pulse. The second stage is the Tx and Rx coil with the SS compensation capacitor to provide the resonance on the Tx and Rx sides. The third stage is the rectifier bridge which consists of four diodes. The diode bridge is connected in parallel to a capacitor, which acts as a filter and supplies the load with pure direct current.

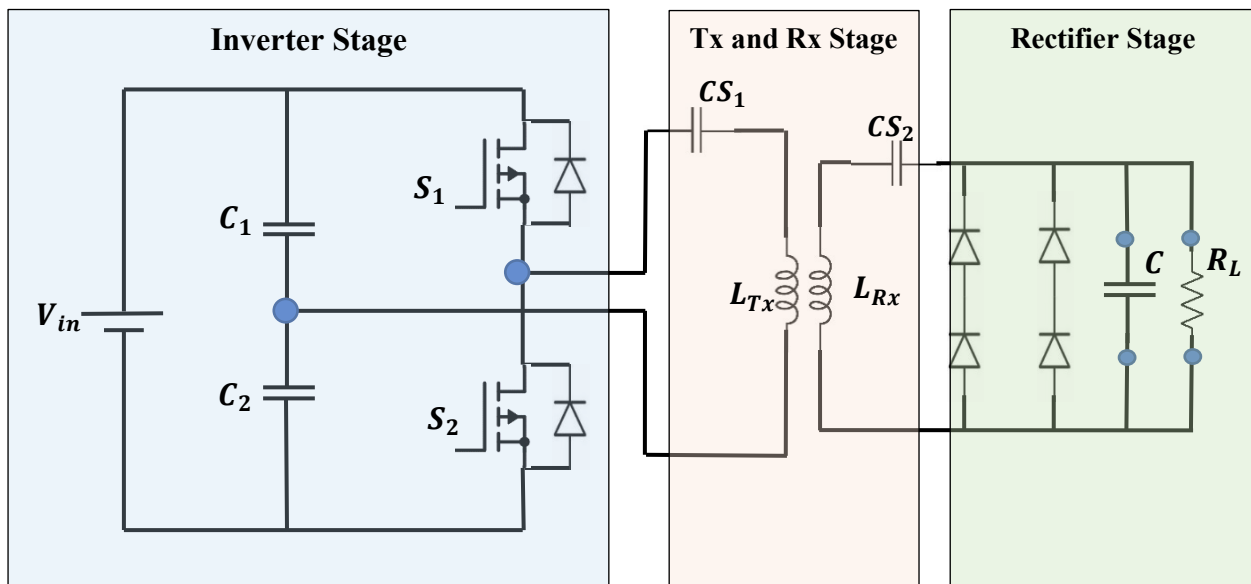


Fig. 3.15 The WPT system circuit.

The entire WPT circuit in MATLAB with the measuring system instruments is shown in Fig. 3.16. The considered values of the circuit elements are given in Table 3.11.

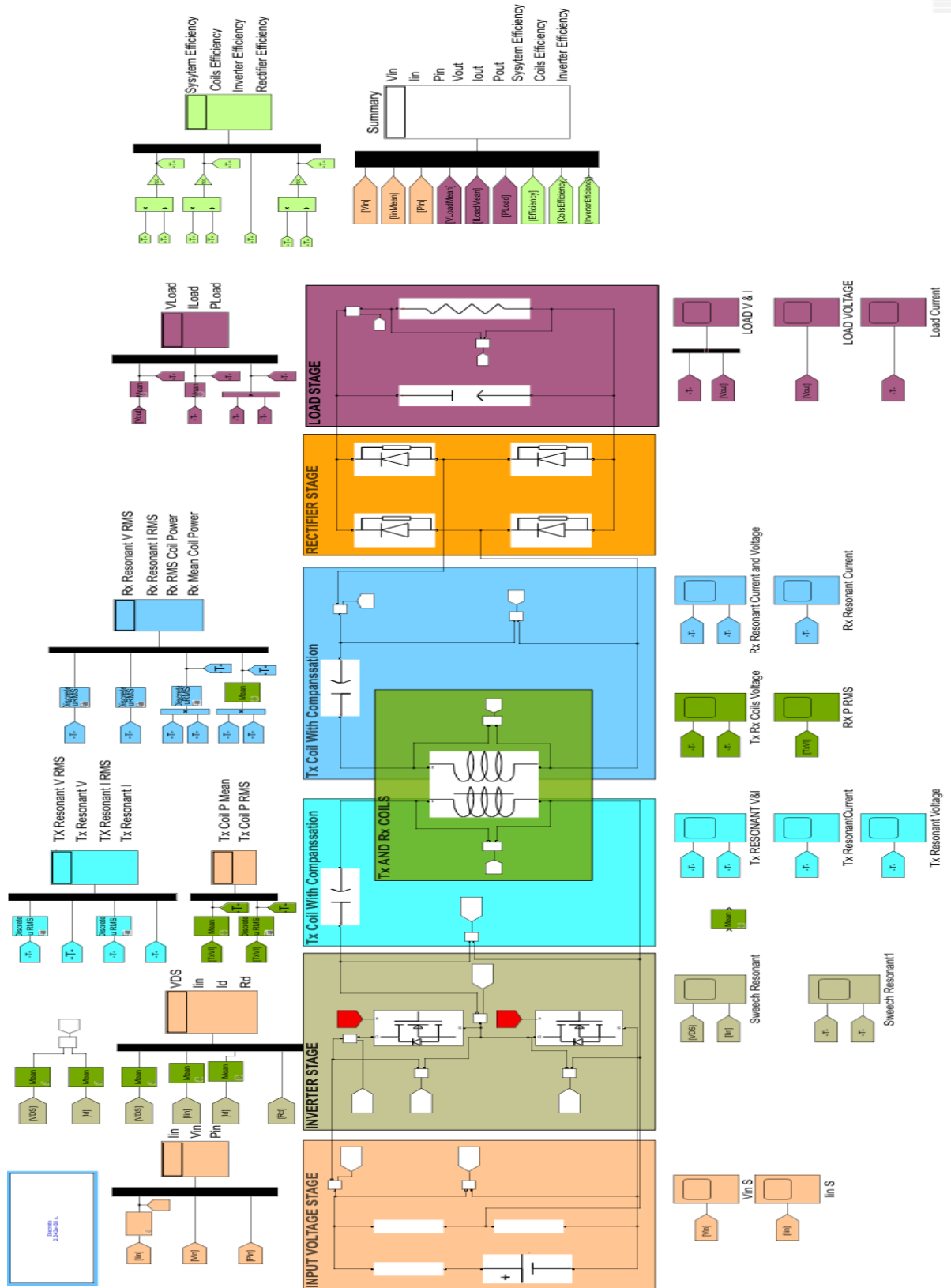


Fig. 3.16 The whole MATLAB WPT circuit with the measurement devices.

Table 3.11 WPT circuit elements.

| Circuit element | Value |
|----------------------|-----------------------------------|
| V_{in} | Input voltage (variable) |
| C_1, C_2 | Dc link Capacitor = 470 μ F |
| T_1, T_2 | MOSFET switch Ron=280 m Ω |
| C_{S1}, C_{S2} | Compensations capacitor(variable) |
| L_{Tx}, L_{Rx} | Tx and Rx Self-inductance |
| D_1, D_2, D_3, D_4 | Rectifier Diode |
| C | Output capacitor = 220 μ F |
| R_L | Load resistance =7 Ω |

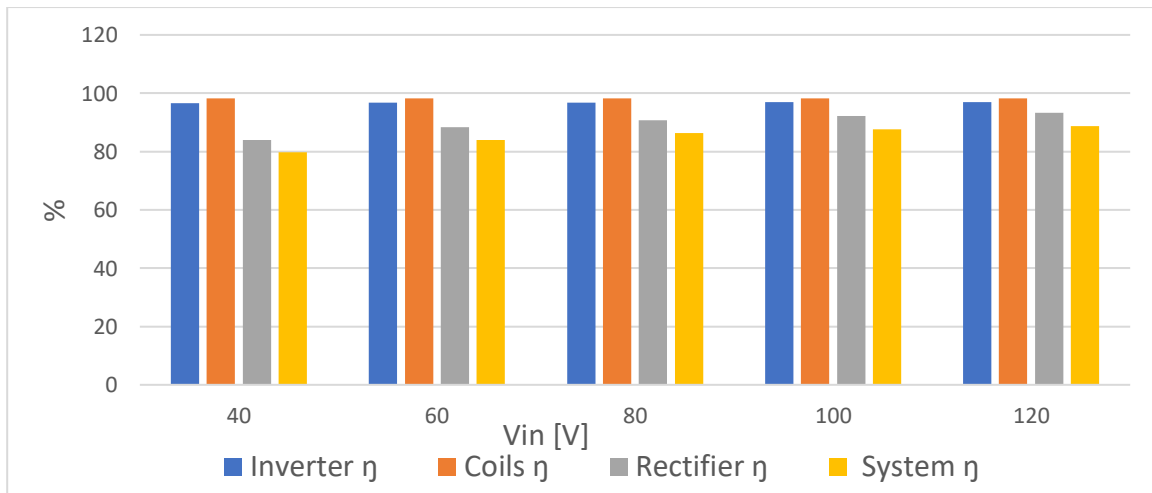
3.5 System efficiency measurement simulation at a different applied voltage

Table 3.12 given the simulation results for the efficiency calculations with different voltages applied with the following parameters: air gap $D = 40$ mm, $R_L = 7 \Omega$, $f_r = 41.7$ kHz, $L = 67.7$ uH and $C_{S1} = C_{S2} = 225 \mu$ F. Simulation results for different V_{in}

Table 3.12 The simulation results for the efficiency calculations for the different voltages applied.

| V_{in} | I_{in} | V_{out} | I_{out} | P_{in} | P_{out} | η |
|----------|----------|-----------|-----------|----------|-----------|--------|
| 40 | 0.95 | 14.58 | 2.08 | 38.1 | 30.4 | 79.7 |
| 60 | 1.36 | 21.93 | 3.13 | 81.84 | 68.7 | 84 |
| 80 | 1.78 | 29.28 | 4.18 | 142 | 122 | 86.3 |
| 100 | 2.19 | 36.64 | 5.23 | 218.6 | 192 | 87.7 |
| 120 | 2.6 | 43.99 | 6.28 | 311.8 | 276 | 88.7 |

The WPT system circuit stages efficiency is shown in Fig.3.17.

**Fig. 3.17** The WPT system stages efficiency of the WPT system.

The inverter losses are shown in Fig.3.18.

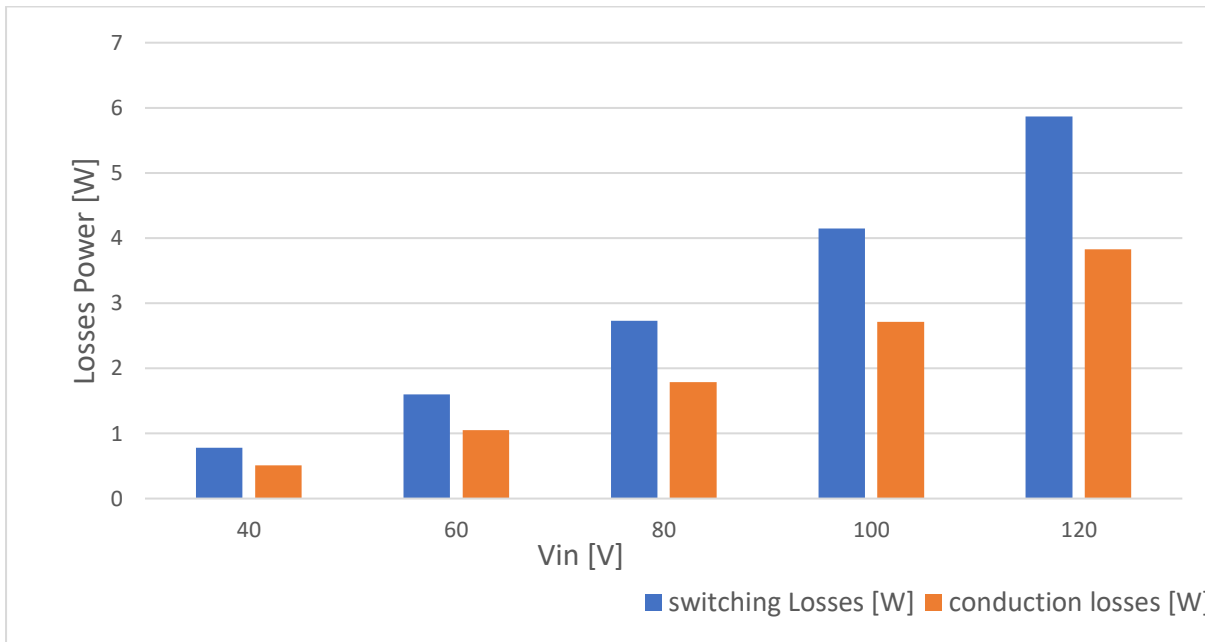


Fig. 3.18 The inverter losses of the WPT system at different V_{in}

3.6 Performance study of the entire WPT system.

This section is concerned with the WPT system performance investigation.

3.6.1 Find the appropriate load resistance for the WPT system

In this simulation experiment, the appropriate load resistance RL_A is found for the WPT system that was previously designed. Then check the result value with the Eq. (3-5) [59] which is used to find it:

$$RL_A = R_{ac Rx} * \sqrt{1 + k^2 Q_{Tx} Q_{Rx}} \quad (3-5)$$

The max. power transfer efficiency PTE theoretical (PTE_{max}) of a WPT system occurs when the equivalent load is at its appropriate value (RL_A), which can be expressed in terms of the Q (quality factors) of the coils (Q_{Tx} and Q_{Rx}) which can be calculated using Eq. (3-6), and the coupling coefficient (k) [38].

$$Q = \frac{\omega_r L}{R_{ac}} \quad (3-6)$$

The simulation process is done at a resonant frequency $f_r = 40\text{kHz}$ using the coil self-inductance value $L_{Tx} = L_{Rx} = 105.8 \mu\text{H}$ and $R_{ac} = 0.125\Omega$, then by applying this value in Eq. (3-6) to get $Q_{Tx} = Q_{Rx} = 212.7$

Coupling factor $k = 0.44$ at distance 30 mm taken from MAXWELL software while simulation the coils, then by applying these values in Eq. (3-5) to get $RL_A \cong 12\Omega$.

The compensation element value $C_{s1} = C_{s2} = 149.6\text{ nF}$, by applied input voltage $V_{in} = 150\text{ V}$, it given the results in Table 3.13, the full resonant is done at switching frequency $f_{sw} = 41.4\text{ kHz}$ which is found by examining the voltage and current wave at MOSFET.

Table 3.13 Simulation result to find RL_A at $V_{in} = 150\text{ V}$.

| $R_L \Omega$ | $I_{in} \text{ A}$ | $V_{out} \text{ V}$ | $I_{out} \text{ A}$ | $P_{in} \text{ W}$ | $P_{out} \text{ W}$ | η |
|--------------|--------------------|---------------------|---------------------|--------------------|---------------------|--------|
| 4 | 0.8 | 20.15 | 5.03 | 120.9 | 101.5 | 83.96 |
| 7 | 1.3 | 34.83 | 4.97 | 196.3 | 173.3 | 88.3 |
| 8 | 1.47 | 39.64 | 4.95 | 221 | 196.5 | 88.89 |
| 9 | 1.63 | 44.42 | 4.93 | 245.5 | 219.2 | 89.29 |
| 10 | 1.79 | 49.15 | 4.91 | 269.8 | 241.6 | 89.54 |
| 11 | 2.02 | 55.71 | 4.88 | 303.5 | 272.3 | 89.72 |
| 12 | 2.11 | 58.5 | 4.87 | 317.8 | 285.2 | 89.75 |
| 13 | 2.27 | 63.12 | 4.85 | 341.5 | 306.5 | 89.74 |
| 14 | 2.43 | 67.71 | 4.83 | 365 | 327.4 | 89.71 |
| 15 | 2.58 | 72.25 | 4.81 | 388.3 | 348 | 89.62 |
| 16 | 2.74 | 76.76 | 4.79 | 411.4 | 368.3 | 89.5 |
| 20 | 3.34 | 94.44 | 4.72 | 502.1 | 446 | 88.82 |
| 30 | 4.77 | 136.3 | 4.45 | 716.3 | 619.2 | 86.45 |

From the above results, the relation between the power efficiency of the WPT system and load resistance is plotted as shown in Fig.3.19.

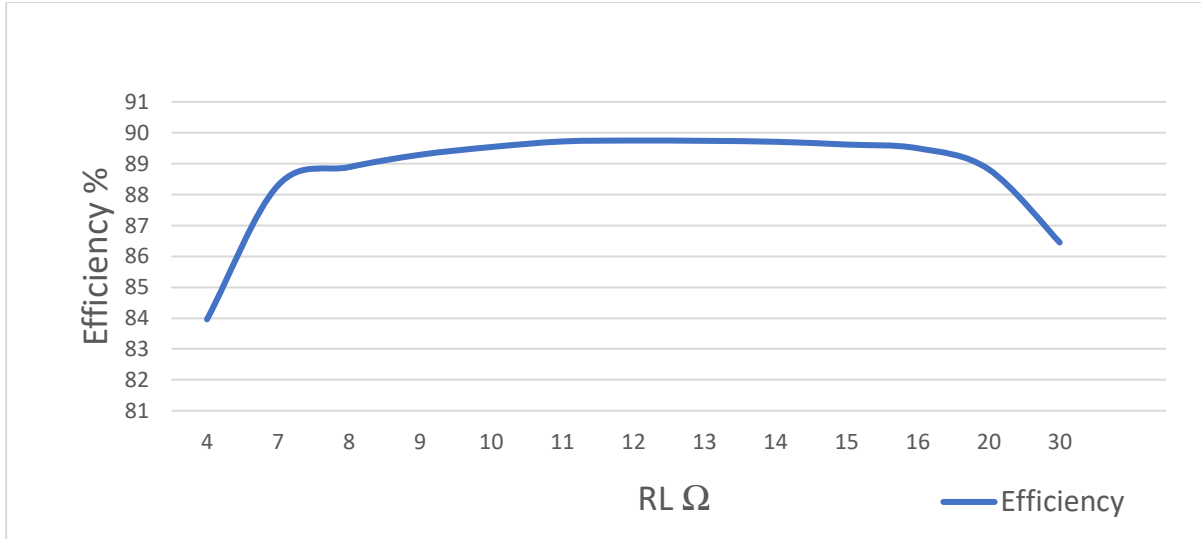


Fig. 3.19 Efficiency curve with various R_L at $V_{in} = 150$ V and $f_r = 40$ kHz

The results show that the maximum efficiency occurs at the $R_L = RL_A$, then the efficiency is decreased when the load resistance goes up or down. Also, the input and output power are gone down when the R_L decreased and vice versa.

3.6.2 The effect of changing the load resistance on the WPT system

In this MATLAB process experiment on the WPT circuit, it is gone to design a WPT with a 250-watt output power system for various R_L and it studied the effect of changing the R_L on the circuit parameters.

The simulation is completed using previously designed circuits and coils with transmitter (Tx) and receiver (Rx) coils self-inductance $L = 68.7 \mu H$ and the air gap between the two coils (Tx and Rx) $D = 40 mm$.

The simulation results exhibited that when the resistance of the load is increased the input applied voltage is decreasing, while the output voltage is slightly affected by the changing R_L . Also, the input current is decreased and the output current is slightly affected by the changing R_L as shown in Fig.3.20.

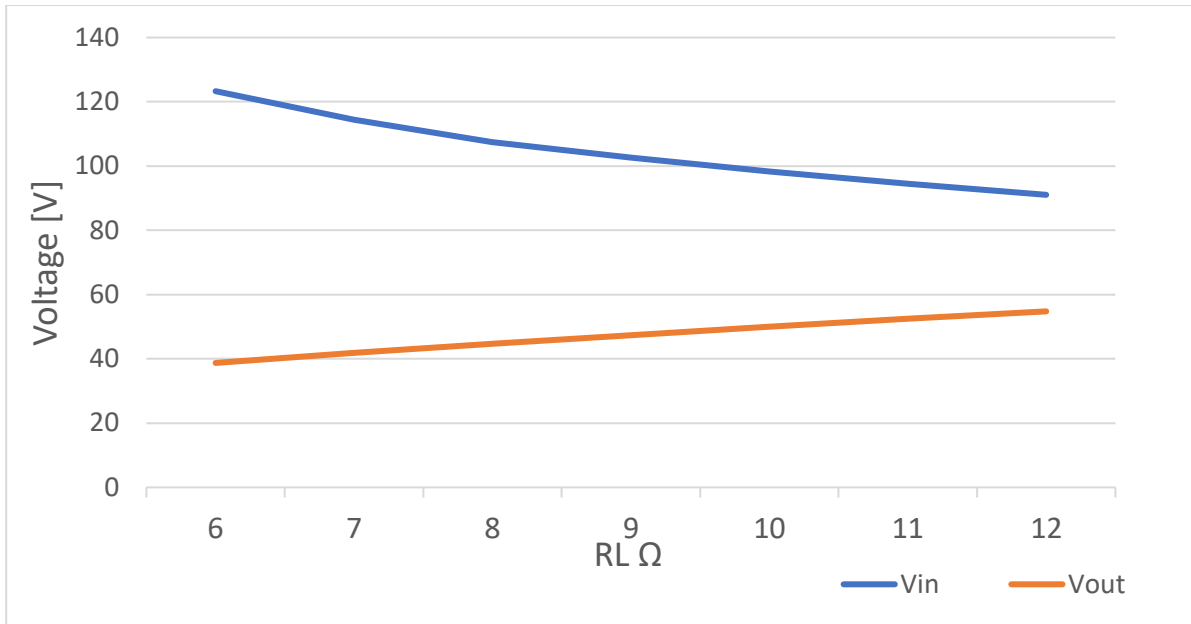


Fig. 3.20 Variation of V_{in} and V_{out} with R_L at 250 W out power.

The input power is significantly decreased until the R_L up closes the value R_{L_A} then the change becomes very small as shown in Fig.3.21, while the efficiency was adversely affected as shown in Fig.3.22.

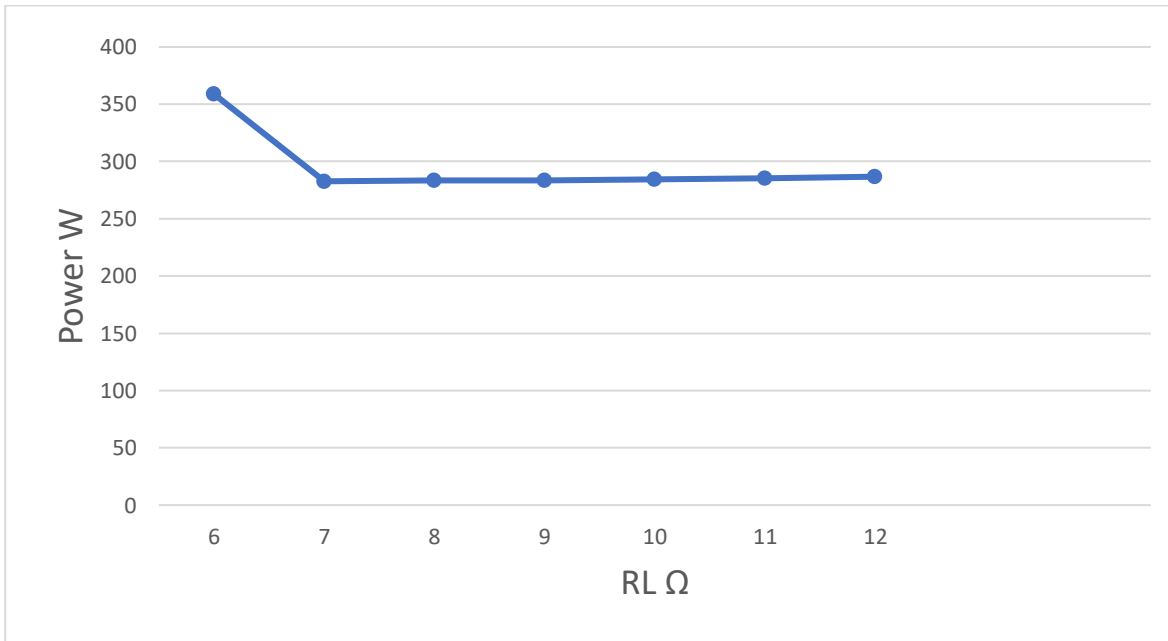


Fig. 3.21 Variation of the input power with changing R_L .

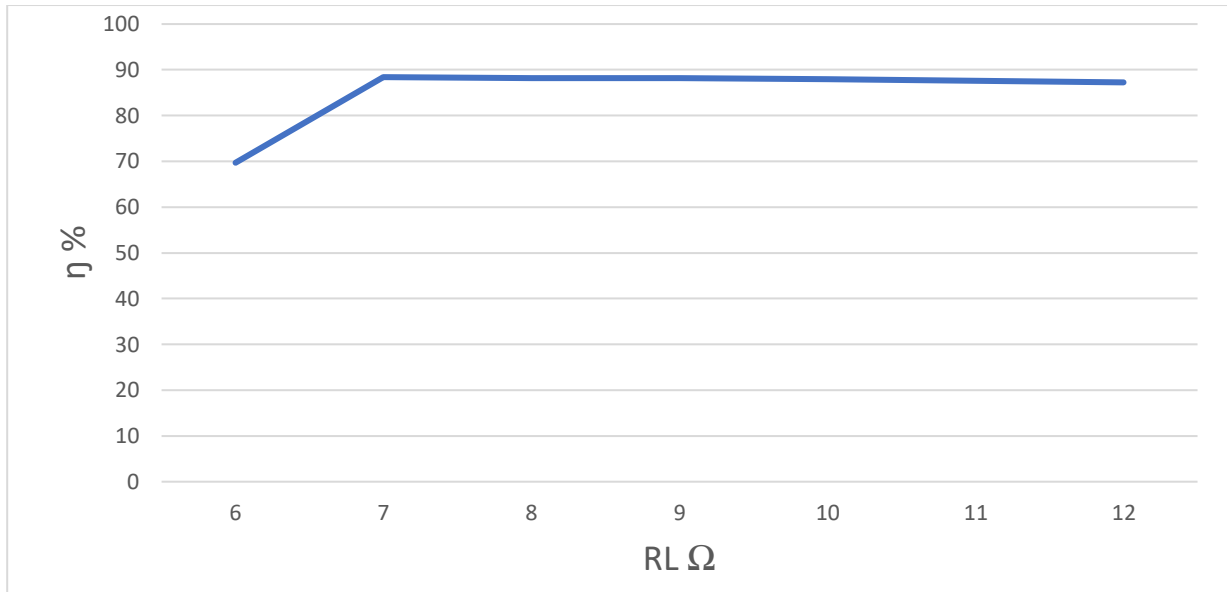


Fig. 3.22 System efficiency with changing R_L .

The switching frequency of the MOSFET must be changing when the load change, and it can be controlled as the values given in Table 3.14 to provide a soft switching for inverter and full resonance in both sides as illustrated in Fig.3.23 and Fig.3.24.

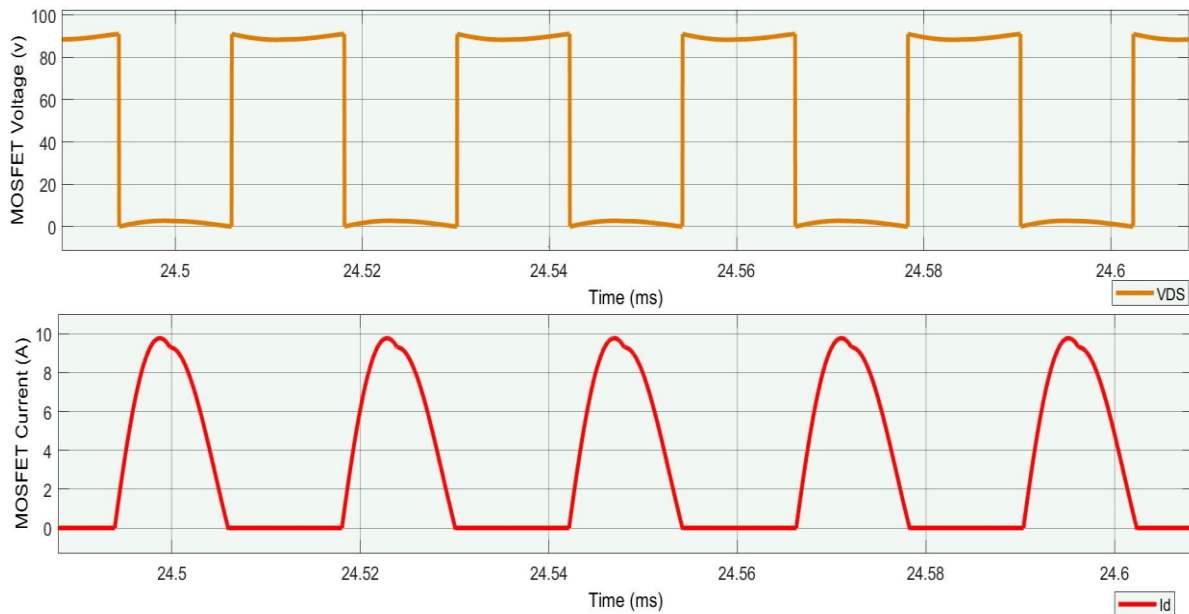


Fig. 3.23 MOSFET voltage and current waveforms.

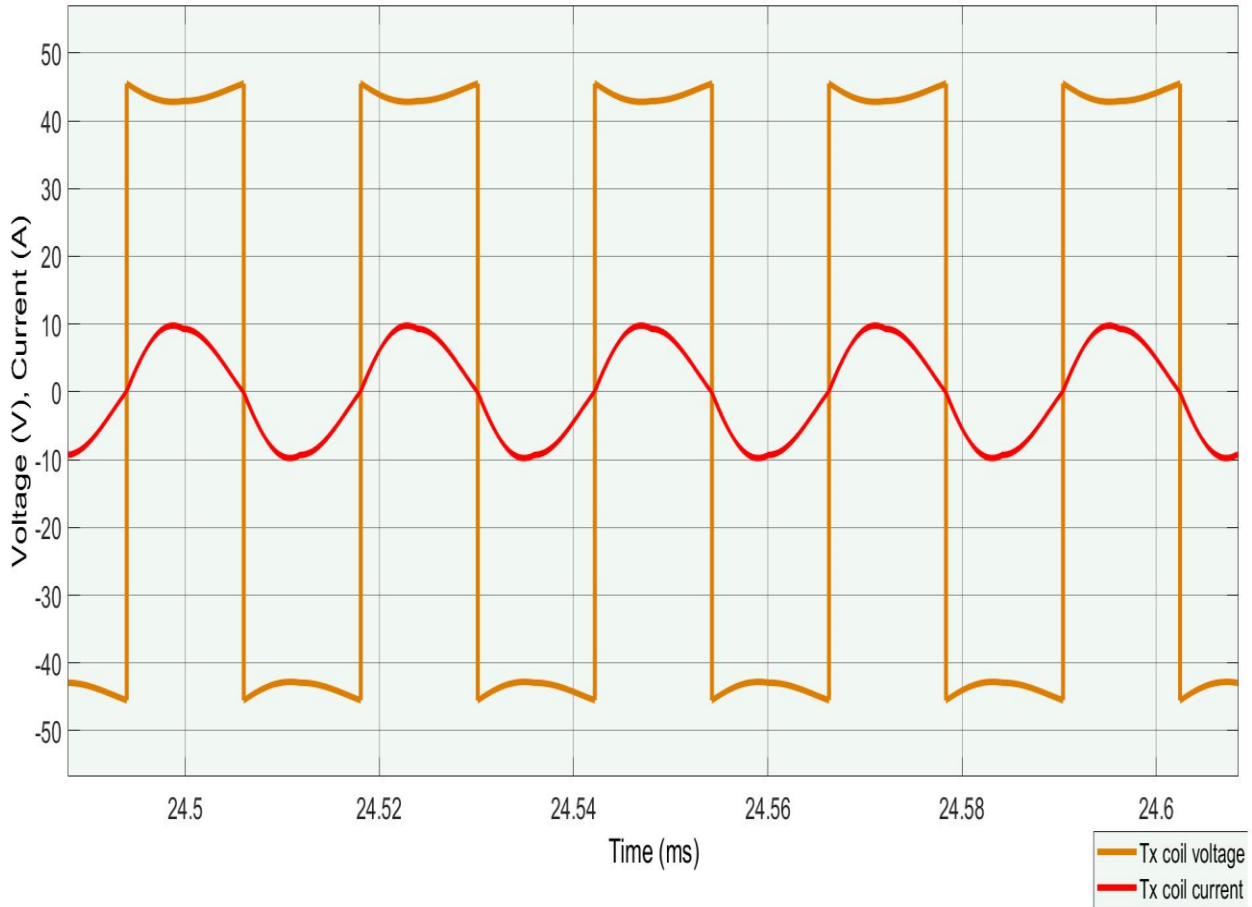


Fig. 3.24 Tx coil voltage and current.

Table 3.14 f_{sw} value for each R_L with 250 W output power

| R_L | f_{sw} (kHz) |
|-------|----------------|
| 6 | 42.3 |
| 7 | 42.7 |
| 8 | 43 |
| 9 | 42.5 |
| 10 | 42 |
| 11 | 41.5 |
| 12 | 41.5 |

3.6.3 The effect of changing resonant frequency (f_r) on the WPT system

In this simulation process, the effect of changing resonant (f_r) frequency on the efficiency is studied and the WPT system output voltage.

The experiment procedure that used previously MATLAB circuit is shown in Fig.3.15. The series compensation element is used in the primary and secondary stages to eliminate the self-inductance reactance and to increase the system efficiency. The considered parameters of the circuit are illustrated in Table 3.15

Table 3.15 The circuit's parameter value to study the resonant frequency effect.

| Parameter | Value |
|-----------------|----------------|
| C_1, C_2 | 470 μ F |
| C | 220 μ F |
| R_L | 7 Ω |
| $L_{Tx}=L_{Rx}$ | 67.7 |
| M At 40 mm | 28.892 μ H |

Different values of the resonance frequency f_r were taken while the other circuit parameters were fixed, and the compensation capacitors were calculated each time according to f_r , as shown in Table 3.16.

Table 3.16 f_r and f_{sw} and compensation capacitor value.

| f_r (kHz) | f_{sw} (kHz) | Compensations Capacitors |
|-------------|----------------|--------------------------|
| 20 | 20.5 | $C_{s1}=C_{s2}=225$ nF |
| 41.7 | 42.7 | $C_{s1}=C_{s2}=935.3$ nF |
| 80 | 82.3 | $C_{s1}=C_{s2}= 58.4$ nF |

The simulation process is employed to get 250-watt output power. From the simulation reset it is noted that when the resonant frequency increases, also the input applied voltage is needed to increase in order to get the same power at the output, and also the input current was inversely proportional to the resonant frequency so the tension on the inverter switches is less than when the resonant frequency increases, while the output voltage and current are remaining constant when the resonant frequency is changed as shown in Fig.3.25 and Fig.3.26.

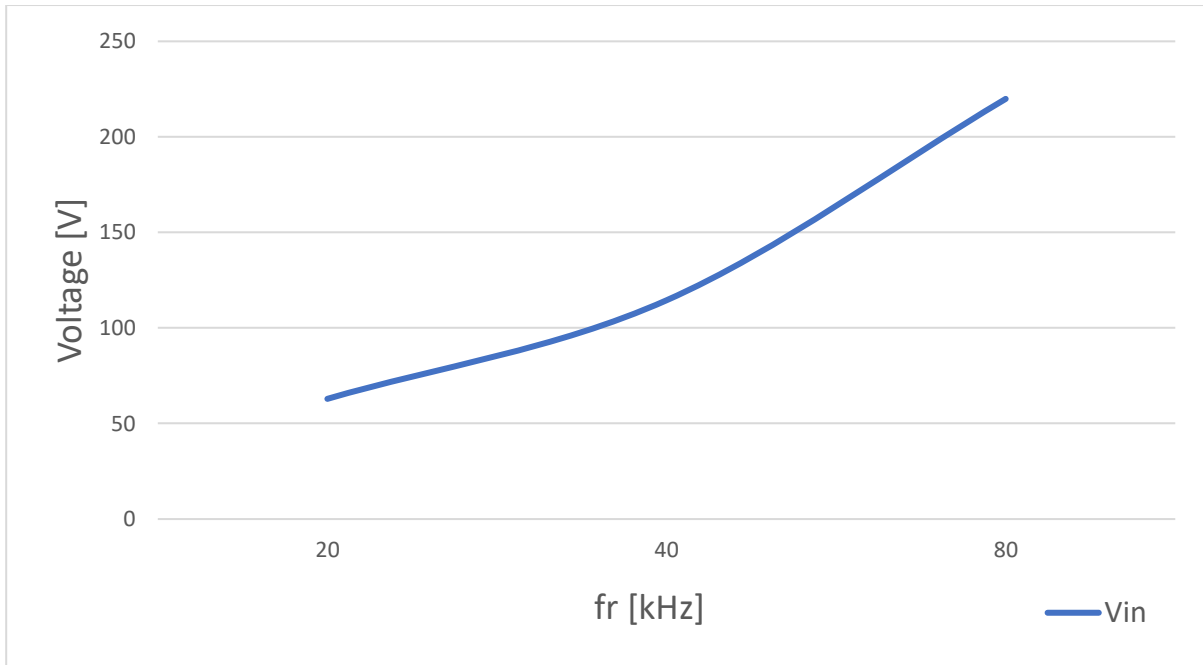


Fig. 3.25 Input voltage at with changing f_r and 250-watt output power.

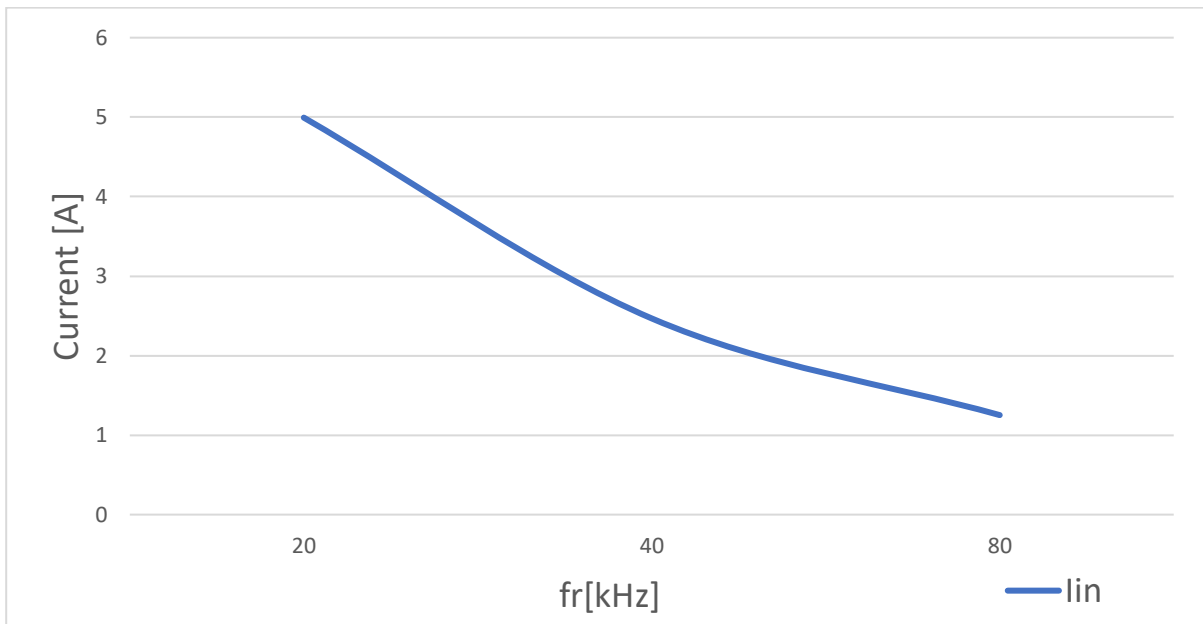


Fig. 3.26 Input current value with changing f_r to get the 250-watt output power.

Also, the system power transfer efficiency is increased as the resonant frequency increasing as shown in Fig.3.27.

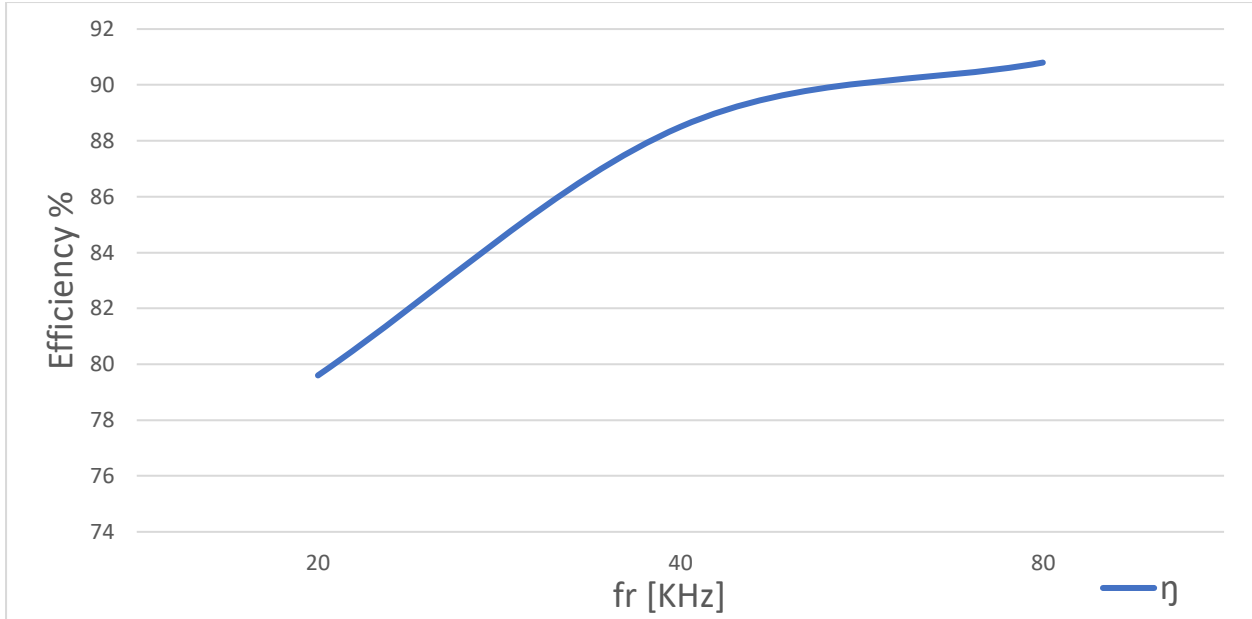


Fig. 3.27 The efficiency of the power transfer of the WPT system with changing f_r and 250-watt output power.

3.6.4 Comparative study of resonant frequency calculation

Based on some mathematical formulas, the resonant frequency for the SS compensation topologies of the WPT system is calculated twice, the first once by using self-inductance and once depending on leakage-inductance. The MATLAB software is used in simulation and then the results are verified practically in chapter four. The previously WPT simulation circuit used, the used coils in Tx and Rx have an inductance value $L_{Tx} = L_{Rx} = L = 105.8 \mu\text{H}$ and the mutual inductance (M) between them at a distance of 30 mm is $(47) \mu\text{H}$, the load resistance R_L is (7Ω) . The resonant frequency f_r for determining the compensated elements of the following two calculations is chosen at 40 kHz.

a. Leakage-inductance-based calculation

In this method, the leakage inductance (L_{leak}) between the transmitter (Tx) and receiver (Rx) coils are obtained as follows:

$$L_{leak Tx} = L_{Tx} - M \quad (3-7)$$

$$L_{leak Rx} = L_{Rx} - M \quad (3-8)$$

Where: $L_{leak Tx}$ is the leakage-inductance-based for transmitter coil, $L_{leak Rx}$ is the leakage inductance for the receiver coil. Thus, $L_{leak Tx} = L_{leak Rx} = L_{leak} = 58 \mu\text{H}$,

By substituting the values of f_r and L_{leak} in the Eq.2.15 the values of $C_{s1} = C_{s2} = 272.95\text{nF}$. The switching frequency f_{sw} should be set to less than f_r . So, at $f_{sw} = 36.6$ kHz the full resonant has occurred.

b. Self-inductance-based calculation:

In this method, the self-inductance-based (L_{Self}) values of the transmitter (Tx) and receiver (Rx) coils are used in the calculations. By substituting f_r and L_{Tx} or L_{Rx} in Eq.2.15, the compensation capacitors are calculated $C_{s1} = C_{s2} = 149.63$ nF. The switching frequency f_{sw} should be set to more than f_r . So, at $f_{sw} = 41.4$ kHz the full resonant has occurred.

The results of the WPT system on leakage-inductance-based and self-inductance-based calculations are illustrated respectively in Table 3.17 and Table 3.18.

Table 3.17 Results based on leakage-inductance calculations.

| V_{in} V | I_{in} A | V_{out} V | I_{out} A | P_{in} W | P_{out} W | $\eta\%$ |
|------------|------------|-------------|-------------|------------|-------------|----------|
| 60 | 1.85 | 25.34 | 3.62 | 111.4 | 91.76 | 82.39 |
| 90 | 2.78 | 38.64 | 5.52 | 251 | 213.3 | 84.98 |
| 120 | 3.72 | 51.93 | 7.41 | 446.4 | 385 | 86.29 |
| 200 | 6.2 | 87.36 | 12.48 | 1240 | 1090 | 87.9 |

Table 3.18 Results based on self-inductance calculations.

| V_{in} V | I_{in} A | V_{out} V | I_{out} A | P_{in} W | P_{out} W | $\eta\%$ |
|------------|------------|-------------|-------------|------------|-------------|----------|
| 60 | 0.57 | 13.89 | 1.98 | 34.41 | 27.57 | 80.12 |
| 90 | 0.81 | 20.87 | 2.98 | 73.68 | 62.24 | 84.48 |
| 120 | 1.06 | 27.85 | 3.97 | 127.7 | 110.8 | 86.83 |
| 200 | 1.71 | 46.47 | 6.63 | 343.5 | 308.5 | 89.81 |

The voltage and current waveforms of the MOSFET switching in leakage-inductance-based are shown in Fig.3.28, and for self-inductance-based, calculations are shown in Fig.3.29.

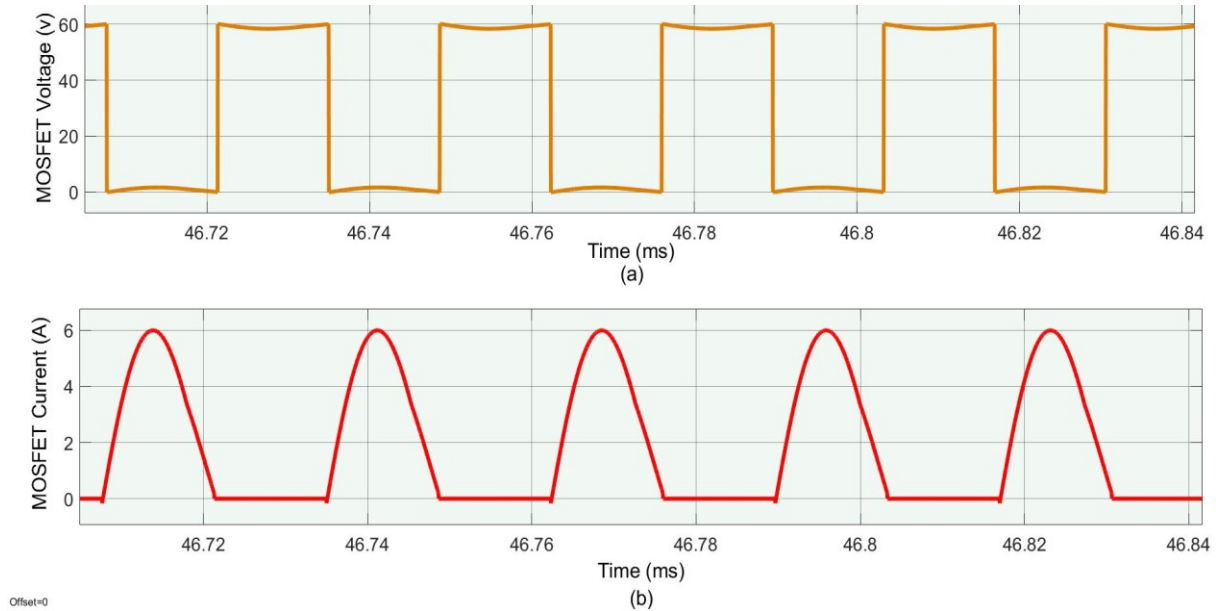


Fig. 3.28 Switching Voltage and current at $V_{in}=60V$ for Leakage-inductance-calculation.

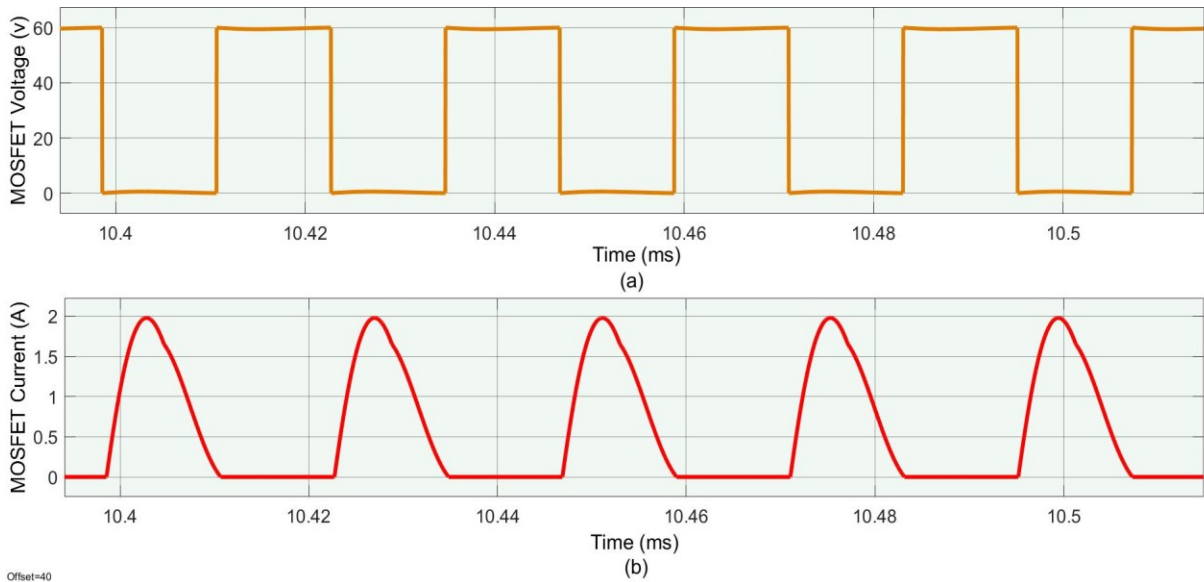


Fig. 3.29 Switching Voltage and current at $V_{in}=60V$ for Self- inductance-based calculation.

The voltage and current waveform before the transmitter (Tx) coil i.e. the input voltage and current for the Tx stage compensation circuit at $V_{in}=60V$ are shown in Fig 3.30. (a & b) for both leakage and self-inductance-based calculations respectively.

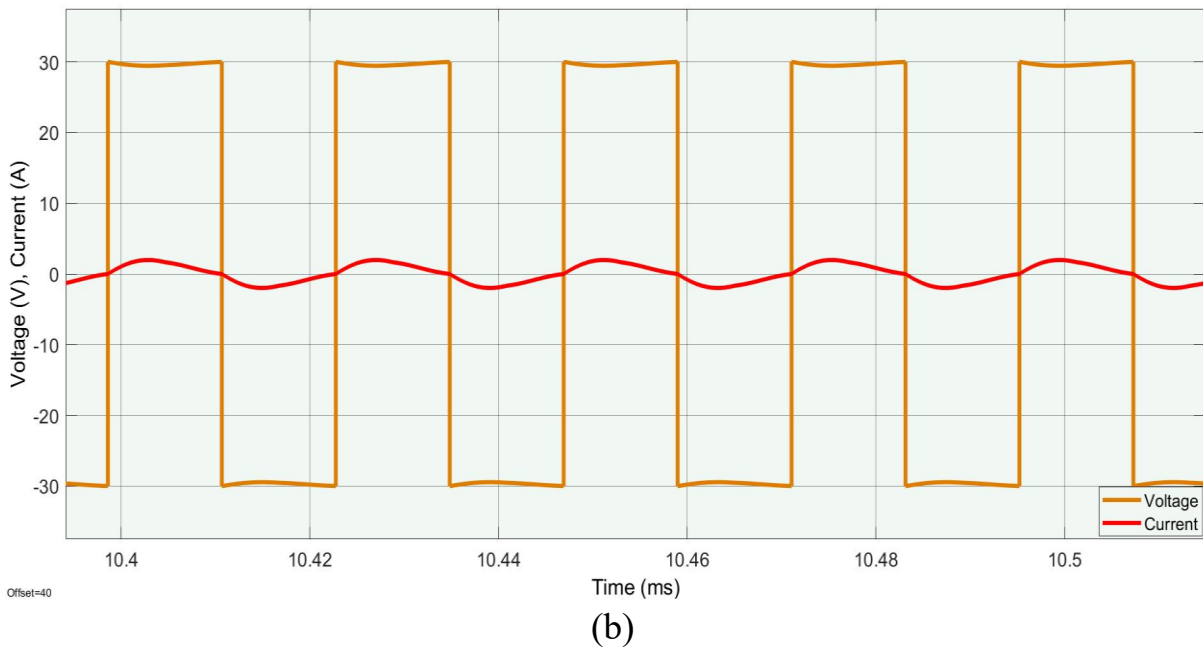
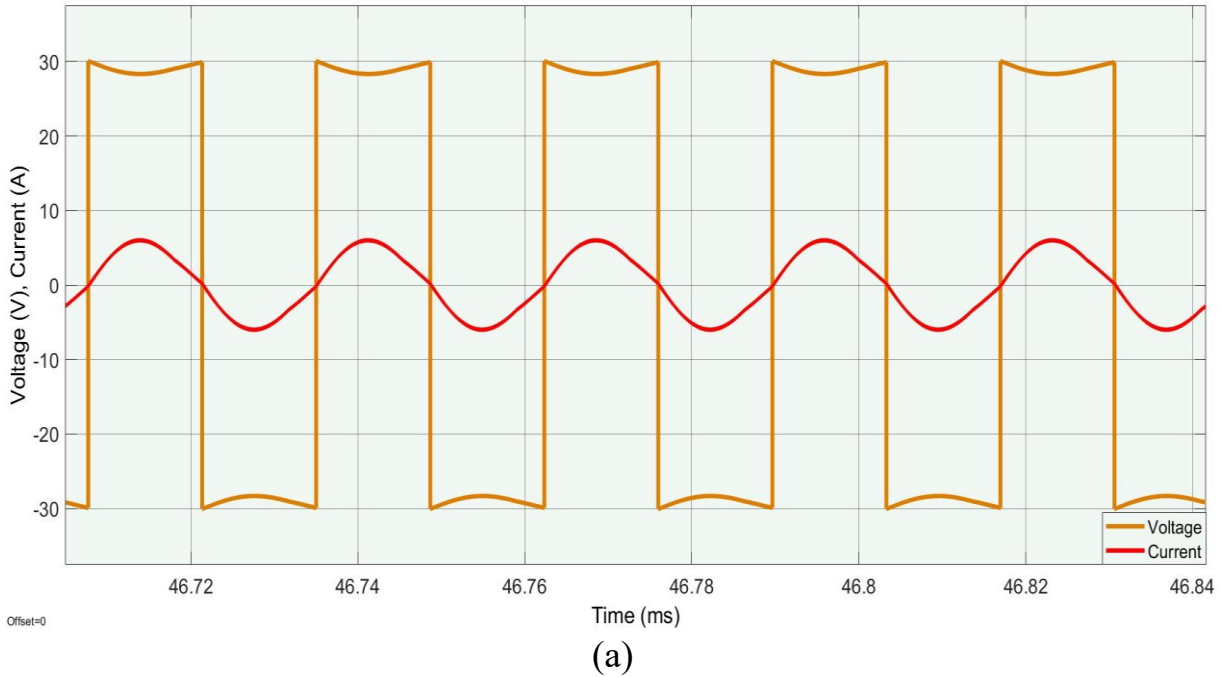
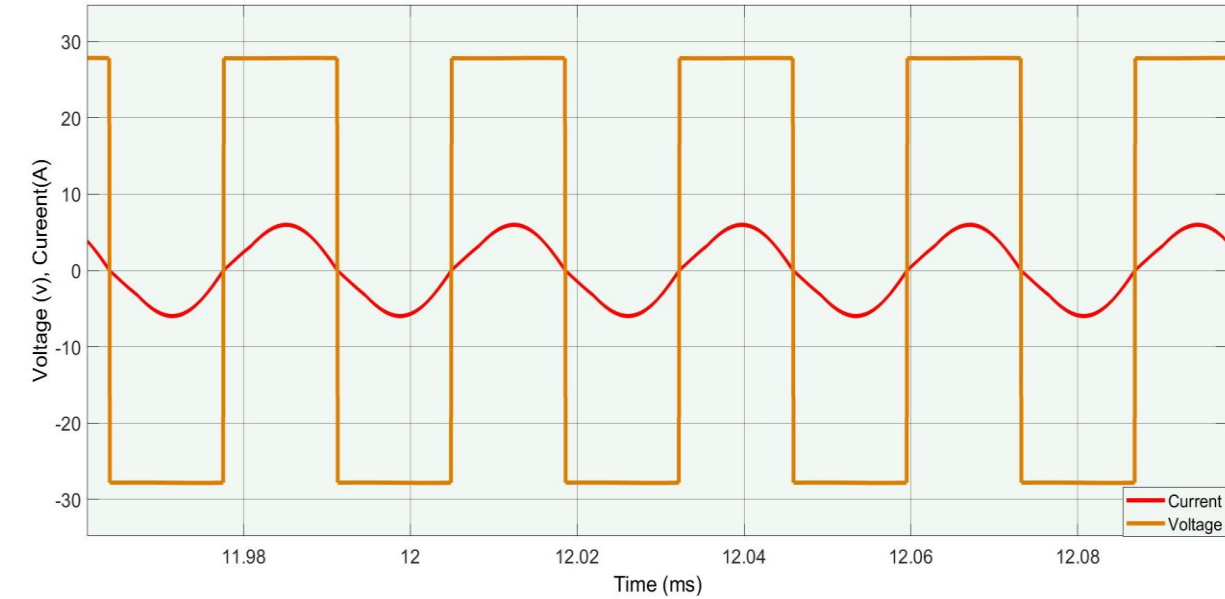
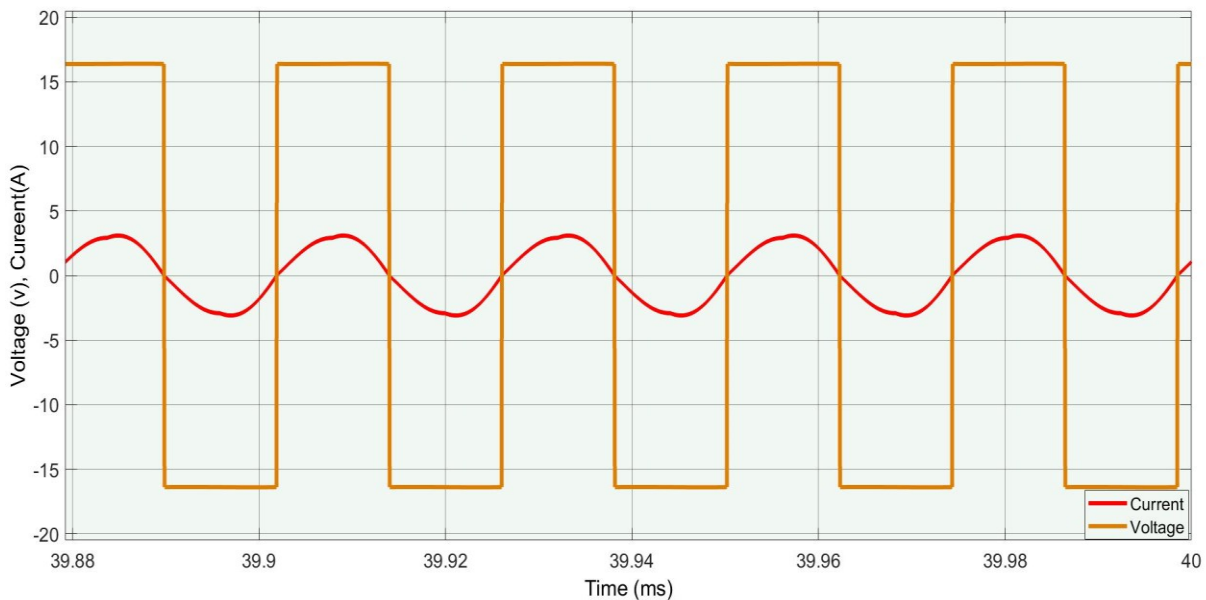


Fig. 3.30 The input voltage and current before the Tx coil at $V_{in}=60V$ (a) L_{leak} -based calculation (b) L_{self} -based calculation.

The voltage and current beyond the Rx circuit i.e. the input voltage and current for the rectifier circuit on the load side at $V_{in}=60V$ are shown in Fig 3.31. (a & b) for both leakage-inductance and self-inductance-based calculations respectively.



(a)



(b)

Fig. 3.31 The input voltage and current for the rectifier circuit at $V_{in}=60V$ (a) L_{leak} -based calculation (b) L_{self} -based calculation

The Tx and Rx Coils Voltage L_{leak} - based and L_{Self} -based calculation at 60 V is illustrated in Fig.3.32. & Fig.3.33.

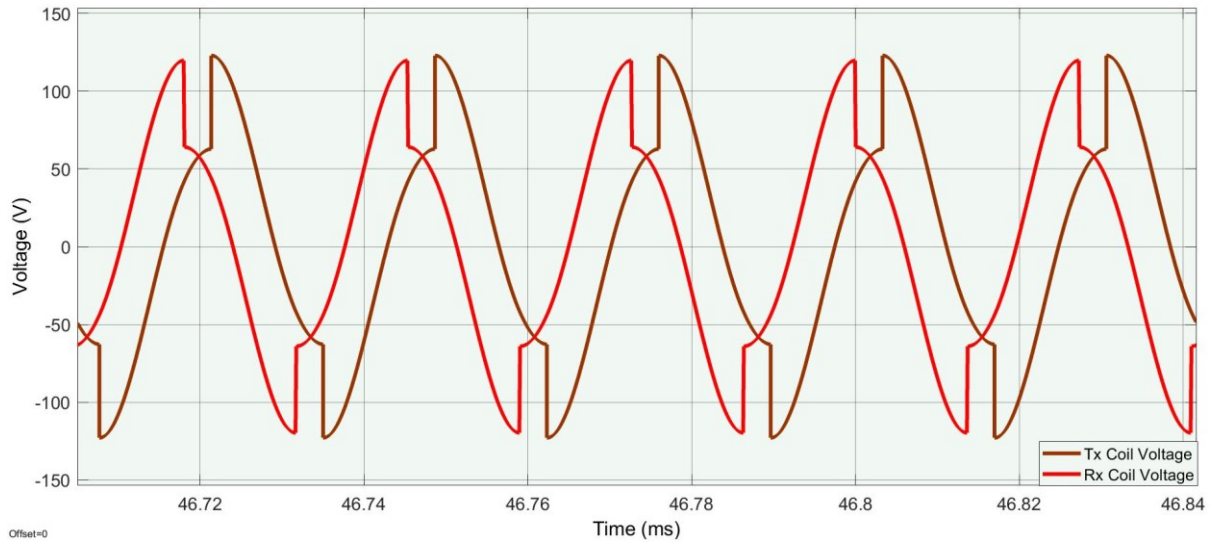


Fig. 3.32 Tx and Rx Coils Voltage L_{leak} -based calculation at $V_{in} = 60$ V.

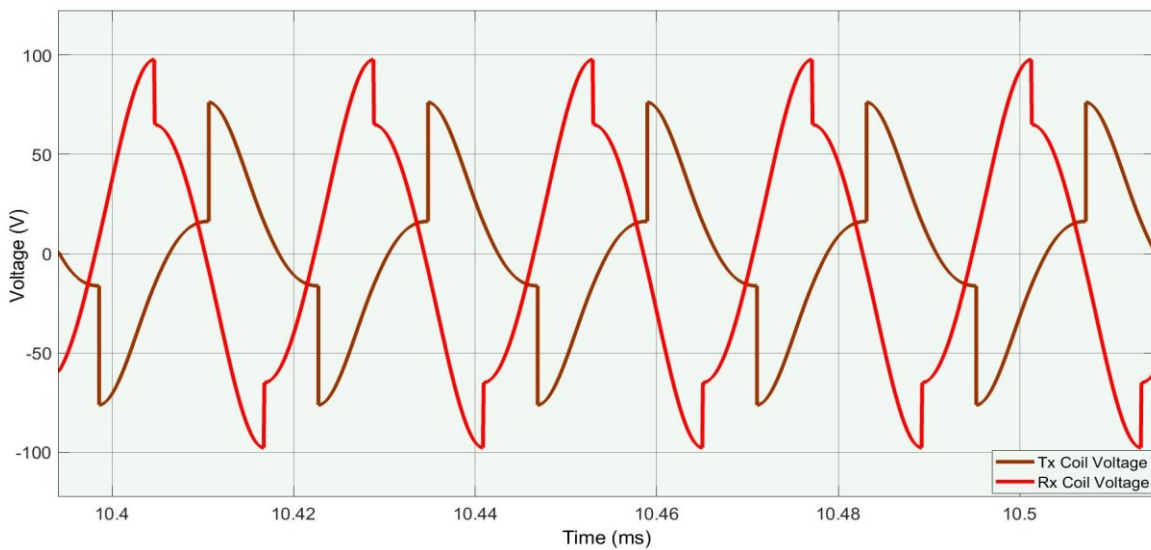


Fig. 3.33 Tx and Rx Coils Voltage L_{Self} -based calculation at $V_{in} 60$ V.

In this section, two assessments for determining the compensator elements of the WPT system have been presented. The first assessment is based on the leakage inductance and the second one is the self-inductance-based on the resonant

frequency calculations. So, the same equation is used with different values of the inductances to determine the compensator elements. From the results that are given in Tables 3.17 & 3.18, also the system output voltage and the delivered power to the load in case of the first assessment is more than for the 2nd assessment at the same input voltage and load condition. Also, it was noted from the experiment that the current across the inverter MOSFET switch in the first assessment is almost twice the value that in the 2nd assessment at the same power deliverable in the output, this causes tension on the inverter switches. Furthermore, it can be seen that the resonant frequency which is based on the leakage-inductance calculation is very sensitive to coil misalignment, so it is preferred to use it in a static WPT system. Also, it was noted that in the 1st method, the voltage on the Tx and Rx coil terminal were Almost equal. Therefore, more attention should be given to choosing the resonant frequency.

3.6.5 Simulation of a 250-watt WPT with a various air gap

In this simulation, the effect of changing the gap between the transmitter (Tx) and receiver (Rx) coils is studied.

The experiment is completed using the previously MATLAB circuit shown in Fig.3.1. The series-compensation elements have been used in the primary and secondary stages. The fixed circuit parameters have been shown in Table 3.19.

Table 3.19 Simulation of a 250-watt WPT with various air gap circuit elements.

| Parameter | Value |
|-----------------|-------------|
| C_1, C_2 | 470 μ F |
| C | 220 μ F |
| R_L | 7 Ω |
| $L_{Tx}=L_{Rx}$ | 67.7 |

The mutual value is taken from Table.3.5 for $D = 40\text{mm}$, $M = 28.8\mu\text{H}$. The simulation results have been shown that when the air-gap increased the applied input voltage decreased to get the specific power (250 W), and also the input current was

inversely proportional with the air-gap, so the tension on the inverter swatches has increased, as the air-gap increases, while the output current and voltage remained constant as shown in Fig.3.34 and Fig.3.35.

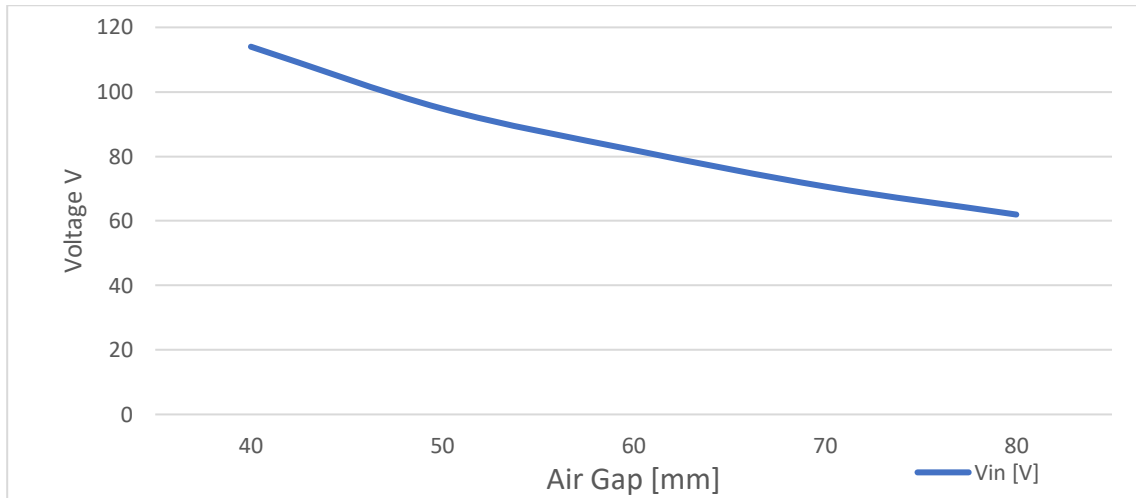


Fig. 3.34 Input applied voltage with changing air-gap and 250-watt output power.

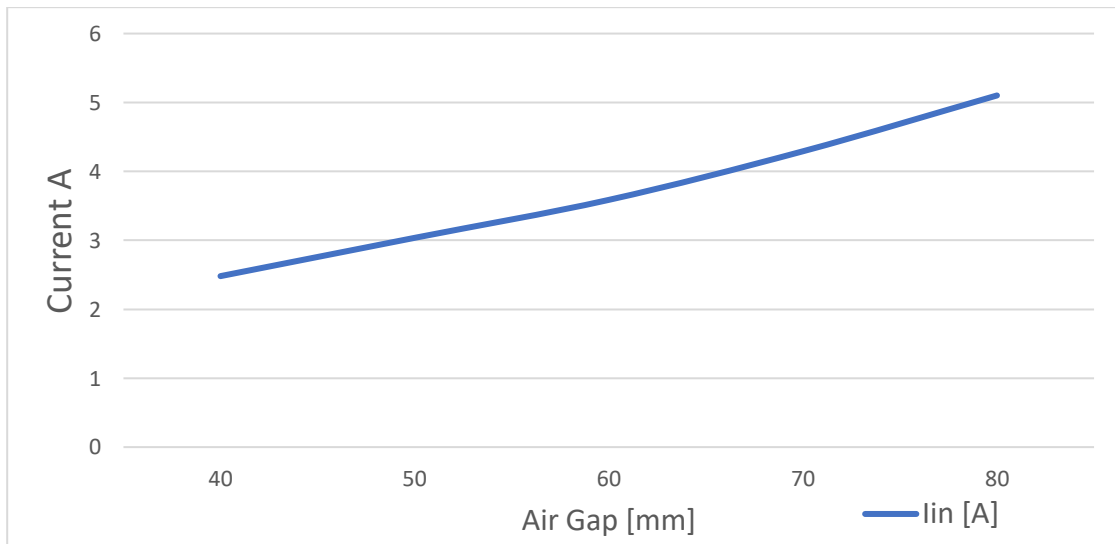


Fig. 3.35 Input current with changing air-gap and 250-watt output power.

Also, the results show in Fig. 3.36 that the system power transfer efficiency decreases as the air-gap increases.

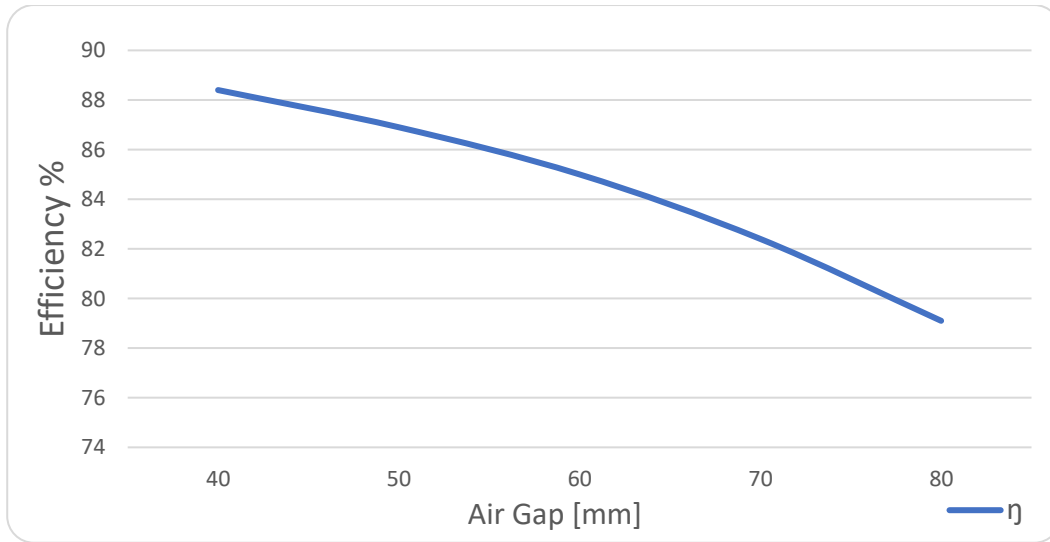


Fig. 3.36 The power efficiency of the WPT system with changing air-gap and 250-watt output power.

CHAPTER FOUR

IMPLEMENTATION OF RESONANT WPT SYSTEM

CHAPTER FOUR

IMPLEMENTATION OF RESONANT WPT SYSTEM

4.1 Introduction

The resonant IPT-WPT system developed in chapter 3 is implemented in this chapter using a conventional Silicon inverter. After that, new switches of Silicon Carbide are used to implement it in the WPT system and then compared between the two systems. Two types of circular coils are used to implement the WPT system, which was simulated in the previous chapter.

4.2 WPT system design

The fundamental working theory of the WPT system is that two circuits operating in the same resonant frequency are magnetically coupled to allow for the exchange of the energy between the transmitter and receiver circuits while dissipating relatively little bit of power. As mentioned in the previous chapter the WPT system consisted of multiple stages for power transfer from the transmitter (Tx) side to the receiver (Rx) side as illustrated in Fig.4.1.

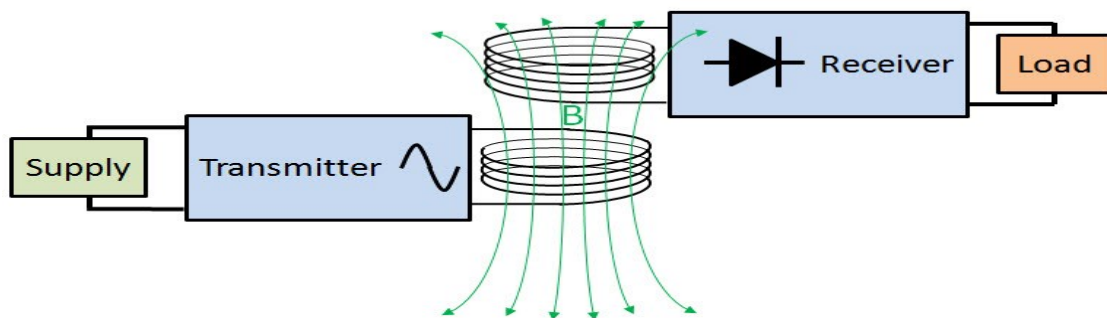


Fig. 4.1 Wireless power transfer system general configuration.

The system consists of the following major devices:

1. DC-AC converter (inverter) with the dc voltage supply.
2. Inductive coils.
3. Compensations circuits.
4. Rectifier circuits.
5. Load.

4.2.1 Inverter design

The principle circuit diagram of the WPT system is realized and it consists of a single-phase half-bridge inverter. The inverter circuit comprises a control circuit and power switches (MOSFET) are arranged in regulation to invert DC power to AC power at the required level and frequency. Two types of inverter were implemented one by using traditional Silicon MOSFET as shown in Fig.4.2, and the other using a new MOSFET device (Silicon Carbide) as shown in Fig.4.3.

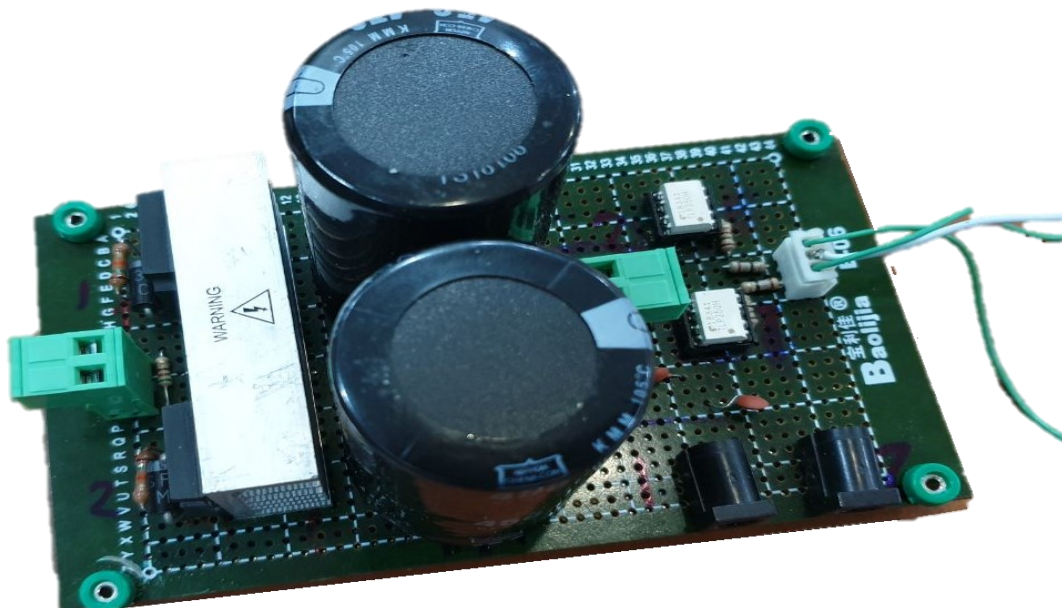


Fig. 4.2 Inverter circuit using Silicon MOSFET.

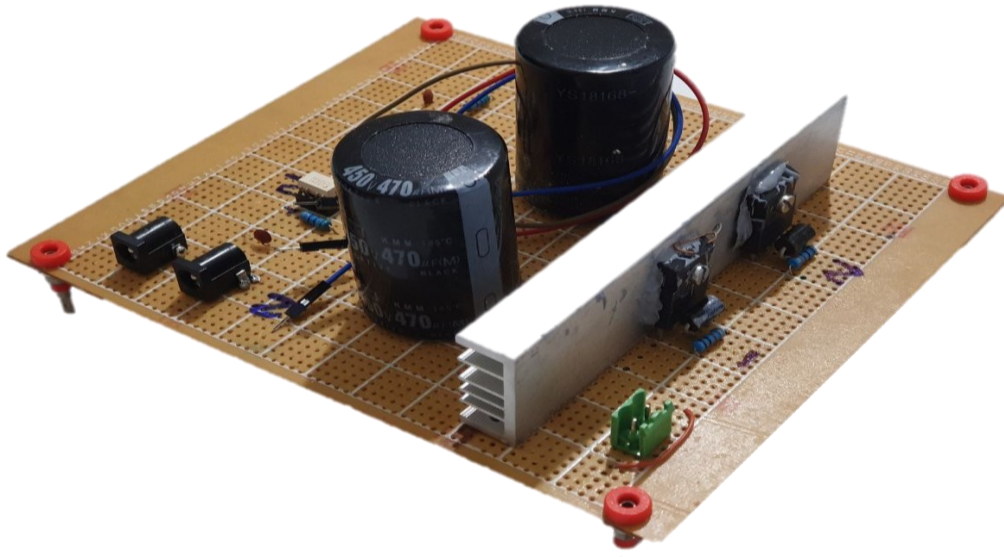


Fig. 4.3 Inverter circuit using Silicon Carbide MOSFET.

The inverter has the following components:

1. DC supply voltage.
2. Trigger circuit.
3. Switching device

4.2.1.1 Input DC supply voltage

A single-phase autotransformer is used with the industrial single-phase uncontrolled full-bridge to convert the input AC supply to the DC source. In order to divide the DC supplied voltage into two series supply voltage to provide the voltage to the half-bridge rectifier, two capacitors are connected in parallel with the supply voltage. The value of the two capacitors is chosen to have $470\ \mu\text{F} - 450\text{V}$, because of the permittivity in the value of the two capacitors that make the upper and lower peaks not equals, so a resistor $220\ \text{K}\Omega - 1\ \text{watt}$ is connected at the terminal of each capacitor to solve this problem.

4.2.1.2 Trigger circuit

Two devices are used to generate a pulse to trigger the MOSFET Arduino Mega 2560 or Signal Generator.

4.2.1.3 Optocoupler

The photocoupler “TLP250H “is an integrated circuit Ic with packaging type DIP8 that consists of gallium-aluminum (GaAl) As infrared LED (light-emitting diode) which is optically paired to an integrated high-gain, high-speed photodetector IC chip. It offers a guarantee to operate at temperature up to (125 ° C) with performance and specifications.

It has also an internal “Faraday shield” in order to provide a common-mode transient immunity of $\pm 40 \text{ kV}/\mu\text{s}$. It is great as the gate drive for the MOSFET and IGBT power devices.

4.2.1.4 Switching device

Two types of MOSFET switches were used to design the inverter to generate a square wave in the WPT system as follow:

a) Silicon MOSFET IRFP460

Third generation Power MOSFETs from Vishay company. It provides the following feature:

- The faster switching than the other generation.
- The production of ruggedized devices and low cost.
- The packaging type is TO-247.
- Low on-resistance $R_{DS(on)} = 0.27\Omega$ at $V_{GS} = 10 \text{ V}$
- $V_{DS} = 500\text{V}$.
- $I_d @ 25^\circ\text{C} = 36$

b) Silicon Carbide MOSFET C2M0080120D

Power MOSFETs from CREE provides the following feature:

- The switching speed is high and low capacitances.
- High blocking voltage $V_{DS} = 1200V$.
- $I_d @ 25^{\circ}C = 36 A$.
- Low on-resistance $R_{DS(on)} = 0.8\Omega$.
- The packaging type is TO-247.

The Benefits of C2M0080120D MOSFET are more than the others:

- Enhanced the efficiency of the system.
- Reduced the requirements for cooling.
- Enhanced the density of power.
- Increased switching frequency of the system.

4.2.2 Coil implementation

As mention in the previous chapter, two types of inductive coils are used in the implementation WPT system, inductive coil, and specific coil for WPT.

4.2.2.1 Inductive coil

A premade inductive coil shown in Fig.4.4 is used firstly in the implementation of a WPT system.



Fig. 4.4 Inductive coils.

Two pairs of modified coils are fixed on a base of wood to allow for horizontal and vertical alignment as shown in Fig.4.5.

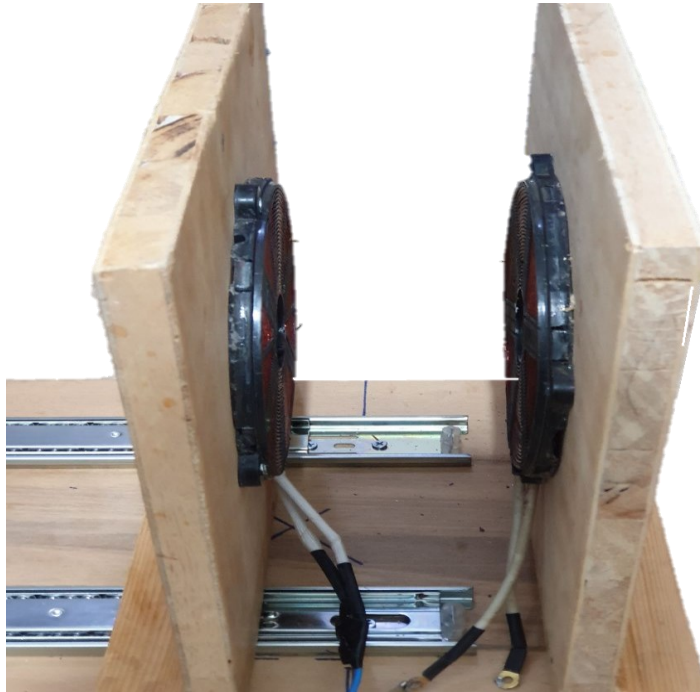


Fig. 4.5 Induction Tx and Rx coils.

The simulation result of the coils obtained from the ANSYS MAXWELL program is approximately matched with the laboratory measurement using LCR-meter as shown in Fig.4.6.



Fig. 4.6 Laboratory measurement L for the inductive coil.

4.2.2.2 Specific coil for the WPT system

Litz wire was used in the implementation of WPT system coils because of its suitable performance in the high frequency and voltage and it is less influenced by the phenomenon of the skin effect than the traditional wire. Two pairs of circular coils are implemented using **5x5x42/38 DN** Litz wire with cross-section radius $r=1.715$ mm and fixed on a plastic transparent plate as shown in Fig.4.7.



Fig. 4.7 Circular Litz wire coils.

The laboratory test of the coils is completed using LCR-meter and the simulation result of the coils obtained from the ANSYS MAXWELL program is approximately matched with the laboratory measurement using LCR- meter

4.2.3 Compensation capacitors

This type of AC high-frequency capacitor is used in the transmitter Tx and receiver Rx stage to work as a compensation element to eliminate the complex part of the impedance and remain a real part that works as a pure resistance.

4.2.4 Rectifier circuit

After the resonant circuit, the rectifier circuit receives the voltage with high-frequency to convert it to DC voltage. The implemented circuit is shown in Fig.4.8, which is consisted of the fast recovery diode and capacitive filter.

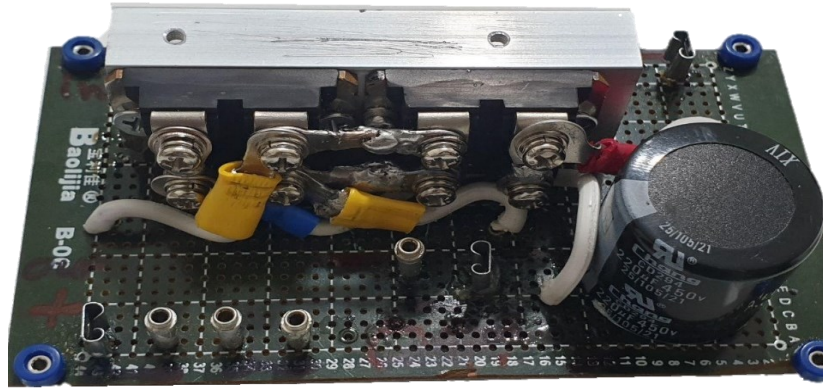


Fig. 4.8 Rectifier circuit.

4.2.4.1 Diode bridge

Two of low loss, soft recovery, and fast recovery DSEI2x101-06A are used for the implementation of the rectifier circuit with $V_{RSM}=600V$ (maximum non-repetitive reverse blocking voltage) at $(25^{\circ}C)$, max. repetitive reverse blocking voltage $V_{RSM}=600V$ at $25^{\circ}C$, average forward current $I_{FVr}=96 A$ at $T_C = 70^{\circ}C$, and reverse recovery time $t_{rr}= 35ns$

4.2.4.2 Output capacitor

The output capacitor works as a smoothing filter with a value of $220 \mu F-250V$.

4.2.5 Output load

The variable sliding resistor 25Ω , 10 A by Zenith Electric Co. Ltd is used in the experiment.

4.3 Implementation of the WPT system with a Silicon inverter

In this experiment, the MATLAB circuit designed and simulated in chapter (3) section (3.4), is implemented using the circular Litz wire with the gap between the coils (40 mm), the compensation circuit is connected in series-series (SS) topologies with value $225nF$ in the Tx and Rx sides. The dead time is set to have a value of $1.180 \mu s$ for the MOSFET applied pulse. The experiment installation is shown in Fig.4.9.

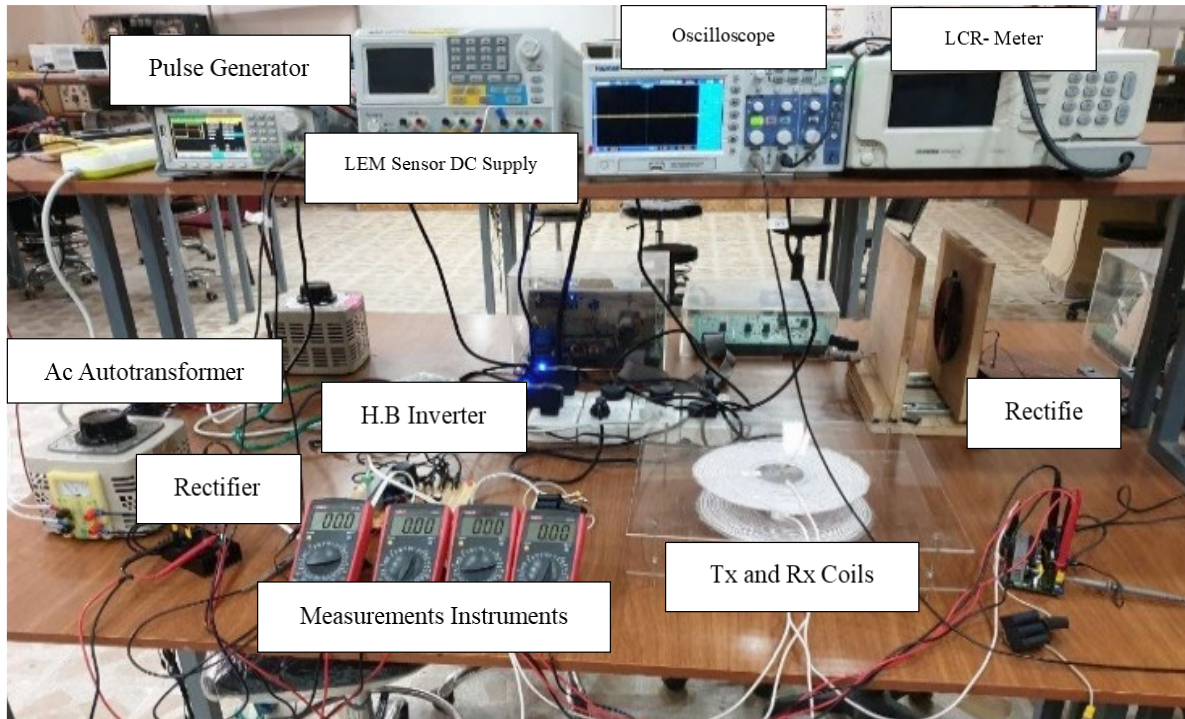


Fig. 4.9 Silicon inverter WPT system experiment.

The experiment results for different V_{in} the applied voltage is given in Table 4.1.

Table 4.1 Experiment result for WPT system with the silicon inverter.

| V_{in} (V) | I_{in} (A) | V_{out} (V) | I_{out} (A) | P_{in} (W) | P_{out} (W) | η |
|--------------|--------------|---------------|---------------|--------------|---------------|--------|
| 40 | 0.94 | 14.5 | 2.05 | 37.6 | 29.7 | 79.1 |
| 60 | 1.39 | 22.2 | 3.15 | 83.4 | 69.9 | 83.8 |
| 80 | 1.8 | 29.15 | 4.2 | 144 | 122 | 85 |
| 100 | 2.2 | 36.06 | 5.245 | 220 | 189 | 86 |
| 120 | 2.62 | 43.6 | 6.314 | 314.4 | 275 | 87.6 |

The simulation result of the WPT system obtained from the MATLAB program is approximately agreed with the laboratory measurement as shown in Fig.4.10 and Fig.4.11.

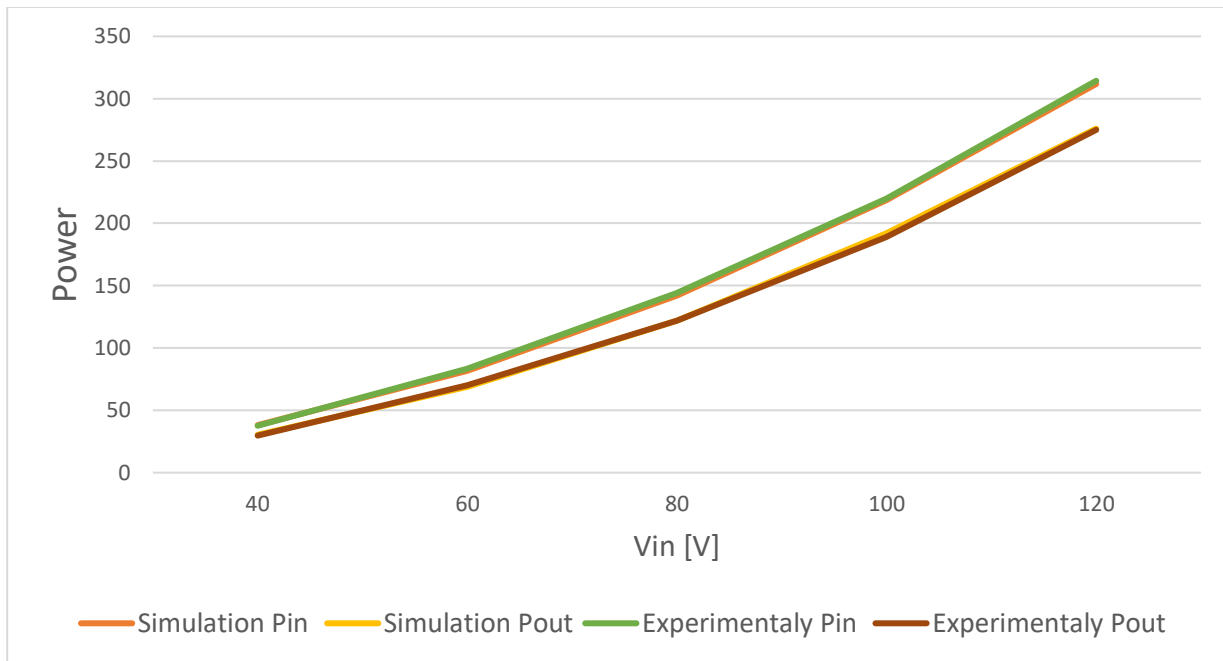


Fig. 4.10 Experimental results verification with simulation for input and output power.

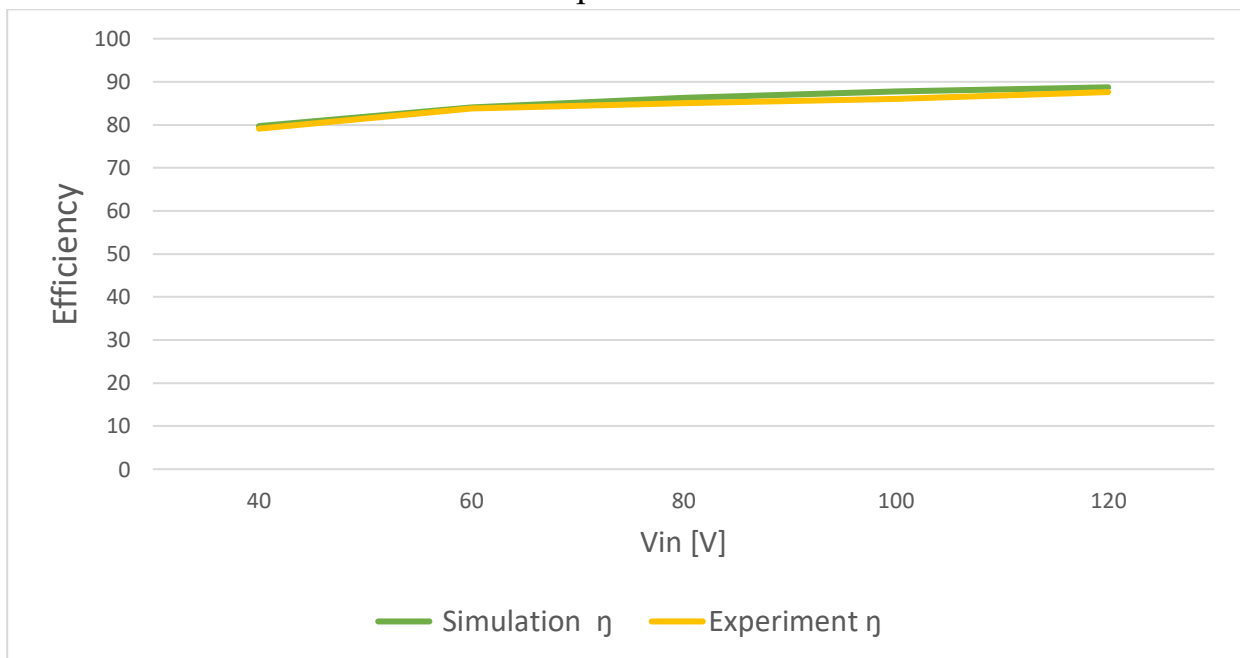


Fig. 4.11 Experimental results verification with simulation for efficiency.

The voltage and current across transmitter and receiver coils at $V_{in} = 50$ V are illustrated in Fig.4.12 and Fig.4.13 which are shown as good resonant is Tx and Rx side.

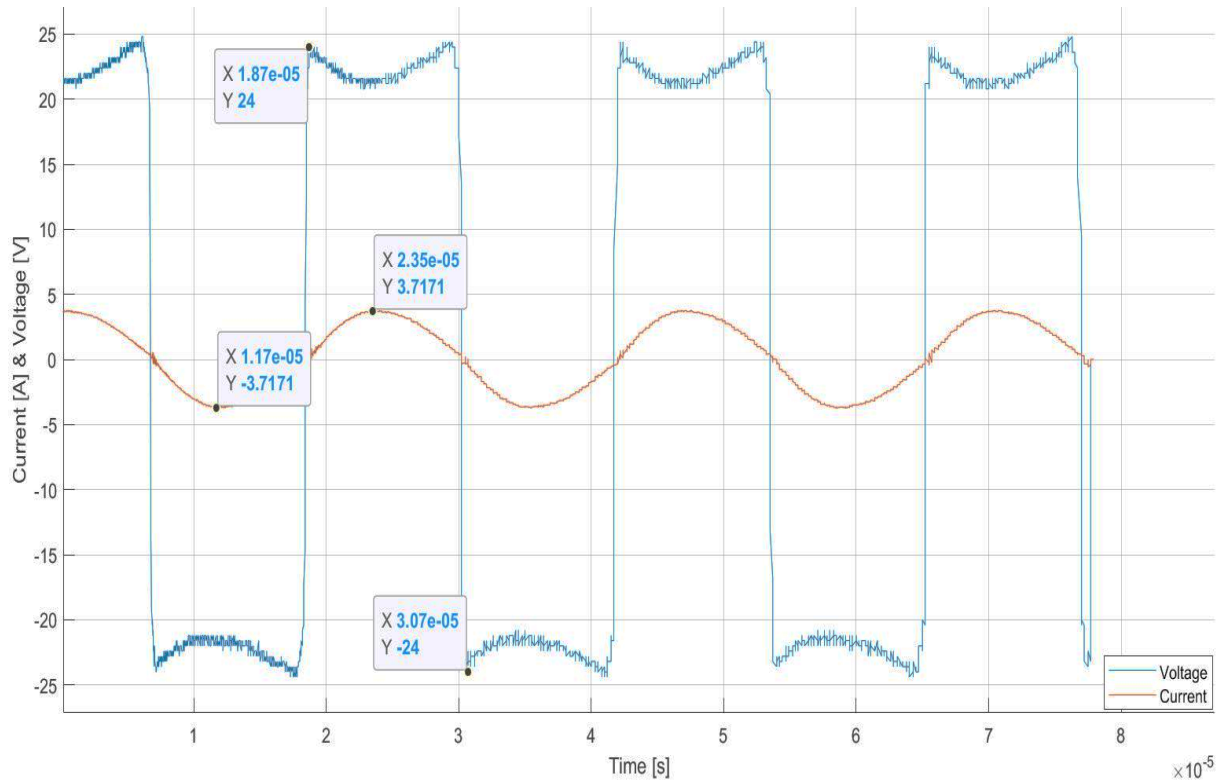


Fig. 4.12 Voltage and current across Tx coil at $V_{in} = 50V$.

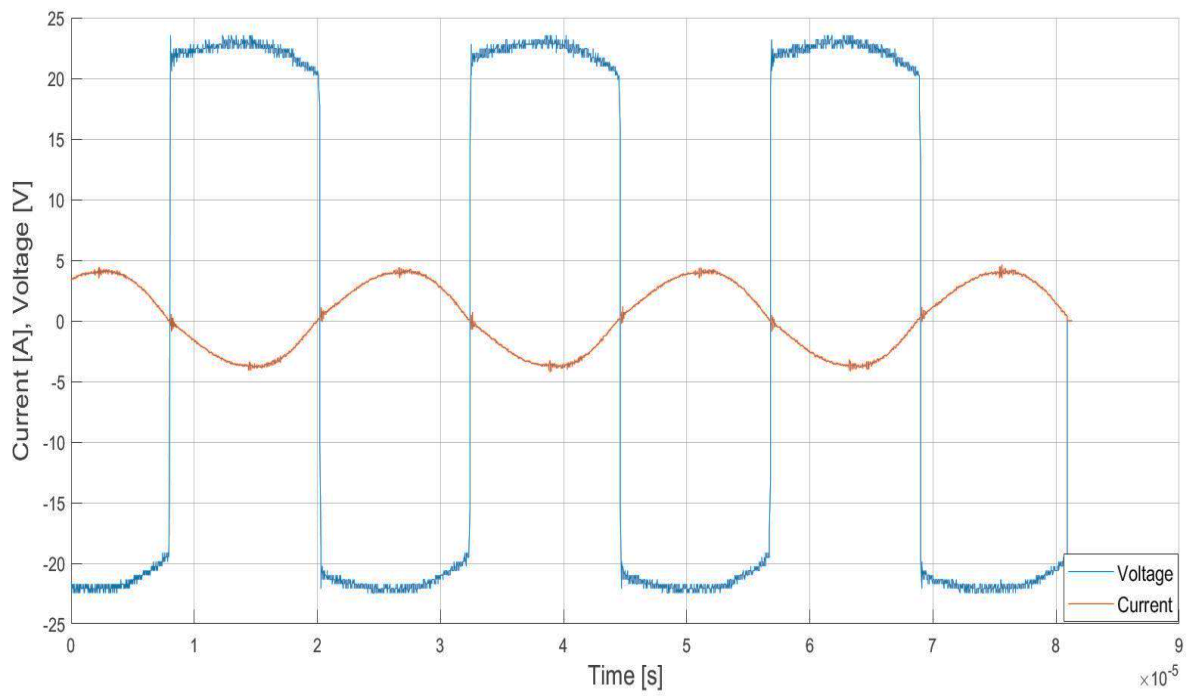


Fig. 4.13 Voltage and current across Rx coil at $V_{in} = 50V$.

4.4 Comparison between WPT system using Silicon and Silicon Carbide inverter

In this experiment, the Silicon carbide inverter is used for the implementation of a WPT system. The same coils and air gap and compensations capacitors used in the previous experiment are used in this system. The dead time is set to have a value of 720 ns for the MOSFET applied pulse.

The experiment results of the WPT system are given in Table 4.2.

Table 4.2. Experiment Results of WPT using Silicon Carbide inverter.

| V_{in} | I_{in} | V_{out} | I_{out} | P_{in} | P_{out} | η |
|----------|----------|-----------|-----------|----------|-----------|--------|
| 40 | 0.99 | 15.9 | 2.24 | 39.6 | 35.6 | 89.9 |
| 60 | 1.42 | 23.7 | 3.32 | 85.2 | 78.6 | 92.3 |
| 80 | 1.85 | 31.3 | 4.36 | 148 | 136.4 | 92.2 |
| 100 | 2.31 | 40.9 | 5.22 | 231 | 213.5 | 92.4 |
| 120 | 2.6 | 45.6 | 6.35 | 312 | 289.5 | 92.8 |

So, when the results are compared with the previous experiment using Silicon inverter, which is shown the input and output of the system using Silicon Carbide inverter are more than the other inverter as shown in the Fig.4.14.

Also, the MOSFET junction temperature remains constant in Silicon Carbide inverter, while in Silicon inverter it rises significantly.

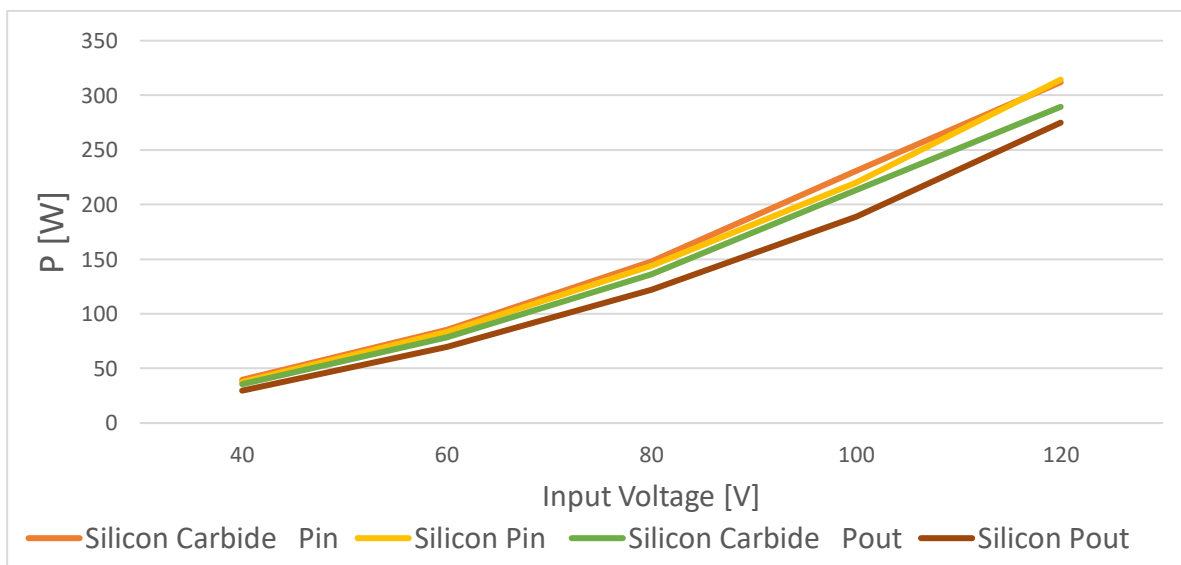


Fig. 4.14 Input and output power comparison between Silicon and Silicon Carbide inverter in the WPT system.

Also, the input current is slightly increased in Silicon Carbide more than the Silicon inverter as shown in Fig.4.15.

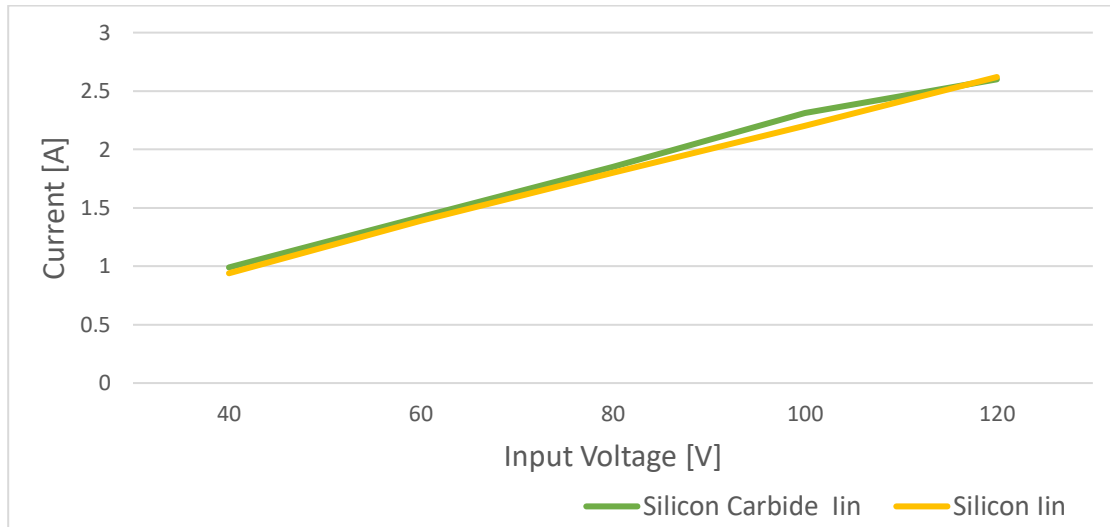


Fig. 4.15 Input current comparison between Silicon and Silicon Carbide inverter in the WPT system.

It can also be shown from the result that the efficiency of the system using Silicon Carbide inverter is more stable and more than the other inverter as shown in Fig.4.16.

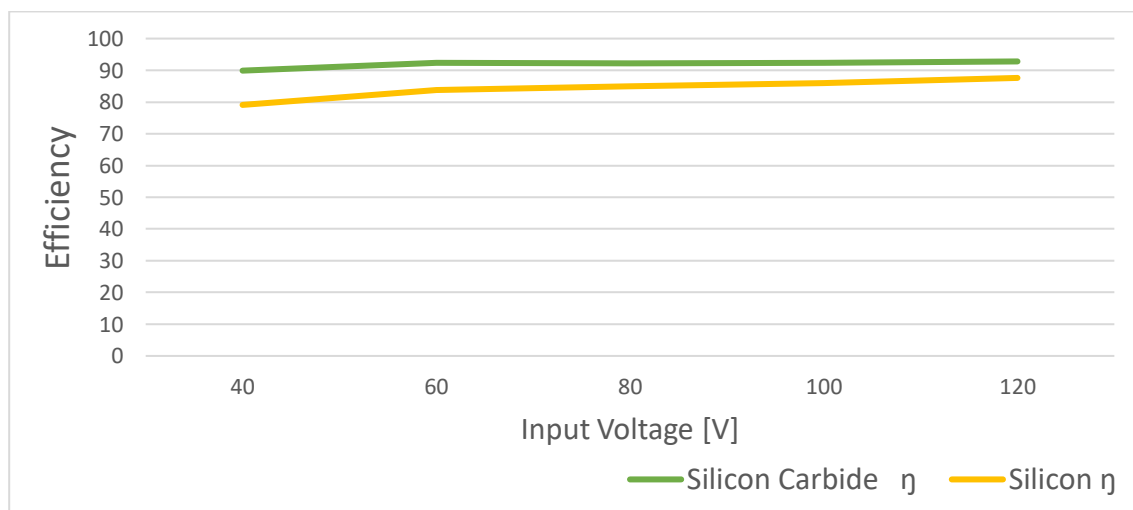


Fig. 4.16 Efficiency comparison between Silicon and Silicon Carbide inverter in the WPT system.

4.5 Implementation of the WPT system with leakage self-inductance-based resonant frequency calculation

This experiment is set to check and prove the results achieved previously about leakage and self-inductance-based resonant frequency calculation in the WPT system.

Fig.4.17 shows the experiment setup in the laboratory which consists of input supply voltage, a half-bridge inverter, transmitter Tx and receiver Rx coils, rectifier, and the load. In addition to some measurement instrumentation and a signal generator for driving the switches of the inverter. The practical results obtained from this experiment are given in Table 4.3 and Table 4.4.

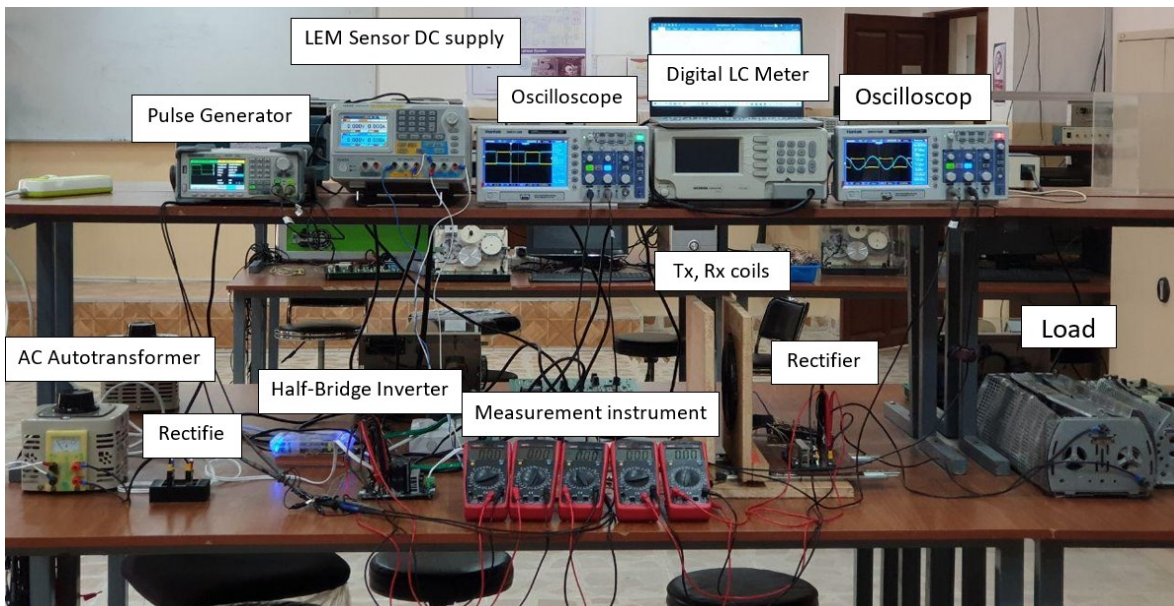


Fig. 4.17 Practical experiment setup of the leakage and self-inductance-based calculation in the WPT system.

Table 4.3. Experimental results based on leakage-inductance calculations.

| V_{in} (V) | I_{in} (A) | V_{out} (V) | I_{out} (A) | P_{in} (W) | P_{out} (W) | η % |
|--------------|--------------|---------------|---------------|--------------|---------------|----------|
| 60.7 | 1.8 | 25.2 | 3.57 | 109.26 | 89.964 | 82.33 |
| 89.6 | 2.65 | 37.6 | 5.26 | 237.44 | 197.776 | 83.29 |
| 120.3 | 3.68 | 49.1 | 7.64 | 442.704 | 375.124 | 84.73 |

| | | | | | | |
|-------|-----|------|------|--------|--------|-------|
| 184.1 | 4.4 | 68.7 | 10.1 | 810.04 | 693.87 | 85.65 |
|-------|-----|------|------|--------|--------|-------|

Table 4.4. Experiment results based on self- inductance calculations.

| V _{in} (V) | I _{in} (A) | V _{out} (A) | I _{out} (W) | P _{in} (W) | P _{out} (W) | η% |
|---------------------|---------------------|----------------------|----------------------|---------------------|----------------------|-------|
| 60.5 | 0.57 | 14 | 1.96 | 34.485 | 27.44 | 79.57 |
| 90.4 | 0.87 | 21.7 | 3.06 | 78.648 | 66.402 | 84.42 |
| 118.9 | 1.09 | 27.8 | 4.02 | 129.601 | 111.756 | 86.23 |
| 200 | 1.7 | 44.6 | 6.67 | 340 | 297.482 | 87.4 |

From the results, above it can be noticed that at the same input applied voltage, the current of input in the leakage-inductance-based calculations is more than the second method of calculation; this causes attention on the MOSFET switches. Also, it is noted that in the input and output power

The Experimental transmitter stage resonant voltage and current signal at V_{in}=60V are shown in Fig.4.18, which show a good resonant on the inverter switch, also receiver stage resonant voltage and current signal at V_{in}=60V Voltage is shown are Fig.4.19.

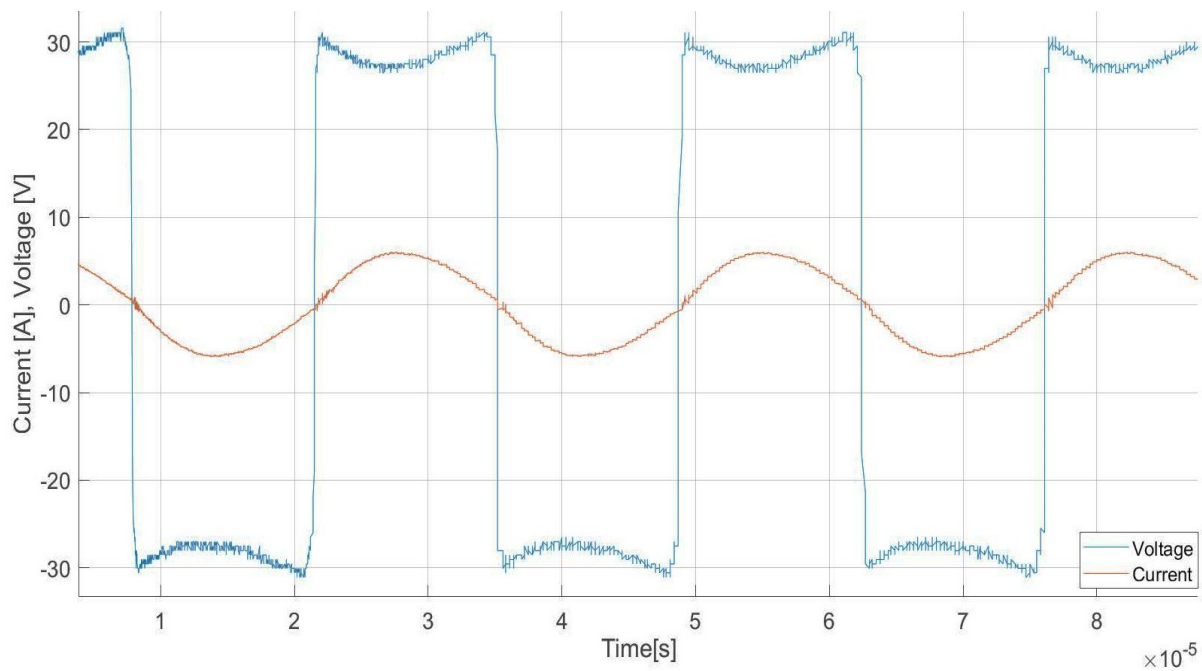


Fig. 4.18 Experimental transmitter stage resonant voltage and current waveform at $V_{in}=60V$ leakage-inductance-based.

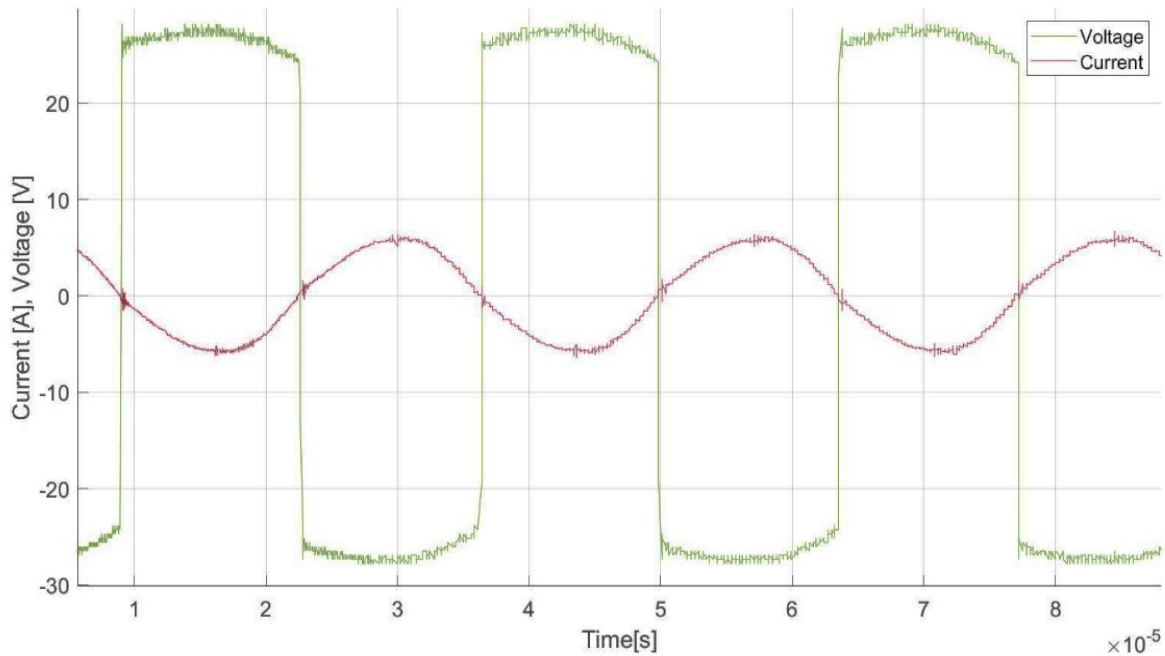


Fig. 4.19 Experimental receiver stage resonant voltage and current waveform at $V_{in}=60V$ leakage-inductance-based.

These experimental results are compared with the simulation counterpart as shown in Fig.4.20 which shows a good agreement between simulation and experimental results.

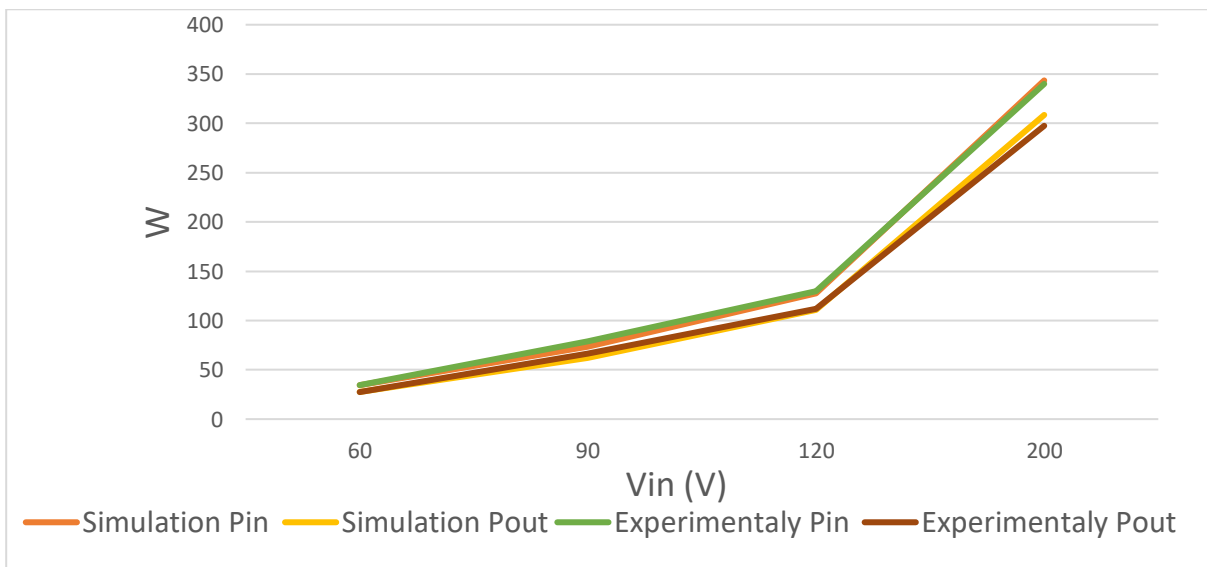


Fig. 4.20 Experimental results verification with simulation for input and output power based on self-inductance calculation.

CHAPTER FIVE

CONCLUSIONS AND FUTURE WORK

CHAPTER FIVE

CONCLUSIONS AND FUTURE WORK

5.1 Conclusions

Near field WPT system has been designed, simulated, and realized practically. Many investigations have been accomplished on the coils and the circuit of the system, these may include the effect of changing coils parameters on the coupling factor and how to improve it. The system efficiency has been improved using a new switch device, which is the Silicon Carbide MOSFET that is used in the inverter stage instead of Silicon MOSFET. It has been illustrated that using the Silicon Carbide inverter in the WPT system circuit improved the power transfer efficiency and made it more stable as well as reduced the junction temperature of the MOSFET, which means that it reduced the need for a large heatsink. Also, a new method to calculate the compensations element was presented, simulation and realization are applied that based on the leakage-inductance instead of self- inductance in which the power delivered to the load at the same input applied voltage was increased.

The main points which are considered by this study can be summarized as:

1. If the wire diameter of the inductive circular coils increases to get the same mutual between two symmetrical coils, the turn number, the wire length, and the L of the coils are decreasing but the volume and the weight of the coil increases.
2. If the inner diameter of the Tx and Rx of the circular coils increased, the coupling factor and the coils outer radius r_{out} are also increased, but the turn number is decreased with that effect, while the L is slightly less.

3. When the gap between turns of Tx and Rx of the circular coils increases, the coupling factor is also increasing, but the self-inductance and the coil's turns number decreasing.
4. The best k was obtained with the circular coils in all percentages of misalignment of the other shapes, and it was found that as the sides of the coils increased the number of turns decreased.
5. The symmetrical coils in which the transmitter Tx and receiver Rx coils are the same, this will give higher energy transfer efficiency when an SS compensation circuit is used. For the asymmetrical coils where the Tx coil is larger than the Rx coil, higher power transfer efficiency was achieved using SP compensation topologies.
6. The maximum power transfer efficiency (PTE_{max}) of a WPT occurs when the equivalent load is at its optimum value (RL_A).
7. The system power transfer efficiency increases as the resonant frequency increased. Also, when the resonant frequency increased the applied input voltage also increased, and the input current was inversely proportional with the resonant frequency to get the same power at the output so the tension on the inverter swatches is less when the resonant frequency increases, while the output voltage and current are remaining constant when the frequency changes.
8. Using the Silicon Carbide inverter in the WPT system provides higher efficiency than the Silicon-inverter, and the dead time has been set in the Silicon Carbide inverter is less than that setup in the Silicon inverter which increases the efficiency. Also, the MOSFET junction temperature in the Silicon Carbide inverter remains constant while in the Silicon inverter it rises significantly reduces the effect of temperature on the MOSFET on resistance.
9. A new compensation calculation has been used based on the Leakage inductance (Leakage-inductance-based calculation) between the two coils of the WPT

system used in the state of the self-inductance-based calculation. The output voltage and the delivered power to the load in case of the leakage-inductance-based calculation method is more than for the self-inductance-based calculation method at the same input voltage and load condition.

10. The current passes through the inverter MOSFET switch in the leakage-inductance-based calculation method is almost twice the value that in the self-inductance-based calculation at the same power deliverable in the output, this causes tension on the inverter switches, also it has been noted that the resonant frequency which is based on the leakage-inductance calculation is very sensitive to coil misalignment so it is preferred to use it in a static WPT system. Therefore, more attention should be given to choosing the f_r

5.2 Future work

The current work can be further extended by considering the following modifications:

1. Using a Gallium Nitride MOSFET to the implementation of the inverter of the WPT system.
2. More attention for using the leakage-inductance-based in the calculate of resonant frequency and the compensation circuit and using it to the implementation of the dynamic WPT system by using good control to make the circuit always operate in the resonant state.
3. Increase efficiency by improving the rectifier circuit.

REFERENCES

References:

- [1] D. M. Vilathgamuwa and J. P. K. Sampath, "Wireless power transfer (WPT) for electric vehicles (EVs)—present and future trends," *Power Syst.*, vol. 91, pp. 33–60, 2015.
- [2] X. Mou and H. Sun, "Wireless power transfer: Survey and roadmap," *IEEE Veh. Technol. Conf.*, vol. 2015, no. 646470, pp. 1–13, 2015.
- [3] Z. Zhang, H. Pang, A. Georgiadis, and C. Cecati, "Wireless Power Transfer - An Overview," *IEEE Transactions on Industrial Electronics*, vol. 66, no. 2. Institute of Electrical and Electronics Engineers Inc., pp. 1044–1058, 01-Feb-2019.
- [4] X. Lu, D. Niyato, P. Wang, D. I. Kim, and H. Zhu, "Wireless charger networking for mobile devices: Fundamentals, standards, and applications," *IEEE Wirel. Commun.*, vol. 22, no. 2, pp. 126–135, 2015.
- [5] X. Lu, P. Wang, D. Niyato, D. I. Kim, and Z. Han, "Wireless Charging Technologies: Fundamentals, Standards, and Network Applications," *IEEE Commun. Surv. Tutorials*, vol. 18, no. 2, pp. 1413–1452, Apr. 2016.
- [6] W. Eberle and F. Musavi, "Overview of wireless power transfer technologies for electric vehicle battery charging," *IET Power Electron.*, vol. 7, no. 1, pp. 60–66, 2013.
- [7] A. Ahmad, M. S. Alam, and R. Chabaan, "A Comprehensive Review of Wireless Charging Technologies for Electric Vehicles," *IEEE Trans. Transp. Electrification*, vol. 4, no. 1, pp. 38–63, 2017.
- [8] Z. Bi, T. Kan, C. C. Mi, Y. Zhang, Z. Zhao, and G. A. Keoleian, "A review of wireless power transfer for electric vehicles: Prospects to enhance sustainable mobility," *Appl. Energy*, vol. 179, pp. 413–425, 2016.
- [9] S. H. Kang, V. T. Nguyen, and C. W. Jung, "Analysis of WPT system using rearranged indirect-fed method for mobile applications," *2015 IEEE Wirel. Power Transf. Conf. WPTC 2015*, pp. 1–4, 2015.
- [10] N. Tesla, "Apparatus for Transmitting Electrical Energy," Patented, p. 4, 1914.
- [11] C. M. Zierhofer and E. S. Hochmair, "Geometric approach for coupling enhancement of magnetically coupled coils," *IEEE Trans. Biomed. Eng.*, vol. 43, no. 7, pp. 708–714, 1996.
- [12] A. Kurs, A. Karalis, R. Moffatt, J. D. Joannopoulos, P. Fisher, and M. Soljacic,

- “Wireless Power Transfer via Strongly Coupled Magnetic Resonances,” *Sicence*, vol. 317, no. 5834, p. 83(4), 2007.
- [13] A. K. RamRakhyani, S. Mirabbasi, and M. Chiao, “Design and optimization of resonance-based efficient wireless power delivery systems for biomedical implants,” *IEEE Trans. Biomed. Circuits Syst.*, vol. 5, no. 1, pp. 48–63, 2011.
- [14] W. Zhong, C. K. Lee, and S. Y. Ron Hui, “General analysis on the use of tesla’s resonators in domino forms for wireless power transfer,” *IEEE Trans. Ind. Electron.*, vol. 60, no. 1, pp. 261–270, 2013.
- [15] M. V. Reddy, “Microwave Power Transmission – A Next Generation Power Transmission System,” *IOSR J. Electr. Electron. Eng.*, vol. 4, no. 5, pp. 24–28, 2013.
- [16] T. Campi, S. Cruciani, F. Maradei, and M. Feliziani, “Near-Field Reduction in a Wireless Power Transfer System Using LCC Compensation,” *IEEE Trans. Electromagn. Compact.*, vol. 59, no. 2, pp. 686–694, 2017.
- [17] F. Liu, Y. Yang, Z. Ding, X. Chen, and R. M. Kennel, “A Multifrequency Superposition Methodology to Achieve High Efficiency and Targeted Power Distribution for a Multiload MCR WPT System,” *IEEE Trans. Power Electron.*, vol. 33, no. 10, pp. 9005–9016, 2018.
- [18] V. Cirimele, L. Pichon, and F. Freschi, “Electromagnetic modeling and performance comparison of different pad-to-pad length ratio for dynamic inductive power transfer,” *IECON Proc. (Industrial Electron. Conf.)*, pp. 4499–4503, 2016.
- [19] S. H. Jasim, “Analytical Comparison on Inductive Wireless Power Transfer System for Biomedical Devices,” *Eng. Technol. J.*, vol. 36, no. 6A, 2018.
- [20] M. Rehman, P. Nallagownden, and Z. Baharudin, “Efficiency investigation of SS and SP compensation topologies for wireless power transfer,” *Int. J. Power Electron. Drive Syst.*, vol. 10, no. 4, pp. 2157–2164, 2019.
- [21] M. Fareq et al., “Solar wireless power transfer using inductive coupling for mobile phone charger,” *Proc. 2014 IEEE 8th Int. Power Eng. Optim. Conf. PEOCO 2014*, pp. 473–476, 2014.
- [22] L. Wu, B. Zhang, and J. Zhou, “Efficiency Improvement of the Parity-Time-Symmetric Wireless Power Transfer System for Electric Vehicle Charging,” *IEEE Trans. Power Electron.*, vol. 35, no. 11, pp. 12497–12508, 2020.
- [23] S. A. Sis and H. Akca, “Maximizing the efficiency of wireless power transfer

- systems with an optimal duty cycle operation,” *AEU - Int. J. Electron. Commun.*, vol. 116, p. 153081, 2020.
- [24] M. Etemadrezaei, “Wireless Power Transfer,” *Power Electron. Handb.*, pp. 711–722, 2018.
- [25] T. Sun, X. Xie, and Z. Wang, “Wireless power transfer for medical microsystems,” *Wirel. Power Transf. Med. Microsystems*, vol. 9781461477, pp. 1–183, 2013.
- [26] M. S.Y.R. Hui, W.X. Zhong, C.K. Lee, “A Critical Review of Recent Progress in Mid-Range Wireless Power Transfer,” *IEEE Trans. Ind. Electron.*, vol. 61, no. 7, pp. 1–4, 2013.
- [27] K. Y. Kim, “Wireless Power Transfer - Principles and Engineering Explorations”, Book, InTech, 2011.
- [28] A. P. Sample, D. J. Yeager, P. S. Powledge, A. V. Mamishev, and J. R. Smith, “Design of an RFID-based battery-free programmable sensing platform,” *IEEE Trans. Instrum. Meas.*, vol. 57, no. 11, pp. 2608–2615, 2008.
- [29] A. M. Jawad, R. Nordin, S. K. Gharghan, H. M. Jawad, and M. Ismail, “Opportunities and challenges for near-field wireless power transfer: A review,” *Energies*, vol. 10, no. 7, pp. 1–28, 2017.
- [30] D. Lam Mung, K. Soe Lwin, and H. Myo Tun, “Design And Construction Of Wireless Charging System Using Inductive Coupling,” *Int. J. Sci. Technol. Res.*, vol. 4-p;azs, no. 06, pp. 282–287, 2015.
- [31] N. Shinohara and N. Shinohara, “Theory of WPT,” *Wirel. Power Transf. via Radiowaves*, pp. 21–52, 2014.
- [32] J. D. Jackson, “Classical Electrodynamics Third Edition,” *Am. J. Phys.*, vol. 67, p. 808, 1999.
- [33] A. Kunwar, “Design and Implementation of an Inductive Power Transfer System for Wireless Charging of Future Electric Transportation,” Ph.D. Thesis, University of Ontario Institute of Technology Oshawa, 2016.
- [34] J. Macharia, “Wireless Inductive Charging for Low Power Devices,” M.Sc Thesis, Helsinki Metropolia University of Applied Sciences, 2017.
- [35] P. Joshi, “Influences and Model How the Resonance Frequency is Influenced Under Such Conditions,” M.Sc Thesis, University of Bergen, 2014.

- [36] Y. Zhang, Z. Zhao, and K. Chen, "Frequency decrease analysis of resonant wireless power transfer," *IEEE Trans. Power Electron.*, vol. 29, no. 3, pp. 1058–1063, 2014.
- [37] I. I. C. on E. Safety, "IEEE Recommended Practice for Measurements and Computations of Radio Frequency Electromagnetic Fields With Respect to Human Exposure to Such Fields, 100 kHz–300 GHz," vol. 2002. 2003.
- [38] S. Li and C. C. Mi, "Wireless power transfer for electric vehicle applications," *IEEE J. Emerg. Sel. Top. Power Electron.*, vol. 3, no. 1, pp. 4–17, 2015.
- [39] Z. U. Zahid et al., "Modeling and control of series-series compensated inductive power transfer system," *IEEE J. Emerg. Sel. Top. Power Electron.*, vol. 3, no. 1, pp. 111–123, 2015.
- [40] I. F. Pellitteri, "WIRELESS CHARGING SYSTEMS FOR ELECTRIC VEHICLE BATTERIES," Ph.D. Thesis, UNIVERSIT  DEGLI STUDI DI PALERMO, 2016.
- [41] S. Chopra, "Contactless Power Transfer for Electric Vehicle Charging Application," M.Sc Thesis, DELFT UNIVERSITY OF TECHNOLOGY, 2011.
- [42] Muhammad H. Rashid, N. Kumar, and A. R. Kulkarni, "Power electronics: devices, circuits and applications." Book, Pearson Education Limited, 2014.
- [43] C. W. Lander, "Power Electronics", Book, 3rd ed. The McGraw-Hill Companies London.1993 ,'
- [44] A. Trzynadlowski, "INTRODUCTION TO MODERN POWER ELECTRONICS", Book, WILEY, 2005.
- [45] G. Vacca, "Technology focus: Silicon carbide," *semiconductorTODAY*, vol. 12, no. 3, pp.72–.2017 ,75
- [46] T. Diekhans and R. W. De Doncker, "A Dual-Side Controlled Inductive Power Transfer System Optimized for Large Coupling Factor Variations and Partial Load," *IEEE Trans. Power Electron.*, vol. 30, no. 11, pp. 6320–6328, 2015.
- [47] T. Diekhans, F. Stewing, G. Engelmann, H. Van Hoek, and R. W. De Doncker, "A systematic comparison of hard- and soft-switching topologies for inductive power transfer systems," 2014 4th Int. Electr. Drives Prod. Conf. EDPC 2014

- Proc., 2014.
- [48] I. Nam, R. Dougal, and E. Santi, “General optimal design method for series-series resonant tank in loosely-coupled wireless power transfer applications,” *Conf. Proc. - IEEE Appl. Power Electron. Conf. Expo. - APEC*, pp. 857–866, 2014.
- [49] Y. Liu, P. A. Hu, and U. K. Madawala, “Maximum power transfer and efficiency analysis of different inductive power transfer tuning topologies,” *Proc. 2015 10th IEEE Conf. Ind. Electron. Appl. ICIEA 2015*, vol. 2, no. 3, pp. 649–654, 2015.
- [50] W. Zhang, S. C. Wong, C. K. Tse, and Q. Chen, “Analysis and comparison of secondary series-and parallel-compensated inductive power transfer systems operating for optimal efficiency and load-independent voltage-transfer ratio,” *IEEE Trans. Power Electron.*, vol. 29, no. 6, pp. 2979–2990, 2013.
- [51] O. H. Stielau and G. A. Covic, “Design of loosely coupled inductive power transfer systems,” *PowerCon 2000 - 2000 Int. Conf. Power Syst. Technol. Proc.*, vol. 1, pp. 85–90, 2000.
- [52] I. Nam, R. Dougal, and E. Santi, “Optimal design method to achieve both good robustness and efficiency in loosely-coupled wireless charging system employing series-parallel resonant tank with asymmetrical magnetic coupler,” *2013 IEEE Energy Convers. Congr. Expo. ECCE 2013*, pp. 3266–3276, 2013.
- [53] C. A. Baguley, S. G. Jayasinghe, and U. K. Madawala, *Theory and control of wireless power transfer systems*. Elsevier Inc., 2018.
- [54] R. L. Steigerwald, “A comparison of half-bridge resonant converter topologies,” *APEC 1987 - 2nd Annu. IEEE Appl. Power Electron. Conf. Expo. Conf. Proc.*, vol. 3, no. 2, pp. 135–144, 2015.
- [55] M. Pinuela, D. C. Yates, S. Lucyszyn, and P. D. Mitcheson, “Maximizing DC-to-load efficiency for inductive power transfer,” *IEEE Trans. Power Electron.*, vol. 28, no. 5, pp. 2437–2447, 2013.
- [56] B. H. Choi, V. X. Thai, E. S. Lee, J. H. Kim, and C. T. Rim, “Dipole-Coil-Based Wide-Range Inductive Power Transfer Systems for Wireless Sensors,” *IEEE Trans. Ind. Electron.*, vol. 63, no. 5, pp. 3158–3167, 2016.
- [57] Q. Zhu, Y. Guo, L. Wang, C. Liao, and F. Li, “Improving the Misalignment Tolerance of Wireless Charging System by Optimizing the Compensate Capacitor,” *IEEE Trans. Ind. Electron.*, vol. 62, no. 8, pp. 4832–4836, 2015.

- [58] M. Kesler, “altamente resonante inalámbrica de transferencia de energía: segura, eficiente, y más de Distancia,” WiTricity Corp, 2013.
- [59] J. P. K. Sampath, A. Alphones, and H. Shimasaki, “Coil design guidelines for high efficiency of wireless power transfer (WPT),” IEEE Reg. 10 Annu. Int. Conf. Proceedings/TENCON, vol. 1, no. c, pp. 726–729, 2017.

الخلاصة

نقل القدرة اللاسلكي (WPT) هو تقنية حديثة تم تقديمها لنقل القدرة الكهربائية دون الحاجة للاسلاك. وتعد تقنية الاقتران الحثي من التقنيات السائدة في الشاحنات اللاسلكية نظرًا لمرونة استخدامها مقارنة بأنظمة الشحن التقليدية. تعتمد كفاءة (WPT) على عدة عوامل اهمها الاقتران بين ملفي الارسال والاستقبال (Coupling)، وعلى خسائر العاكس وخسائر المعدل.

في هذه الدراسة ، صُمم نظامًا لاسلكيًا حثيًا قائمًا على ظاهرة الرنين بين ملفي الارسال والاستقبال لنقل قدرة كهربائية لاسلكيا تصل مداها إلى 250 واط مع الأخذ بنظر الاعتبار عدة امور اهمها تأثير تردد الرنين ، وكفاءة النظام ، وعامل اقتران الملفات الحثية وخسائر النظام. وقد تمت محاكاة نظام (WPT) المصمم باستخدام (MATLAB) و (ANSYS MAXWELL) وقد تم إجراء العديد من التحريات على ملفات الاقتران ودائرة النقل عموماً، مثل تأثير تغيير معاملات الملفات على عامل الاقتران وكيفية تحسينه وتحريات اخرى على بعض عناصر الدائرة لتحسين كفاءة النظام. وأخيراً ، نفذ نظام (WPT) المصمم في المختبر عملياً بغية التحقق من نتائج المحاكاة المقدمة.وقدمت طريقة جديدة لحساب عناصر التعويضات على أساس محاثة التسرب بدلاً من الحث الذاتي، وقد تمت ابرازها في نتائج المحاكاة وتحقيقها عملياً.



جامعة نينوى
كلية هندسة الالكترونيات

تصميم وتنفيذ نظام لنقل الطاقة لاسلكيا

زكريا عمار الاطرقجي

شهادة الماجستير في
هندسة الالكترونيك

بإشراف

الدكتور احمد ذنون يونس
الدكتور ياسر محمد امين



جامعة نينوى

كلية هندسة الالكترونيات

تصميم وتنفيذ نظام لنقل الطاقة لاسلكيا

رسالة تقدم بها

زكريا عمار الاطرقجي

إلى

مجلس كلية هندسة الالكترونيات

جامعة نينوى

كجزء من متطلبات نيل شهادة الماجستير

في

هندسة الالكترونيك

بإشراف

الدكتور احمد ذنون يونس

الدكتور ياسر محمد امين